Numerical Modeling of Atmospheric Flows

Nashat Ahmad

NASA Langley Research Center

Presented at: Hampton University

January 29th, 2020

Lewis Fry Richardson

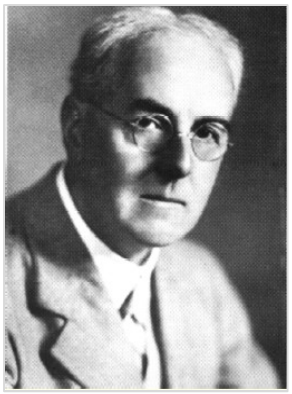

Richardson (1881-1953)

First numerical forecast in 1922 – by hand!

Richardson's Forecast Factory

COMPUTING FORM P XIII. Divergence of horizontal momentum-per-area. Increase of pressure

The equation is typified by: $-\frac{\partial R_{86}}{\partial t} = \frac{\partial M_{\chi 86}}{\partial e} + \frac{\partial M_{\chi 86}}{\partial n} - M_{\chi 86}\frac{\tan\phi}{a} + m_{\chi 8} - m_{\chi 8}{}^{\bullet} + \frac{2}{a}M_{\chi 86}$. (See Ch. 4/2 #5.)

* In the equation for the lowest stratum the corresponding term $-m_{\chi 8}$ does not appear

	Longitude 11° East $\delta e = 441 \times 10^6$			Latitude 5400 km North $\delta n = 400 \times 10^6$			Instant 1910 May 20d 7h G.M.T. $a^{-1}.\tan\phi = 1{\cdot}78 \times 10^{-9}$	Interval, δt 6 hours $a = 6{\cdot}36 \times 10^8$				
REF.:—				previous 3 columns	previous column		Form P XVI	Form P XVI	equation above	previous column	previous column	previous column
h	$\frac{\delta M_E}{\delta e}$	$\frac{\delta M_N}{\delta n}$	$-\frac{M_N \tan\phi}{a}$	$\mathrm{div}'_{EN} M$	$-g\delta t\,\mathrm{div}'_{EN} M$		m_H	$\frac{2M_H}{a}$	$-\frac{\partial R}{\partial t}$	$+\frac{\partial R}{\partial t}\delta t$	$g\frac{\partial R}{\partial t}\delta t$	$\frac{\partial p}{\partial t}\delta t$
	$10^{-5}\times$	$10^{-5}\times$	$10^{-5}\times$	$10^{-5}\times$	$100\times$	Leave the subsequent columns to be filled up after the vertical velocity has been computed on Form P XVI	$10^{-5}\times$	$10^{-5}\times$	$10^{-5}\times$		$100\times$	$100\times$
h_0							0					0
h_2	−61	−245	−6	−312	656		−83		−229	49·5	483	483
h_4	367	−257	2	112	−236		165	0·06	−136	29·4	287	770
h_6	93	−303	−16	−226	478		63	0·11	−124	26·8	262	1032
h_8	32	−55	−12	−35	74		138	0·07	−110	23·8	233	1265
h_a	−256	38	−8	−226	479			0·03	−88	19·0	186	1451
	NOTE: $\mathrm{div}'_{EN} M$ is a contraction for $\frac{\delta M_E}{\delta e} + \frac{\delta M_N}{\delta n} - M_N\frac{\tan\phi}{a}$				SUM = 1451 $= \frac{\partial p_a}{\partial t}\delta t$							check by $\Sigma - g\delta t\,\mathrm{div}'_{EN} M$

Lewis Fry Richardson

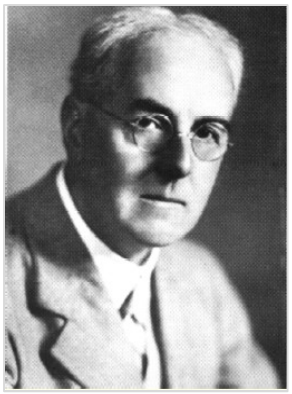

Richardson (1881-1953)

First numerical forecast in 1922 – by hand!

Richardson's Forecast Factory

COMPUTING FORM P XIII. Divergence of horizontal momentum-per-area. Increase of pressure

The equation is typified by: $-\frac{\partial R_{86}}{\partial t} = \frac{\partial M_{\chi 86}}{\partial e} + \frac{\partial M_{\chi 86}}{\partial n} - M_{\chi 86}\frac{\tan\phi}{a} + m_{\chi 8} - m_{\chi 8}{}^{\bullet} + \frac{2}{a}M_{\chi 86}$. (See Ch. 4/2#5.)

* In the equation for the lowest stratum the corresponding term $-m_{\chi 8}$ does not appear

	Longitude 11° East $\delta e = 441 \times 10^6$			Latitude 5400 km North $\delta n = 400 \times 10^6$			Instant 1910 May 20d 7h G.M.T. $a^{-1}.\tan\phi = 1{\cdot}78 \times 10^{-9}$		Interval, δt 6 hours $a = 6{\cdot}36 \times 10^8$			
REF.:—				previous 3 columns	previous column		Form P XVI	Form P XVI	equation above	previous column	previous column	previous column
h	$\frac{\delta M_E}{\delta e}$	$\frac{\delta M_N}{\delta n}$	$-\frac{M_N\tan\phi}{a}$	$\mathrm{div}'_{EN}M$	$-g\delta t\,\mathrm{div}'_{EN}M$		m_H	$\frac{2M_H}{a}$	$-\frac{\partial R}{\partial t}$	$+\frac{\partial R}{\partial t}\delta t$	$g\frac{\partial R}{\partial t}\delta t$	$\frac{\partial p}{\partial t}\delta t$
	$10^{-5}\times$	$10^{-5}\times$	$10^{-5}\times$	$10^{-5}\times$	$100\times$	Leave the subsequent columns to be filled up after the vertical velocity has been computed on Form P XVI	$10^{-5}\times$	$10^{-5}\times$	$10^{-5}\times$		$100\times$	$100\times$
h_0							0					0
h_2	−61	−245	−6	−312	656		−83		−229	49·5	483	483
h_4	367	−257	2	112	−236		165	0·06	−136	29·4	287	770
h_6	93	−303	−16	−226	478		63	0·11	−124	26·8	262	1032
h_8	32	−55	−12	−35	74		138	0·07	−110	23·8	233	1265
h_a	−256	38	−8	−226	479			0·03	−88	19·0	186	1451
	NOTE: $\mathrm{div}'_{EN}M$ is a contraction for $\frac{\delta M_E}{\delta e} + \frac{\delta M_N}{\delta n} - M_N\frac{\tan\phi}{a}$				SUM = 1451 $= \frac{\partial p_a}{\partial t}\delta t$							check by $\Sigma - g\delta t\,\mathrm{div}'_{EN}M$

Δp = 145mb in 6hrs

Charney, von Neuman, Fjørtoft

- Barotropic vorticity equation
  - "Numerical integration of the barotropic vorticity equation," *Tellus*, Vol. 2, pp. 237-254.
- ENIAC
  - 20,000 vacuum tubes, 70,000 resistors, 5million hand-soldered joints, 27 tons in weight, 150kW power requirement
  - 5,000 instructions/s (iPhone 6 executes on the order of billion instructions/s)
- NWP operations started in May 1955
  - US Weather Bureau
  - Air Weather Service (USAF)
  - Naval Weather Service

Charney (1917-1981)

von Neumann (1903-1957)

Fjørtoft (1913-1998)

First 48hr forecast on ENIAC in 1949 using barotropic filtered model

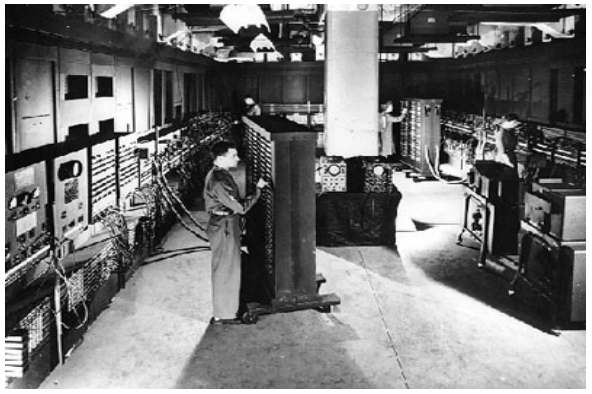

ENIAC (1946)

Atmospheric Modeling

TABLE 1. History of rapidly updated model and assimilation systems at NCEP as of late 2015.

Model and assimilation system	Horizontal grid spacing (km)	No. of vertical levels	Assimilation frequency (h)	Implementation (month/year)		Geographical domain
				NCEP	ESRL	
RUC1	60	25	3	1994		CONUS
RUC2	40	40	1	4/1998		CONUS
RUC20	20	50	1	2/2002		CONUS
RUC13	13	50	1	5/2005		CONUS
Rapid Refresh	13	51	1	5/2012	2010	North America
Rapid Refresh v2	13	51	1	2/2014	1/2013	North America
Rapid Refresh v3	13	51	1	Estimated spring 2016	1/2015	North America
HRRR	3	51	1	9/2014	2010	CONUS
HRRR v2	3	51	1	Estimated spring 2016	4/2015	CONUS

Benjamin et al., MWR 2016

Atmospheric Modeling

TABLE 1. History of rapidly updated model and assimilation systems at NCEP as of late 2015.

Model and assimilation system	Horizontal grid spacing (km)	No. of vertical levels	Assimilation frequency (h)	Implementation (month/year)		Geographical domain
				NCEP	ESRL	
RUC1	60	25	3	1994		CONUS
RUC2	40	40	1	4/1998		CONUS
RUC20	20	50	1	2/2002		CONUS
RUC13	13	50	1	5/2005		CONUS
Rapid Refresh	13	51	1	5/2012	2010	North America
Rapid Refresh v2	13	51	1	2/2014	1/2013	North America
Rapid Refresh v3	13	51	1	Estimated spring 2016	1/2015	North America
HRRR	3	51	1	9/2014	2010	CONUS
HRRR v2	3	51	1	Estimated spring 2016	4/2015	CONUS

Benjamin et al., MWR 2016

Atmospheric Modeling

TABLE 1. History of rapidly updated model and assimilation systems at NCEP as of late 2015.

Model and assimilation system	Horizontal grid spacing (km)	No. of vertical levels	Assimilation frequency (h)	Implementation (month/year)		Geographical domain
				NCEP	ESRL	
RUC1	60	25	3	1994		CONUS
RUC2	40	40	1	4/1998		CONUS
RUC20	20	50	1	2/2002		CONUS
RUC13	13	50	1	5/2005		CONUS
Rapid Refresh	13	51	1	5/2012	2010	North America
Rapid Refresh v2	13	51	1	2/2014	1/2013	North America
Rapid Refresh v3	13	51	1	Estimated spring 2016	1/2015	North America
HRRR	3	51	1	9/2014	2010	CONUS
HRRR v2	3	51	1	Estimated spring 2016	4/2015	CONUS

Benjamin et al., MWR 2016

Atmospheric Modeling

- NCEP Models
  - High Resolution Rapid Refresh (HRRR)
    - Horizontal Resolution: 3km (51 Vertical Levels)
    - Availability: September 2014 onwards
    - Data Format: grib2 – **File size: 400MB**
    - 15min output
  - Rapid Refresh (RAP)
    - Horizontal Resolution: 13km (51 Vertical Levels)
    - Availability: May 2012 onwards
    - Data Format: grib2 **– File size 12MB**
    - Hourly output
- Rapid Update Cycle (RUC) Model
  - Replaced by RAP/HRRR
  - Lower fidelity
  - Useful if data required is earlier than 2012

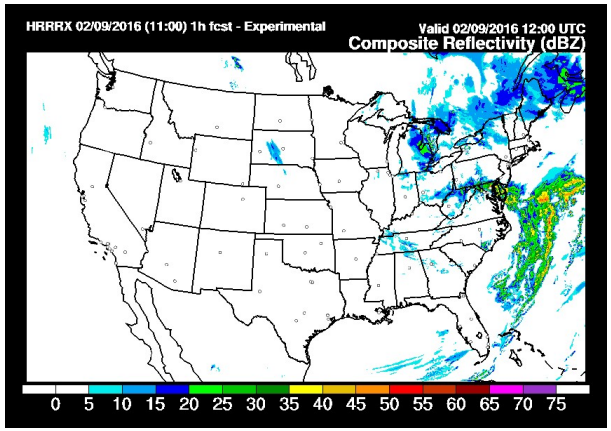

HRRR Model Domain

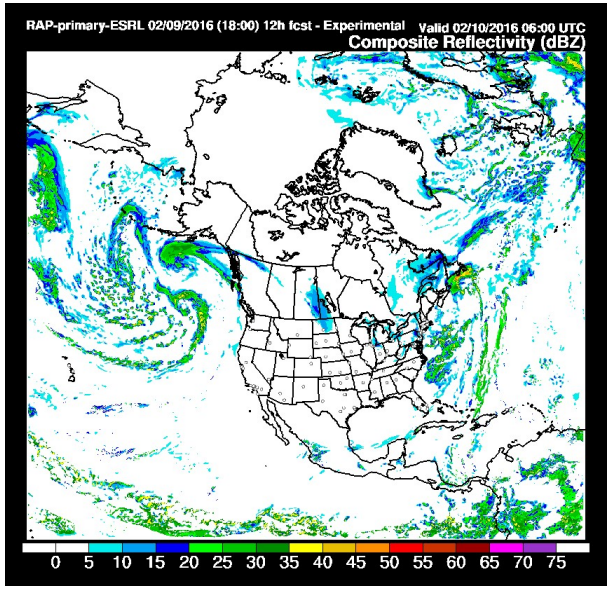

RAP Version 3 Model Domain

Atmospheric Scales and Predictability

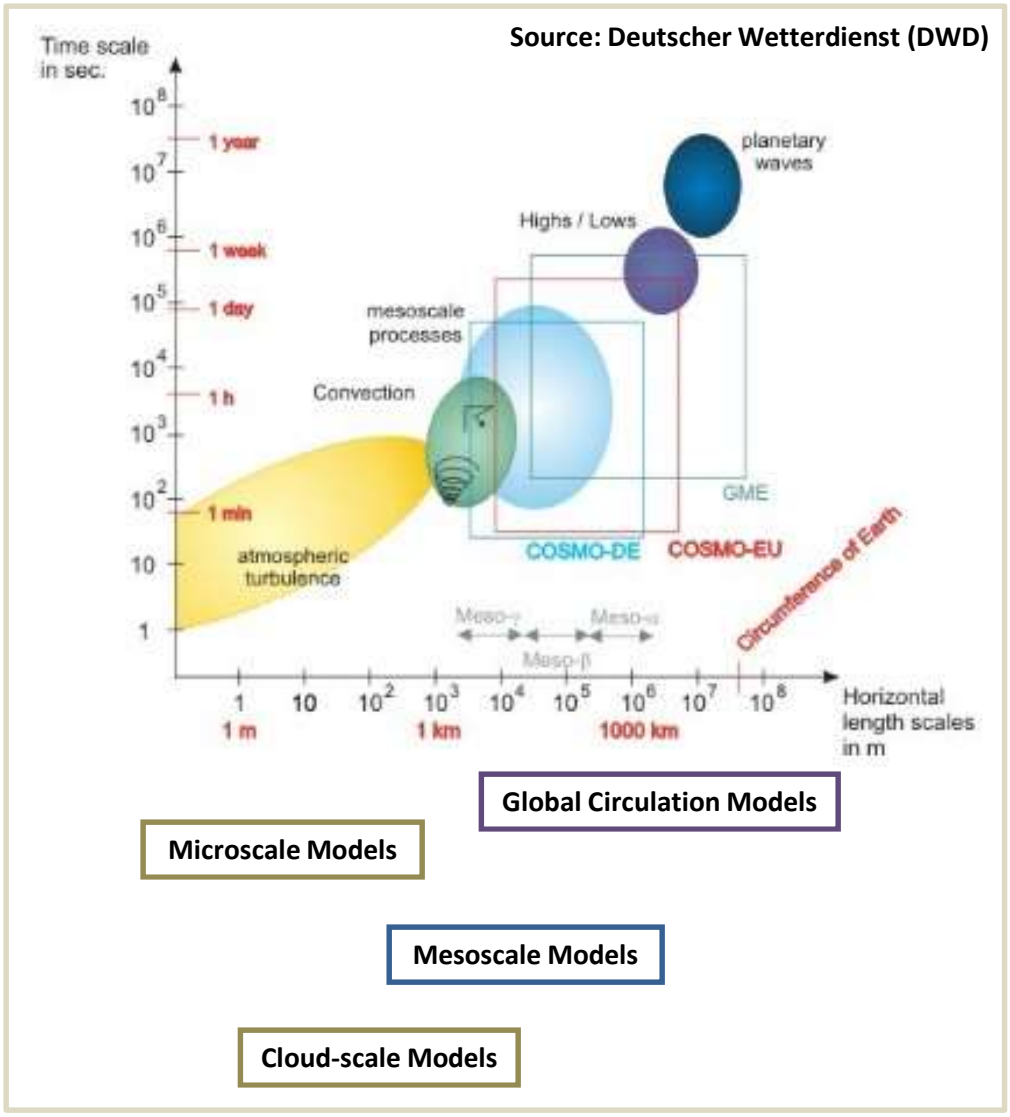

Lorenz pointed out that even if we assume that the physical processes are perfectly understood, there is a limit on predictability due to incomplete knowledge of initial conditions. Lorenz assumed that we know the physical processes in mid-latitudes reasonably well and calculated the upper bound on predictability at around ten days.

The smaller the spatial and temporal scale of an atmospheric process larger is the uncertainty associated with the forecast of that process.

Lorenz (1917-2008)

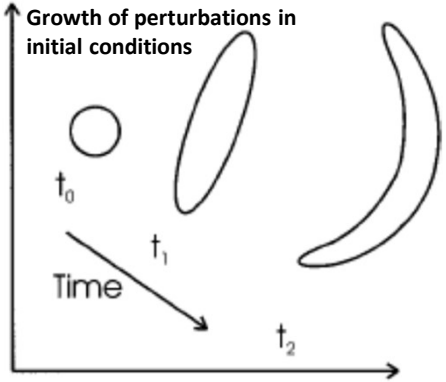

Toth (Wea. Forecasting, Vol. 12)

Atmospheric Models

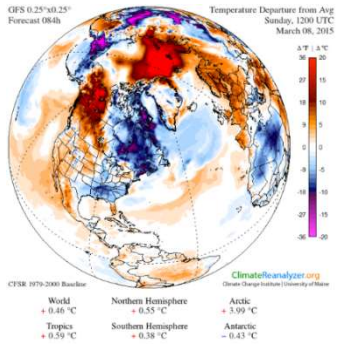

- Global Weather Prediction Models
  - Horizontal grid resolutions on the order of 0.5 to 1 degree
  - Limited vertical resolution and simpler physics options
  - Suitable for simulating large scale synoptic flows
  - Examples:
    - Global Forecast System (GFS) – National Centers for Environmental Prediction (NCEP)
    - Navy Global Environmental Model (NAVGEM) – Fleet Numerical Meteorology and Oceanography Center (FNMOC)
    - FV3 (Geophysical Fluid Dynamics Lab) – designed for massively parallel architectures (>120,000 cores)
- Mesoscale Weather Prediction Models
  - Horizontal grid resolution on the order of 1-5km
  - Vertical grid resolution on the order of meters
  - Comprehensive physics schemes (turbulence, cloud microphysics, and atmospheric radiation)

Atmospheric Models

- Cloud-Scale Models
  - Horizontal grid resolutions on the order of 100s of meters
  - Detailed cloud microphysics (limited boundary layer physics)
  - Small domain sizes (usually no underlying terrain)
  - Example(s):
    - Terminal Area Simulation System (TASS) – Fred Proctor (NASA)
    - Weather Research and Forecast (WRF) model – NCEP/NCAR

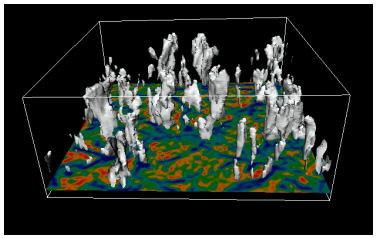

Moeng (NCAR)

- Microscale Models
  - Horizontal grid resolution on the order of 10s of meters or lower
  - Detailed treatment of turbulence
  - Underlying geometry resolved
  - Mostly used for atmospheric dispersion and may have applications for sUAS
  - Examples(s)
    - FEFLO – Rainald Löhner (GMU)
    - FLUENT

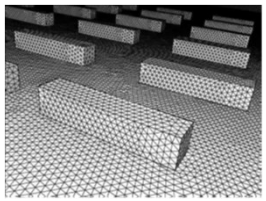

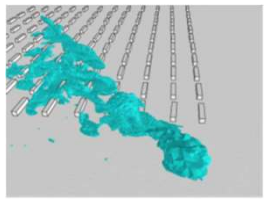

MUST Experiment – Dugway Proving Ground
Camelli and Löhner (AIAA 2006-1419)

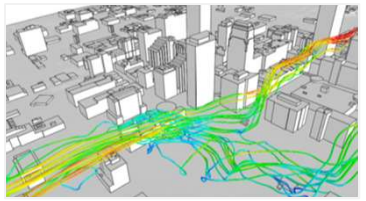

Oklahoma City
Camelli et al. (Geoinformatica)

Mesoscale Atmospheric Models

- Weather Research and Forecast (WRF) Model
  - Developed jointly by: NOAA, NCAR, Academia
  - NOAA and others
  - Users: NOAA, NASA, DoD, Industry, Academia
- Coupled Ocean/Atmosphere Mesoscale Prediction System (COAMPS)
  - Developed by: Navy
  - Users: Navy, Academia
- Operational Multiscale Environment model with Grid Adaptivity (OMEGA)
  - Developed by SAIC
  - Defense Threat Reduction Agency
  - Users: DoD, Industry, Academia
- Other mesoscale models in use but not as widely as others, include RAMS (Colorado State U.), ARPS (U. Oklahoma), MM5 (Penn State), UW-NMS (U. Wisconsin), NUMA (Naval Postgraduate School)

Atmospheric Models

Numerics
Completeness
Order of Accuracy
Data Requirements
Stability & Robustness
Computational Requirements

Data Assimilation
Initial Conditions
Boundary Conditions

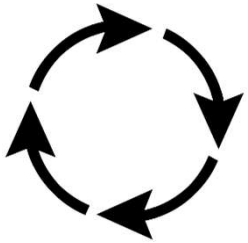

Physics
Dynamics
Turbulence
Thermodynamics
Cloud Microphysics
Radiation Transfer
Surface Physics
Atmospheric Chemistry
Particle Physics

Operational Constraints
CPU Performance
Available Storage
Resolution of Input Data
Spatial / Temporal
Communication Bandwidth
Required Output
Time

Atmospheric Models

$$\frac{\partial U}{\partial t}+\frac{\partial F}{\partial x}+\frac{\partial H}{\partial z}=\frac{\partial F_v}{\partial x}+\frac{\partial H_v}{\partial z}+\psi+S$$

$$U=\begin{bmatrix}\rho\\ \rho u\\ \rho w\\ \rho\theta\end{bmatrix},\qquad F=\begin{bmatrix}\rho u\\ \rho u^2+p\\ \rho uw\\ \rho\theta u\end{bmatrix},\qquad H=\begin{bmatrix}\rho w\\ \rho uw\\ \rho w^2+p\\ \rho\theta w\end{bmatrix},\qquad \psi=\begin{bmatrix}0\\ 0\\ \rho g\\ 0\end{bmatrix}$$

S is the source term. $\boldsymbol{F_v}$ and $\boldsymbol{H_v}$ are viscous flux terms.

$$p=C_0\left(\rho\theta\right)^{\gamma}\qquad C_0=\frac{R_d^{\gamma}}{p_0^{R_d/C_v}}$$

θ – potential temperature
R_d – gas constant (dry air)
p_0 – base-state pressure
g – gravity
u, w – velocity components
p – pressure
ρ – density
γ – ratio of specific heats

$$\theta=T\left(\frac{p_0}{p}\right)^{\frac{R_d}{c_p}}$$

Atmospheric Models

$$\frac{\partial U}{\partial t}+\frac{\partial F}{\partial x}+\frac{\partial H}{\partial z}=\frac{\partial F_v}{\partial x}+\frac{\partial H_v}{\partial z}+\psi+S$$

$$U=\begin{bmatrix}\rho\\ \rho u\\ \rho w\\ \rho\theta\end{bmatrix},\qquad F=\begin{bmatrix}\rho u\\ \rho u^2+p\\ \rho uw\\ \rho\theta u\end{bmatrix},\qquad H=\begin{bmatrix}\rho w\\ \rho uw\\ \rho w^2+p\\ \rho\theta w\end{bmatrix},\qquad \psi=\begin{bmatrix}0\\ 0\\ \rho g\\ 0\end{bmatrix}$$

S is the source term. $\boldsymbol{F_v}$ and $\boldsymbol{H_v}$ are viscous flux terms.

Thermodynamics
Cloud Microphysics
Radiation Transfer
Surface Layer Physics
Atmospheric Chemistry

Atmospheric Models

$$\frac{\partial U}{\partial t}+\frac{\partial F}{\partial x}+\frac{\partial H}{\partial z}=\frac{\partial F_v}{\partial x}+\frac{\partial H_v}{\partial z}+\psi+S$$

$$U=\begin{bmatrix}\rho\\ \rho u\\ \rho w\\ \rho\theta\end{bmatrix},\qquad F=\begin{bmatrix}\rho u\\ \rho u^2+p\\ \rho uw\\ \rho\theta u\end{bmatrix},\qquad H=\begin{bmatrix}\rho w\\ \rho uw\\ \rho w^2+p\\ \rho\theta w\end{bmatrix},\qquad \psi=\begin{bmatrix}0\\ 0\\ \rho g\\ 0\end{bmatrix}$$

S is the source term. ***F*$_v$** and ***H*$_v$** are viscous flux terms.

Turbulence

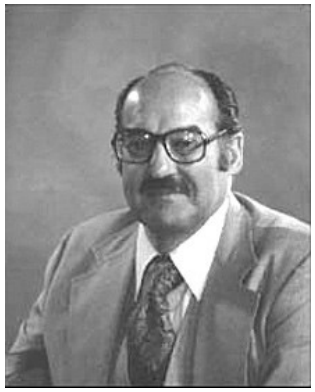

Smagorinsky (1924-2005)

Atmospheric Models

$$\frac{\partial U}{\partial t}+\frac{\partial F}{\partial x}+\frac{\partial H}{\partial z}=\frac{\partial F_v}{\partial x}+\frac{\partial H_v}{\partial z}+\psi+S$$

$$U=\begin{bmatrix}\rho\\ \rho u\\ \rho w\\ \rho\theta\end{bmatrix},\qquad F=\begin{bmatrix}\rho u\\ \rho u^2+p\\ \rho uw\\ \rho\theta u\end{bmatrix},\qquad H=\begin{bmatrix}\rho w\\ \rho uw\\ \rho w^2+p\\ \rho\theta w\end{bmatrix},\qquad \psi=\begin{bmatrix}0\\ 0\\ \rho g\\ 0\end{bmatrix}$$

Dynamics

Charney (1917-1981)

Lorenz (1917-2008)

Cressman (1919-2008)

Definitions

Hyperbolic conservation law written in quasilinear form in 1D:

$$u_t + A(u)u_x = 0$$

Where $A(u)$ is the coefficient Jacobian matrix which has real eigenvalues:

$$s^1 \le s^2 \le \cdots \le s^m$$

and diagonalizable, i.e., there are nonzero vectors $r^1, r^2, \cdots, r^m$ such that

$$Ar^p = s^p r^p \quad for\ p = 1, 2, \cdots, m$$

Matrix $R = \left[r^1 \mid r^2 \mid \cdots \mid r^m \right]$ is nonsingular and has an inverse R^{-1}

Riemann Problem

The Riemann problem is solved by taking the initial data (u_l , u_r) and decomposing the jump $u_r - u_l$ into eigenvectors of $A(u)$:

$$u_r - u_l = \alpha^1 r^1 + \cdots + \alpha^m r^m$$

$$u_r - u_l = R\alpha$$

$$\alpha = R^{-1}\left(u_r - u_l\right)$$

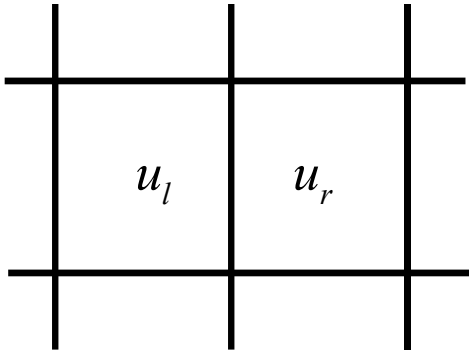

The jump in u across the *p*th wave in the solution of the Riemann problem is denoted by:

$$\mathcal{W}^p = \alpha^p r^p$$

Wave Propagation Method

If the Riemann problem consists of m waves $\mathcal{W}^p$ traveling at speeds s^p (these speeds may be positive or negative), then the cell average can be updated as follows:

$$\mathrm{U}_i^{n+1} = \mathrm{U}_i^n - \frac{\Delta t}{\Delta z}\left[\sum_{p=1}^{m}\left(s^p\right)^+ \mathcal{W}_{i-1/2}^p + \sum_{p=1}^{m}\left(s^p\right)^- \mathcal{W}_{i+1/2}^p\right]$$

$$s^+ = \max\left(s,0\right), \quad s^- = \min\left(s,0\right)$$

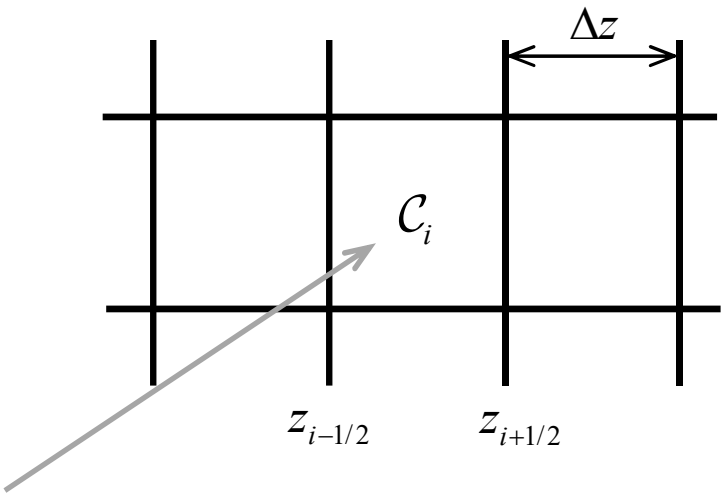

Cell average is affected by all right-going waves from $z_{i-1/2}$ and all left-going waves from $z_{i+1/2}$

Wave Propagation Method

LeVeque introduces the following shorthand notation:

$$\mathcal{A}^{-}\Delta \mathrm{U}_{i-1/2} = \sum_{p=1}^{m} \left(s^{p}\right)^{-} \mathcal{W}_{i-1/2}^{p}$$

$$\mathcal{A}^{+}\Delta \mathrm{U}_{i-1/2} = \sum_{p=1}^{m} \left(s^{p}\right)^{+} \mathcal{W}_{i-1/2}^{p}$$

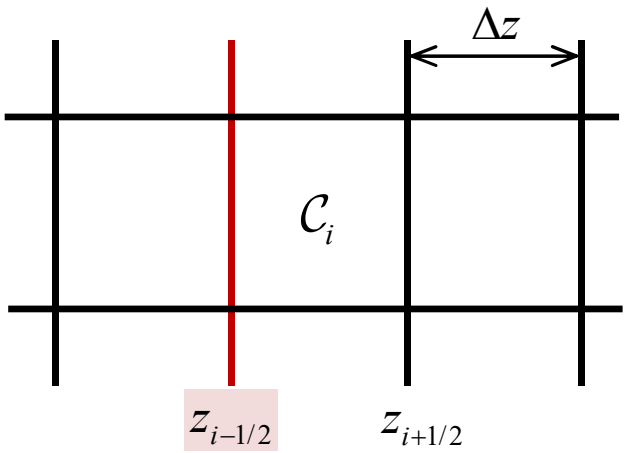

Rewriting the update in U as:

$$\mathrm{U}_{i}^{n+1} = \mathrm{U}_{i}^{n} - \frac{\Delta t}{\Delta z}\left[\mathcal{A}^{+}\Delta U_{i-1/2} + \mathcal{A}^{-}\Delta U_{i+1/2}\right]$$

$\mathcal{A}^{+}\Delta U_{i-1/2}$ measures the net effect of all right-going waves from $z_{i-1/2}$

$\mathcal{A}^{-}\Delta U_{i-1/2}$ measures the net effect of all left-going waves from $z_{i-1/2}$

These net effects are also called *fluctuations*

Wave Propagation Method

LeVeque introduces the following shorthand notation:

$$\mathcal{A}^{-}\Delta \mathrm{U}_{i-1/2} = \sum_{p=1}^{m} \left(s^{p}\right)^{-} \mathcal{W}_{i-1/2}^{p}$$

$$\mathcal{A}^{+}\Delta \mathrm{U}_{i-1/2} = \sum_{p=1}^{m} \left(s^{p}\right)^{+} \mathcal{W}_{i-1/2}^{p}$$

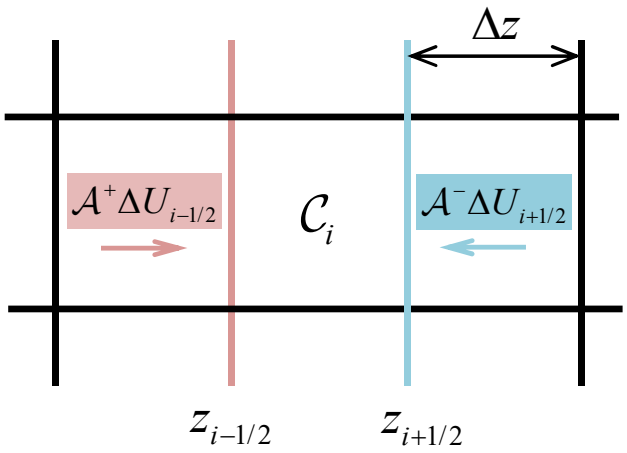

Rewriting the update in U as:

$$\mathrm{U}_{i}^{n+1} = \mathrm{U}_{i}^{n} - \frac{\Delta t}{\Delta z}\left[\mathcal{A}^{+}\Delta U_{i-1/2} + \mathcal{A}^{-}\Delta U_{i+1/2}\right]$$

Within cell $\mathcal{C}_i$ the right-going fluctuation from the left edge and the left-going fluctuation from the right edge modify the cell average.

Conservation is enforced by the following condition:

$$A_{i-1/2}(U_i - U_{i-1}) = F_i(U_i) - F_{i-1}(U_{i-1})$$

$A_{i-1/2}$ is the Roe matrix

f-waves

Use flux-based wave decomposition, in which the flux differences are written directly as a linear combination of the right eigenvectors:

$$F_i(U_i) - F_{i-1}(U_{i-1}) = \sum_{p=1}^{m} \beta_{i-1/2}^{p} r_{i-1/2}^{p} \equiv \sum_{p=1}^{m} Z_{i-1/2}^{p}$$

***f*-waves**

$$\beta_{i-1/2} = R_{i-1/2}^{-1}(F_i(U_i) - F_{i-1}(U_{i-1})).$$

Since we are dealing directly with the fluxes, discretization errors can be avoided when including the source term due to gravity.

$$\beta_{i-1/2} = \mathrm{R}_{i-1/2}^{-1}(\mathrm{F}_i(\mathrm{U}_i) - \mathrm{F}_{i-1}(\mathrm{U}_{i-1}) - \Delta z \psi_{i-1/2})$$

f-waves

The update of U can now be written as:

$$\mathrm{U}_i^{n+1} = \mathrm{U}_i^n - \frac{\Delta t}{\Delta z}\left[\mathcal{A}^+\Delta \mathrm{U}_{i-1/2} + \mathcal{A}^-\Delta \mathrm{U}_{i+1/2}\right]$$

Fluctuations which contribute to the cell-averaged quantity $\mathrm{U_i}$ due to the wave propagation across cell interfaces are given by:

$$\mathcal{A}^-\Delta \mathrm{U}_{i-1/2} = \sum_p Z^p_{i-1/2} \quad \text{if} \quad s^p_{i-1/2} < 0$$

$$\mathcal{A}^+\Delta \mathrm{U}_{i-1/2} = \sum_p Z^p_{i-1/2} \quad \text{if} \quad s^p_{i-1/2} > 0$$

$s^p_{i-1/2}$ are the wave speeds given by the eigenvalues of the hyperbolic system

Higher-order Correction

Second-order accuracy is achieved by adding a correction term:

$$\mathrm{U}_i^{n+1} = \mathrm{U}_i^n - \frac{\Delta t}{\Delta z}\left[\mathcal{A}^+ \Delta \mathrm{U}_{i-1/2} + \mathcal{A}^- \Delta \mathrm{U}_{i+1/2}\right] - \frac{\Delta t}{\Delta z}\left[\tilde{F}_{i+1/2} - \tilde{F}_{i-1/2}\right]$$

Where,

$$\tilde{F}_{i-1/2} = \frac{1}{2}\sum_{p=1}^{m} \mathrm{sgn}(s_{i-1/2}^p)\left[1 - \frac{\Delta t}{\Delta x}\left|s_{i-1/2}^p\right|\right]\tilde{Z}_{i-1/2}$$

Details: LeVeque, Finite Volume Methods for Hyperbolic Problems, 2002.

Riemann Solution in the Normal Direction

In 2D: $u_t + Au_x + Bu_y = 0$

In the normal Riemann solver, decompose,

$\Delta U = U_{ij} - U_{i-1,j}$ into $\mathcal{A}^+\Delta\mathrm{U}$ and $\mathcal{A}^-\Delta\mathrm{U}$

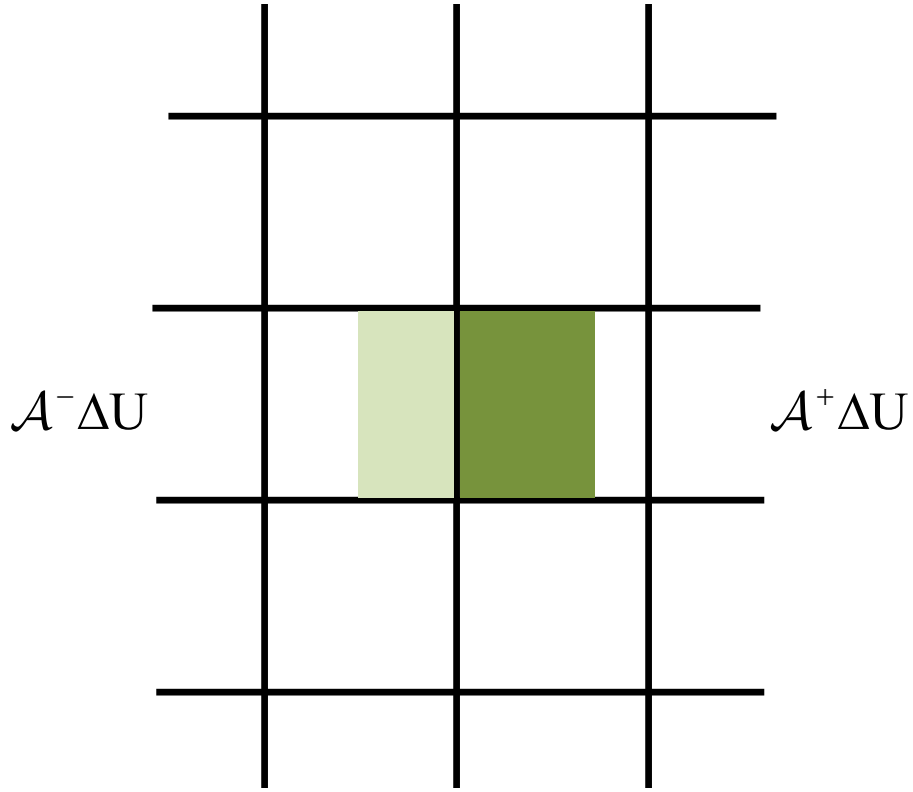

In dimensional-splitting the normal Riemann solver is called successively in each direction.

Riemann Solution in the Transverse Direction

In 2D: $u_t + Au_x + Bu_y = 0$

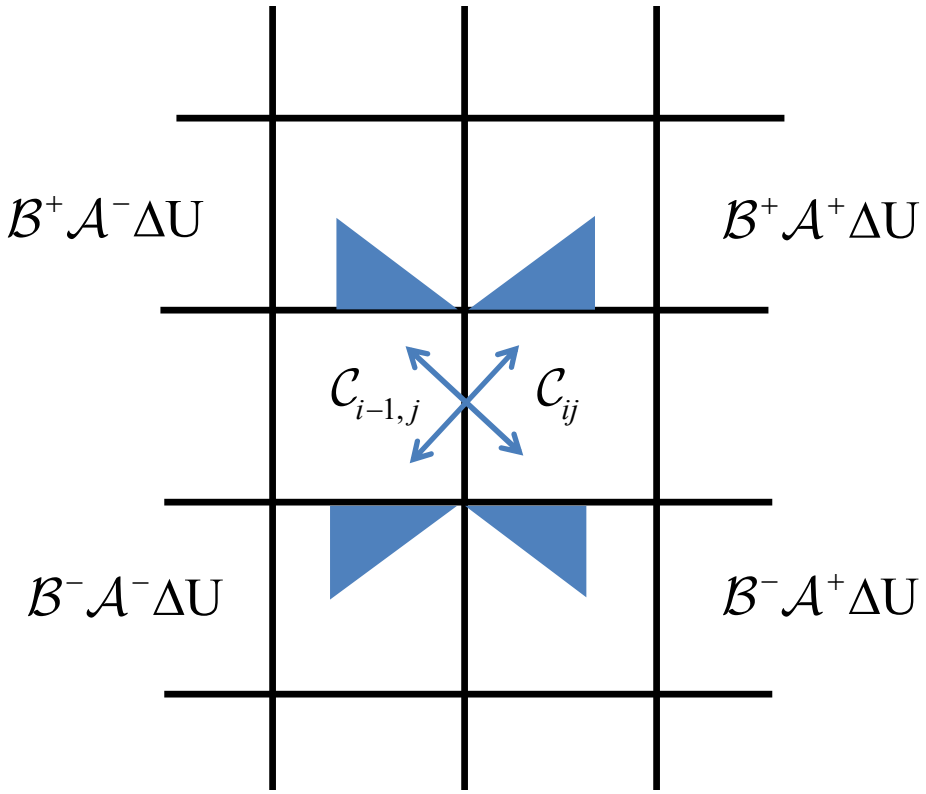

Decompose $\mathcal{A}^+\Delta\mathrm{U}$ and $\mathcal{A}^-\Delta\mathrm{U}$ into eigenvectors of B to obtain $\mathcal{B}^\pm\mathcal{A}^\pm\Delta\mathrm{U}$

This wave decomposition of $\mathcal{A}^\pm\Delta\mathrm{U}$ can be thought of as solving a second Riemann problem in the transverse direction – however it is not based on left and right states.

Details: LeVeque, Finite Volume Methods for Hyperbolic Problems, 2002.

Rayleigh-Taylor Instability

Almgren et al., Astrophysical Journal, 2010

$$(x, z) \in [0,0.5] \times [0,1]$$

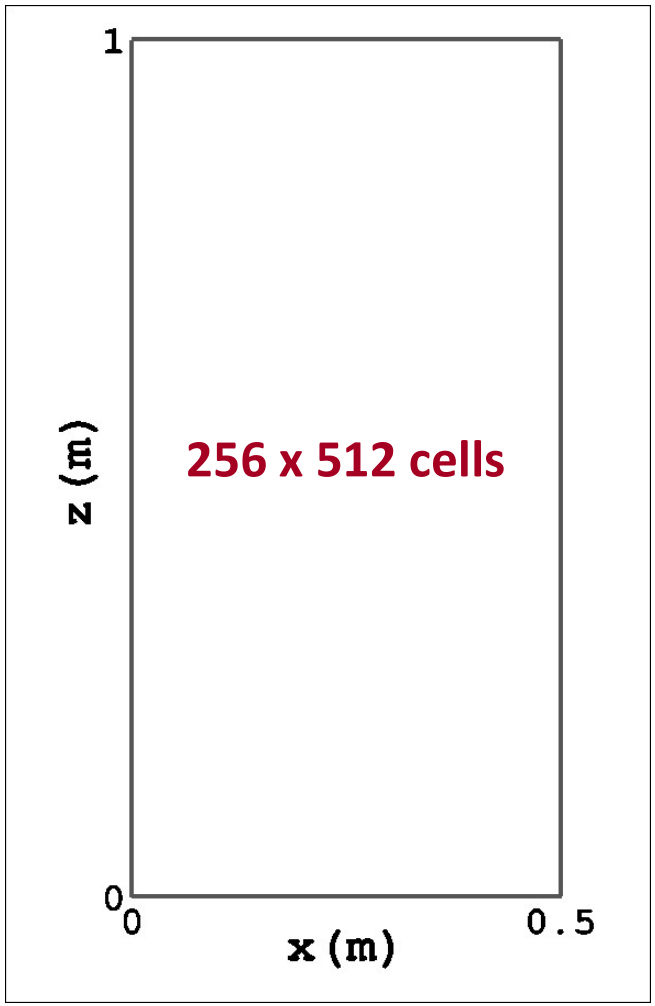

Rayleigh-Taylor Instability

$$(x, z) \in [0,0.5] \times [0,1]$$

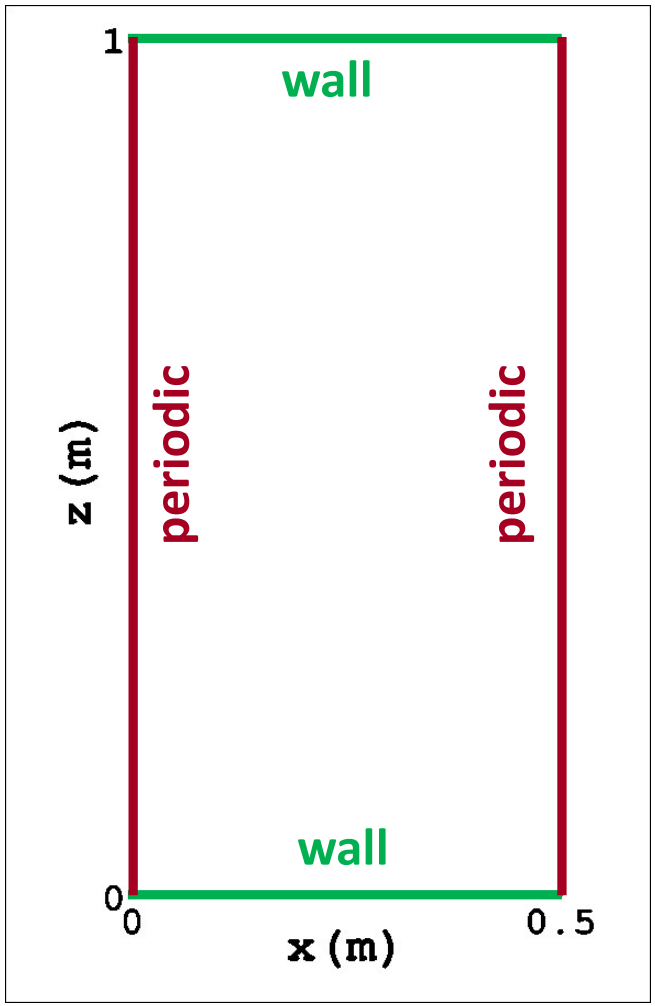

Rayleigh-Taylor Instability

$$p(z) = p_0 - \rho_1 g L_z / 2 - \rho_2 g (z - L_z / 2)$$

$$g = 1$$

$$p(z) = p_0 - \rho_1 g z$$

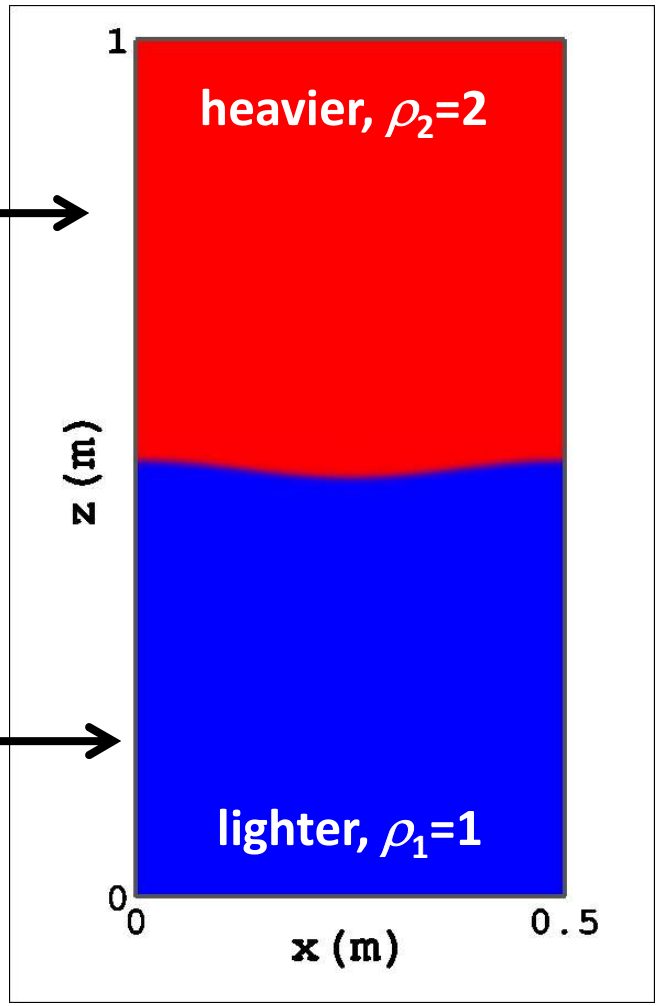

Rayleigh-Taylor Instability

Introduce a single-mode perturbation at the interface

$$\rho(x,z) = \rho_1 + \frac{\rho_2 - \rho_1}{2}\left[1 + \tanh\left(\frac{z - \psi(x)}{0.005}\right)\right]$$

$$\psi(x) = \frac{L_z}{2} + 0.01\frac{\cos(4\pi x) + \cos(4\pi(L_x - x))}{2}$$

$$t \in [0, 2.5]$$

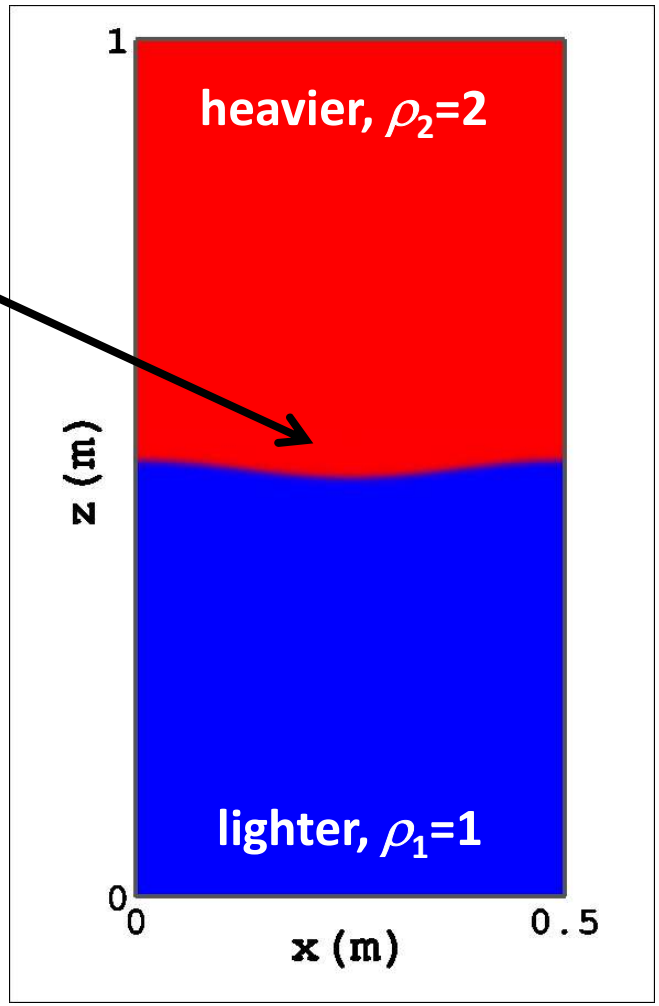

Rayleigh-Taylor Instability

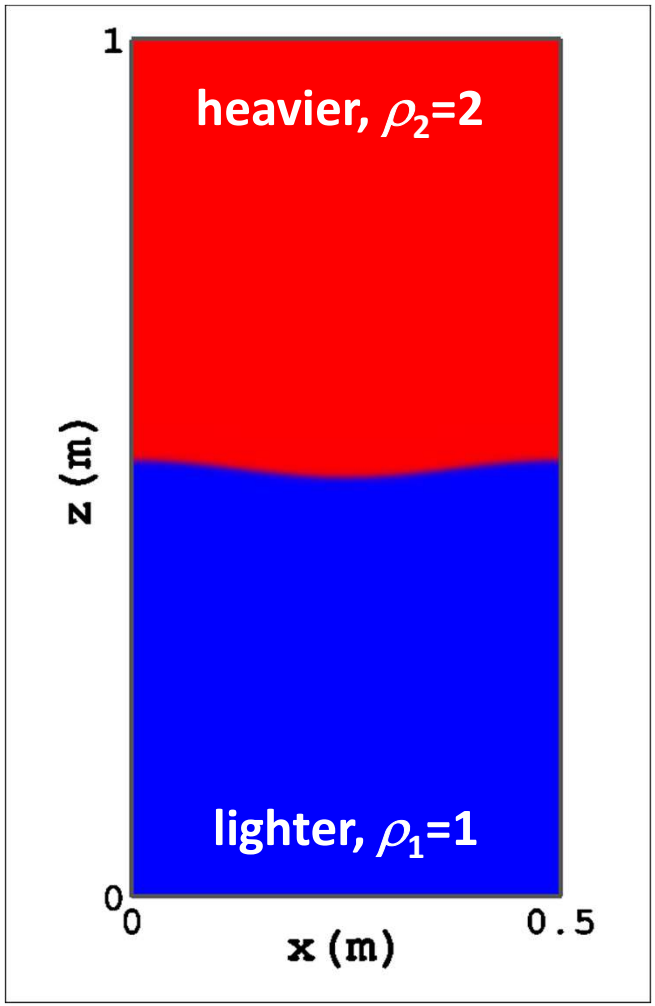

Ahmad (AIAA-2018-3498)

Kelvin-Helmholtz Waves

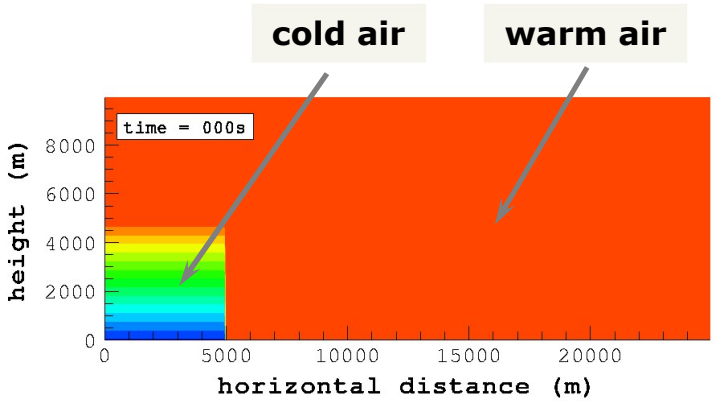

(1) Cold pool of air collapses due to negative buoyancy

Ahmad (AIAA-2009-556)

Kelvin-Helmholtz Waves

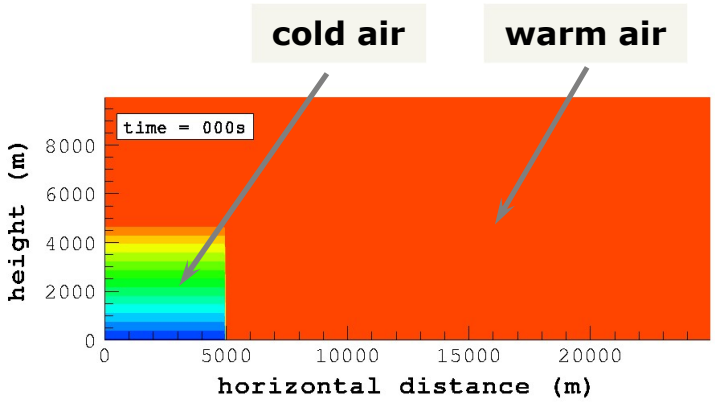

(1) Cold pool of air collapses due to negative buoyancy

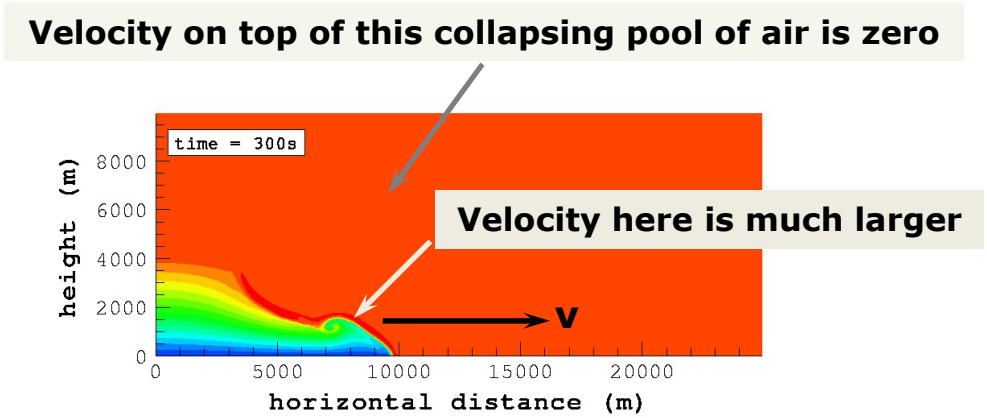

(2) As the pool collapses it builds up speed

Kelvin-Helmholtz Waves

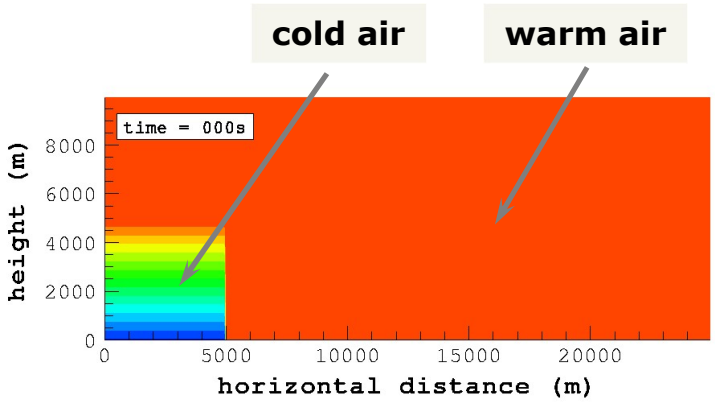

(1) Cold pool of air collapses due to negative buoyancy

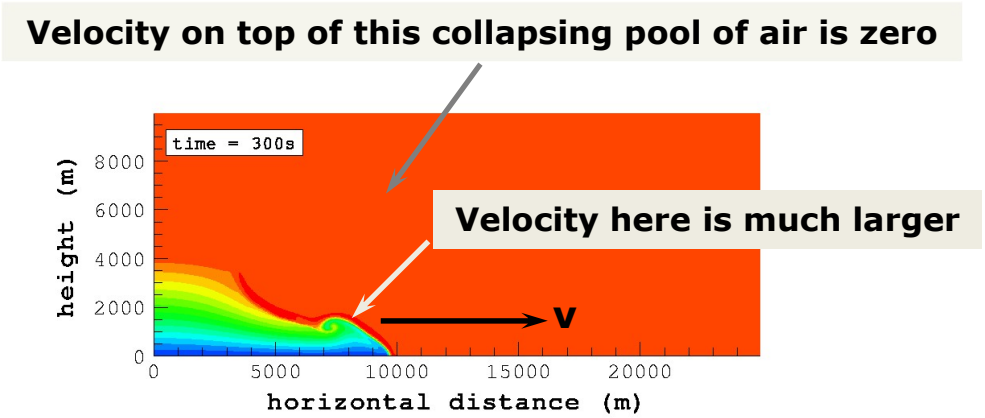

(2) As the pool collapses it builds up speed

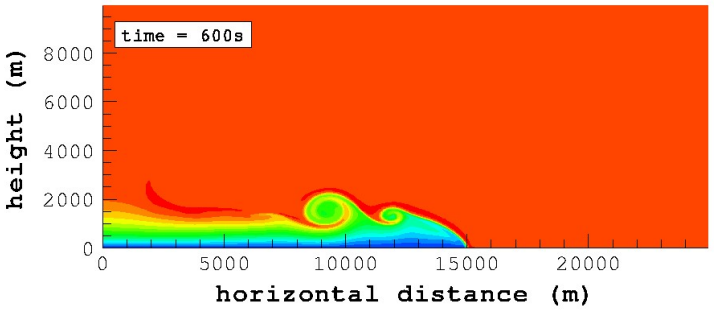

(3) Large amount of shear is generated because of difference in velocities of the top and bottom layers

Kelvin-Helmholtz Waves

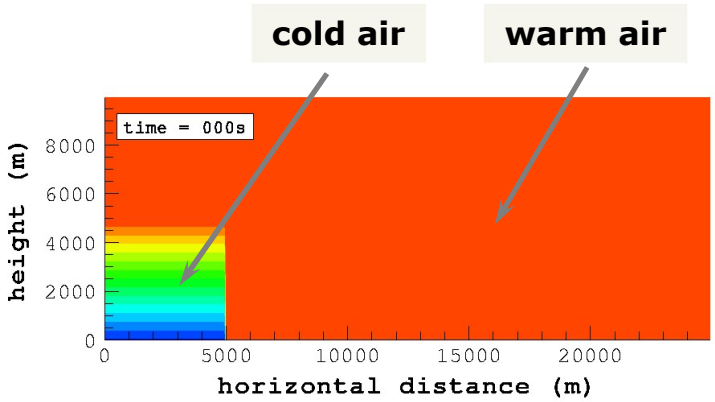

(1) Cold pool of air collapses due to negative buoyancy

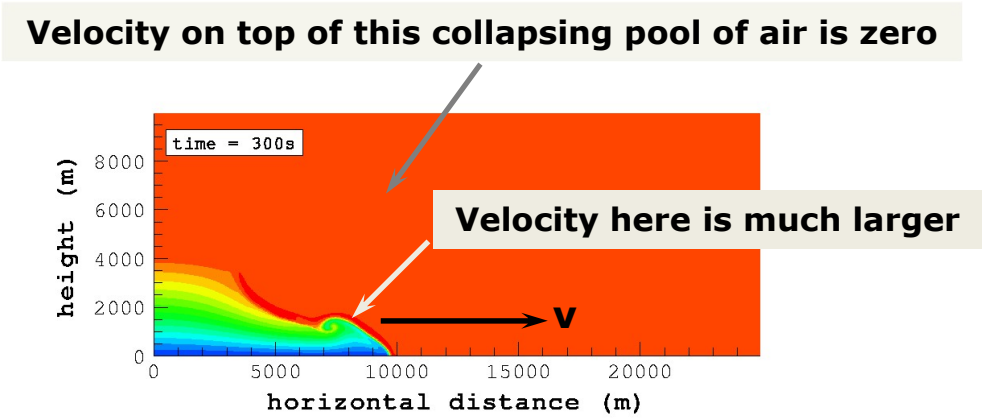

(2) As the pool collapses it builds up speed

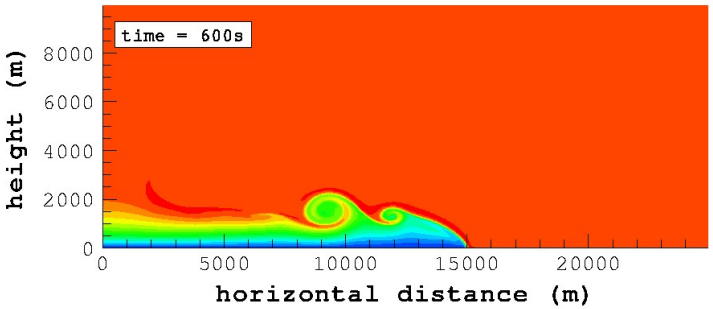

(3) Large amount of shear is generated because of difference in velocities of the top and bottom layers

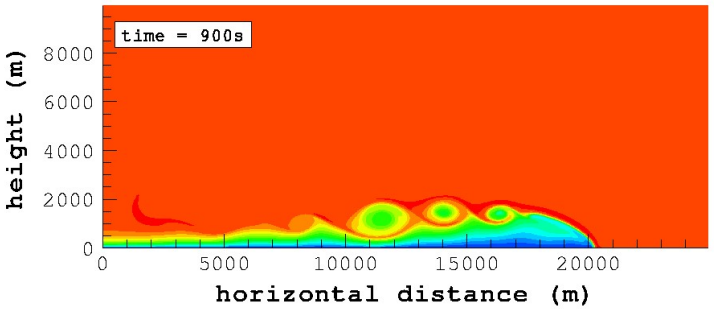

(4) The shear creates Kelvin-Helmholtz waves. Breaking of these waves generates turbulence.

Kelvin-Helmholtz Waves

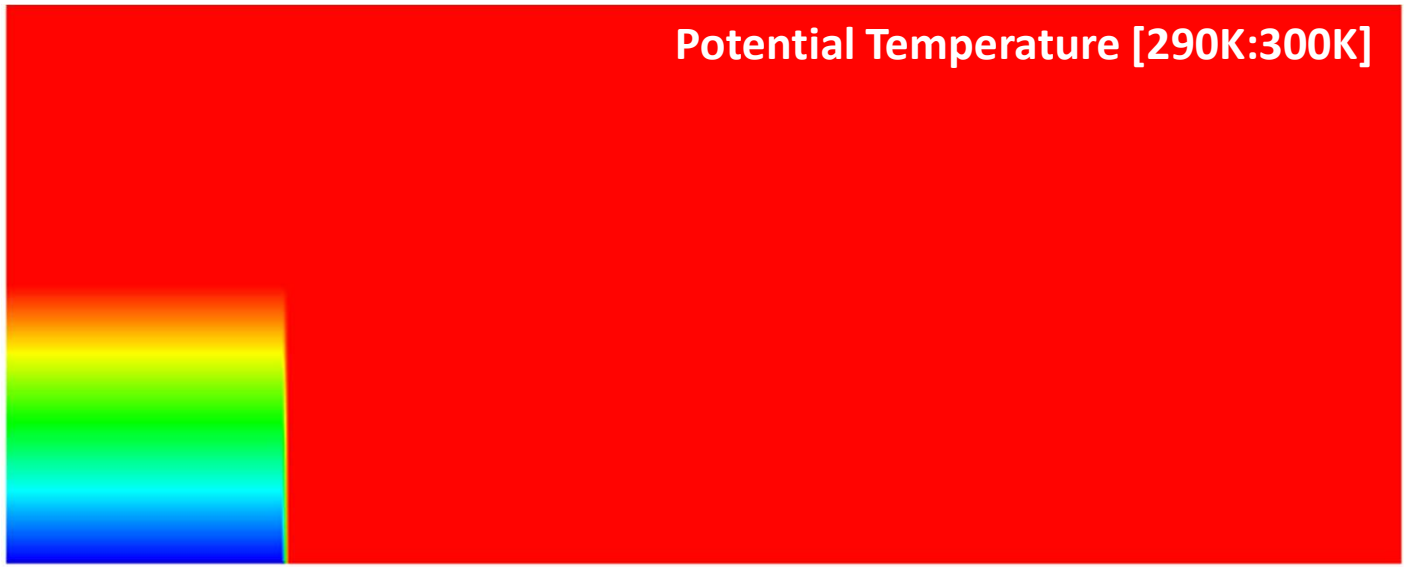

Convection in Neutral Atmosphere

$$(x, y, z) \in [0, 4000] \times [0, 4000] \times [0, 4000] \text{m}$$

Top and bottom boundaries: walls
Side boundaries: outflow

Atmosphere in hydrostatic balance

Neutral stability, $N = 0$

N is the Brunt-Väisälä frequency

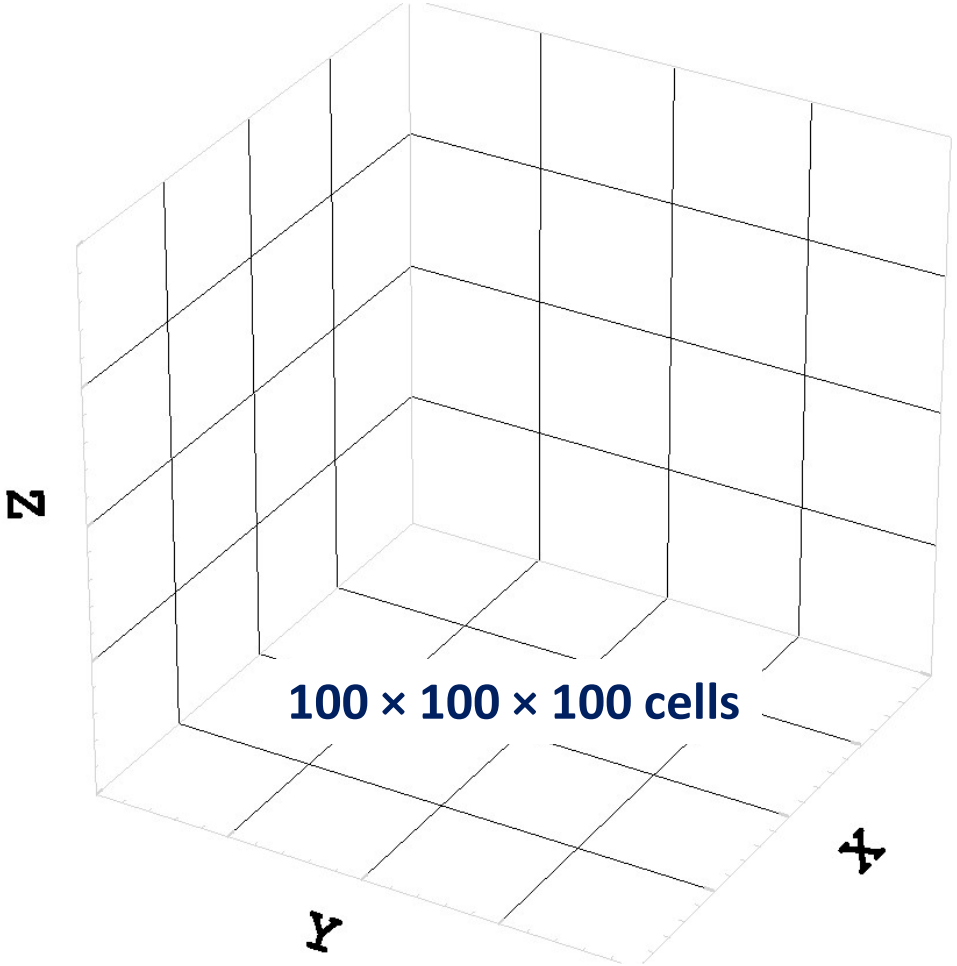

Convection in Neutral Atmosphere

A thermal perturbation is introduced

$$\theta(x,y,z) = \theta_0 + \Delta\theta\left(1.0 - \frac{L}{R}\right) \quad if \quad L \le R$$

$$L = \sqrt{(x-x_b)^2 + (y-y_b)^2 + (z-z_b)^2}$$

$$\Delta\theta = 2\mathrm{K}$$

$$[x_b, y_b, z_b] = [2000, 2000, 500]\mathrm{m}$$

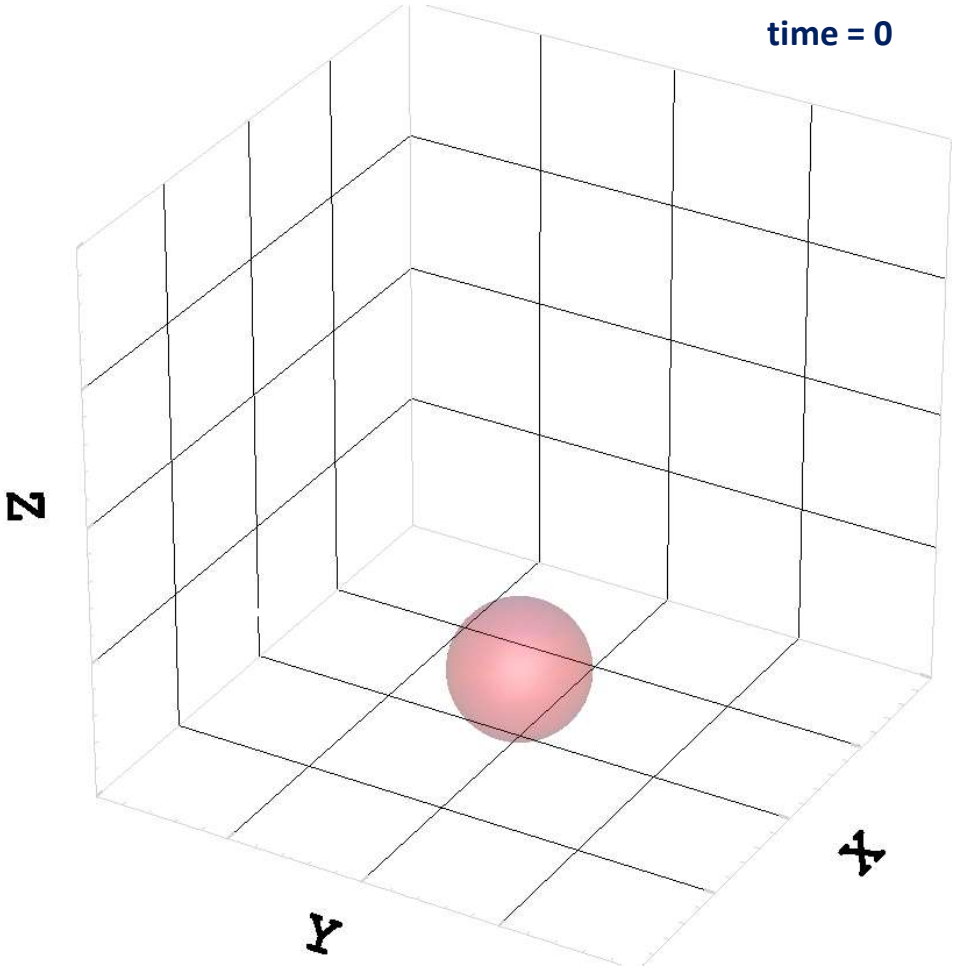

Convection in Neutral Atmosphere

A thermal perturbation is introduced

$$\theta(x,y,z) = \theta_0 + \Delta\theta\left(1.0 - \frac{L}{R}\right) \quad if \quad L \le R$$

$$L = \sqrt{(x-x_b)^2 + (y-y_b)^2 + (z-z_b)^2}$$

$$\Delta\theta = 2\mathrm{K}$$

$$[x_b, y_b, z_b] = [2000, 2000, 500]\mathrm{m}$$

$$yz - plane \ \ (x = 2000\mathrm{m})$$

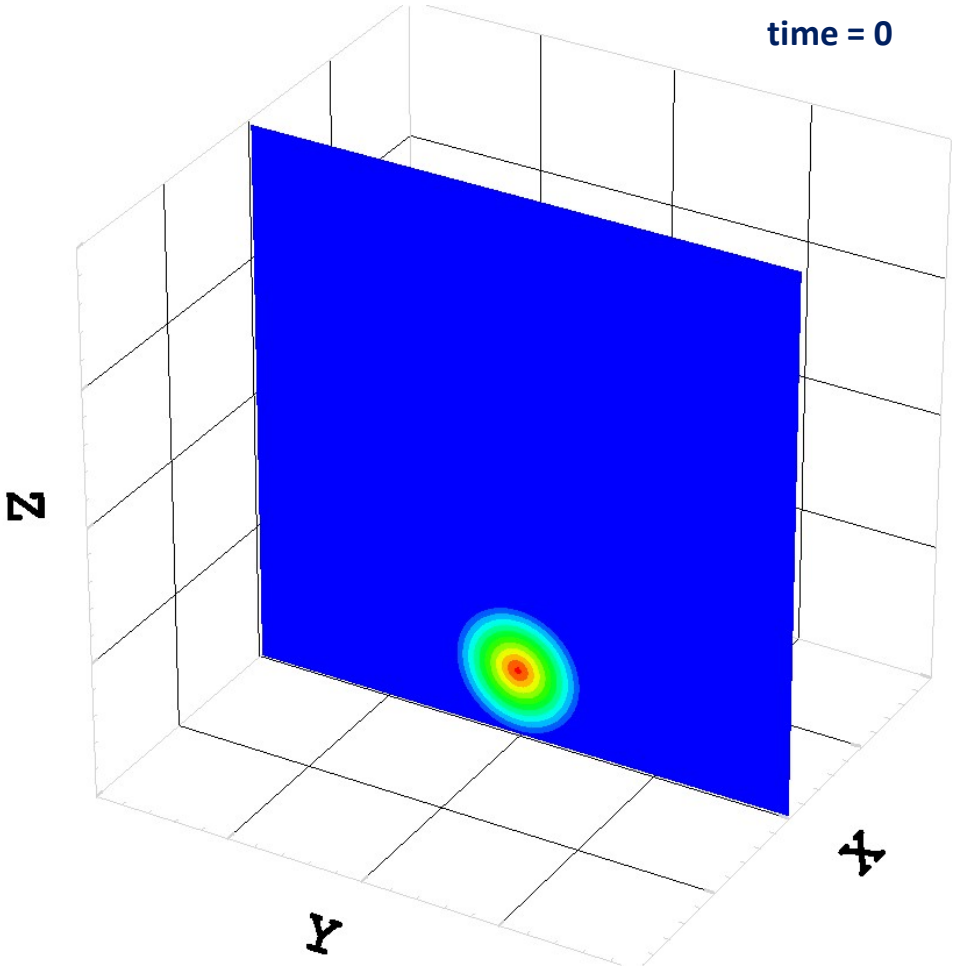

Convection in Neutral Atmosphere

$$\left[p'_{\min}, p'_{\max}\right] = \left[-20, 4\right] \mathrm{Pa}$$

Introduction of the perturbation generates an initial shock wave that quickly propagates out of the domain

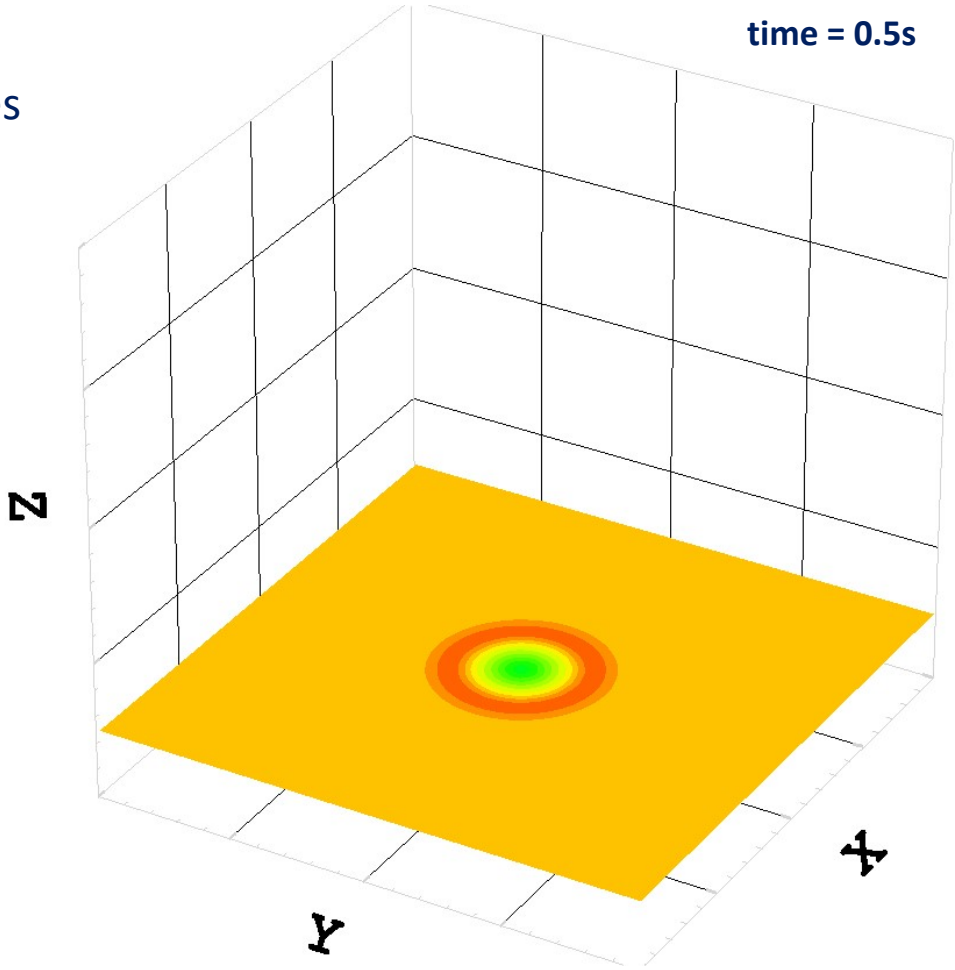

$$xy - plane \ \left(z = 500\mathrm{m}\right)$$

Convection in Neutral Atmosphere

$$\left[p'_{\min}, p'_{\max}\right] = \left[-20, 4\right] \mathrm{Pa}$$

Introduction of the perturbation generates an initial shock wave that quickly propagates out of the domain

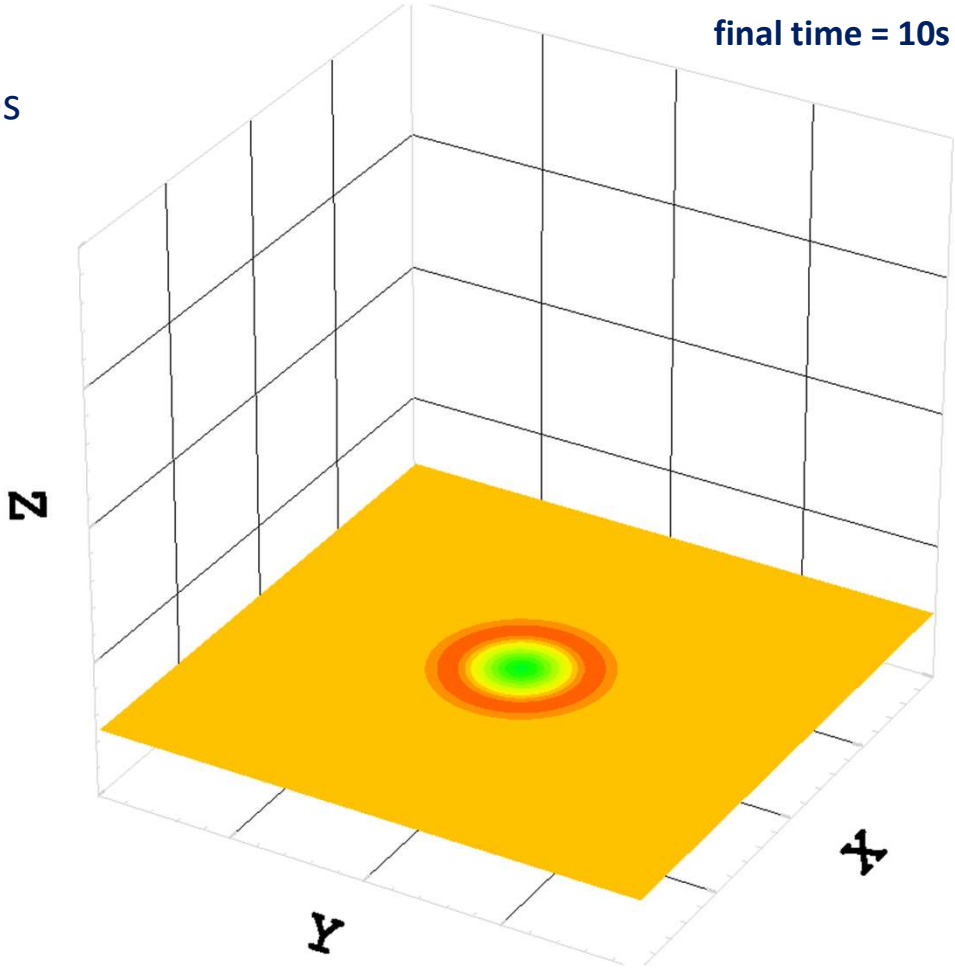

$$xy - plane \ \left(z = 500\mathrm{m}\right)$$

Convection in Neutral Atmosphere

$$\left[w_{\min}, w_{\max}\right] = \left[-0.01, 0.35\right] \mathrm{ms}^{-1}$$

Flow field starts to develop inside and around bubble core

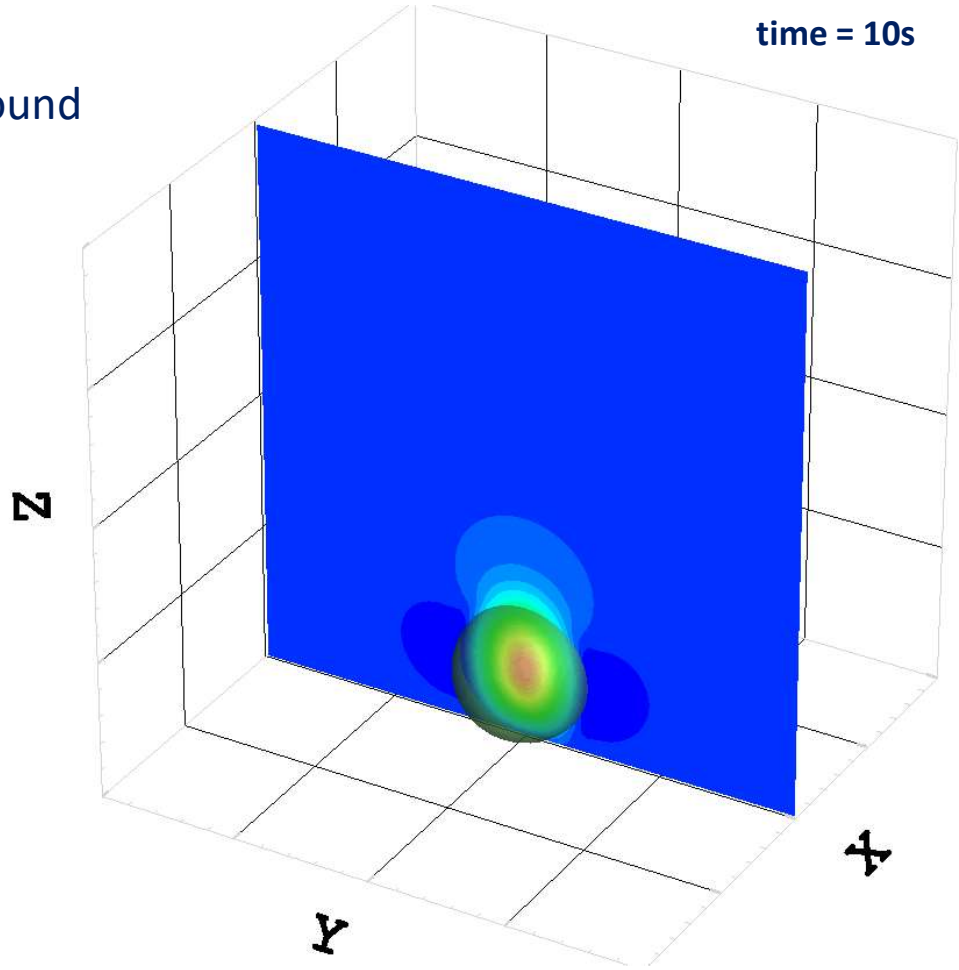

$$yz - plane \ \left(x = 2000\mathrm{m}\right)$$

Convection in Neutral Atmosphere

potential temperature isosurface = 0.08K

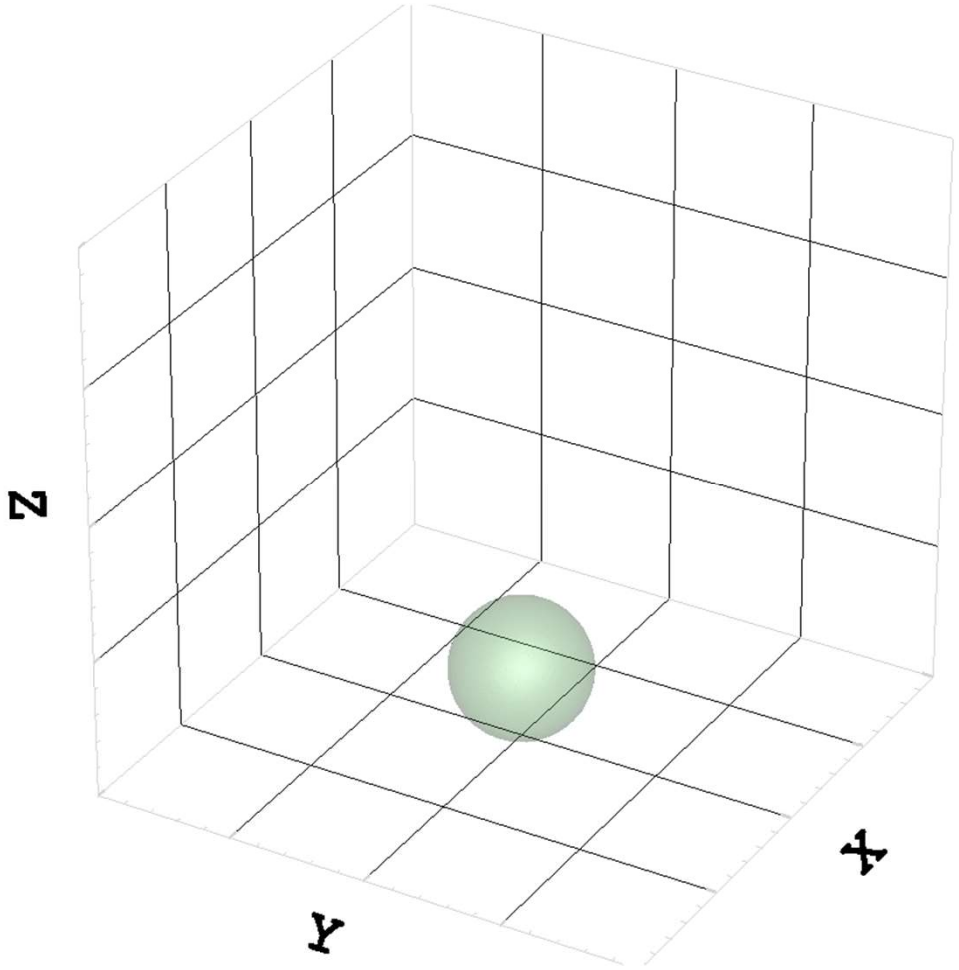

Ahmad (AIAA-2018-3498)

Convection in Neutral Atmosphere

potential temperature isosurface = 0.08K

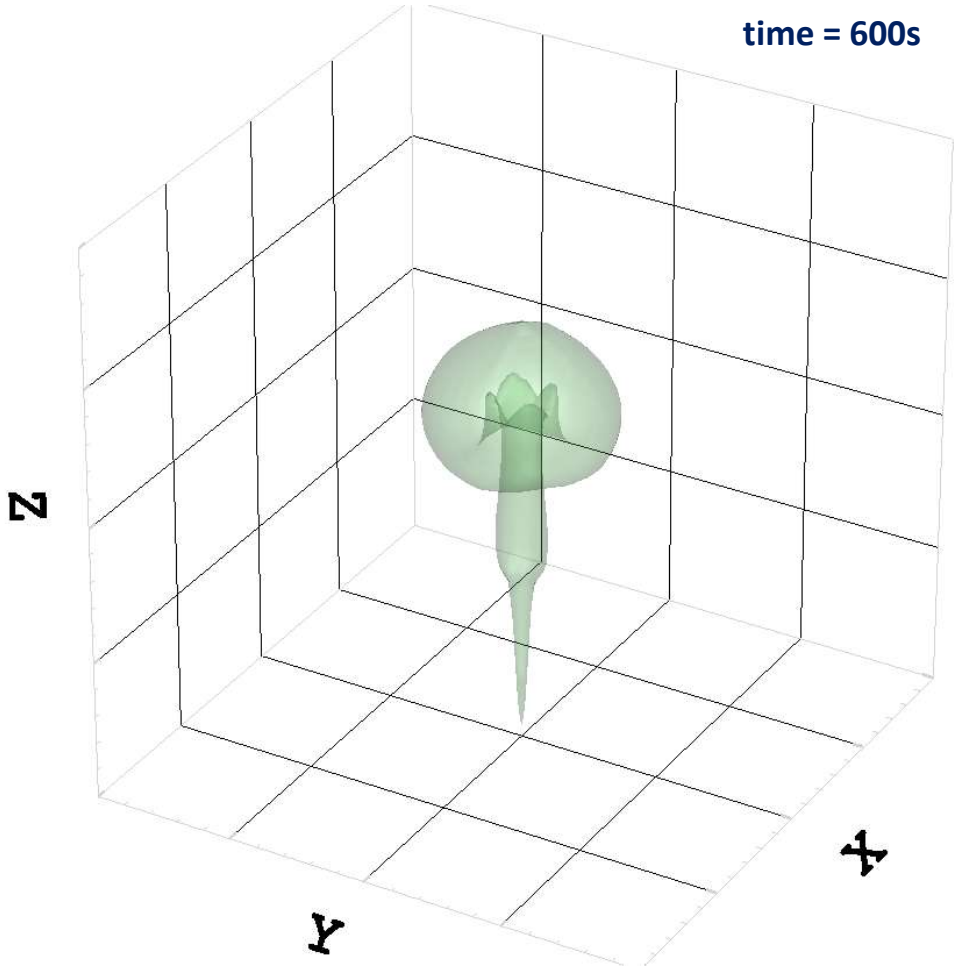

Ahmad (AIAA-2018-3498)

Convection in Neutral Atmosphere

potential temperature isosurface = 0.08K

w^+ isosurface = 6m/s

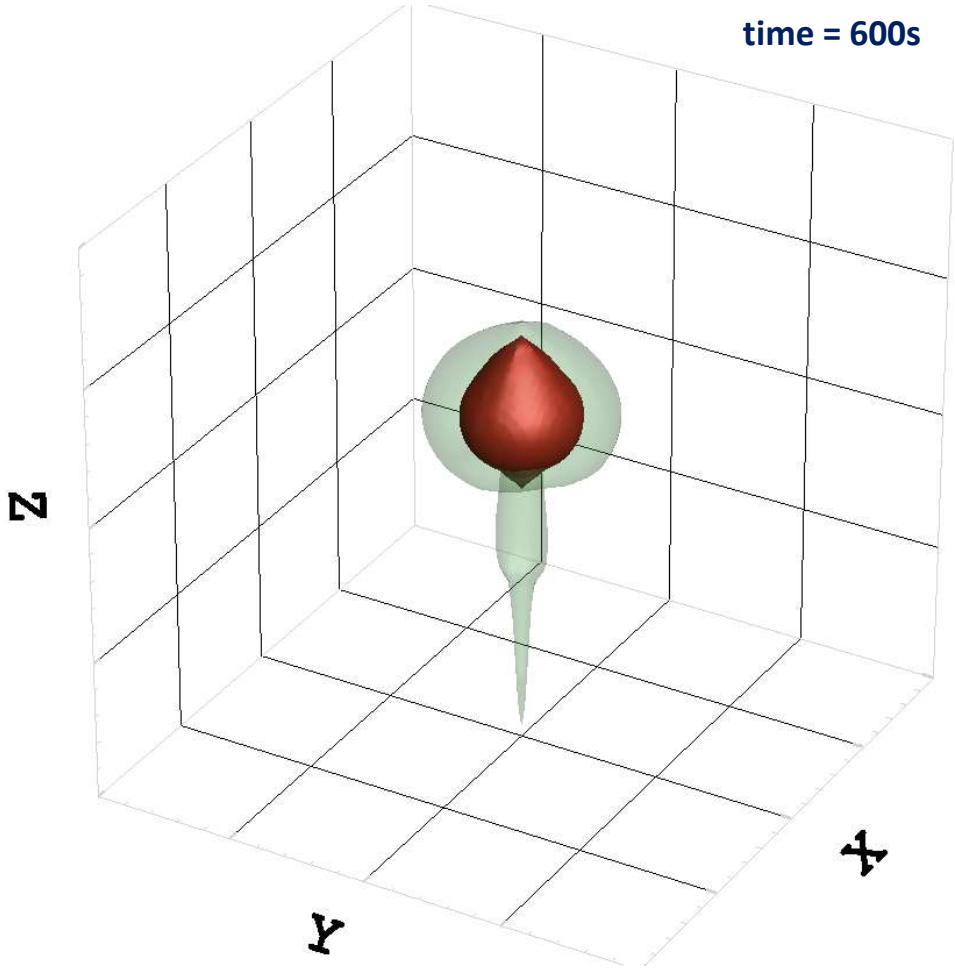

Ahmad (AIAA-2018-3498)

Convection in Neutral Atmosphere

potential temperature isosurface = 0.08K

w^+ isosurface = 6m/s

w^- isosurface = -0.5m/s

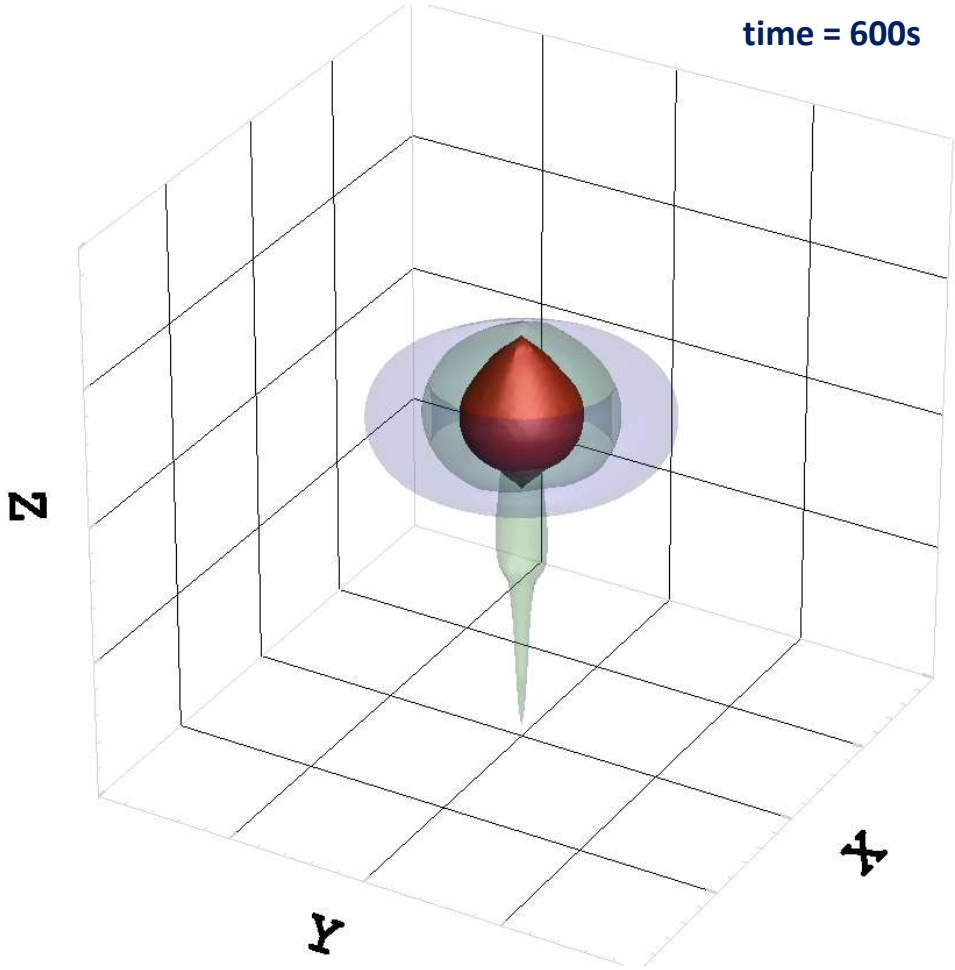

Ahmad (AIAA-2018-3498)

Convection in Neutral Atmosphere

potential temperature isosurface = 0.08K

w^+ isosurface = 6m/s

w^- isosurface = -0.5m/s

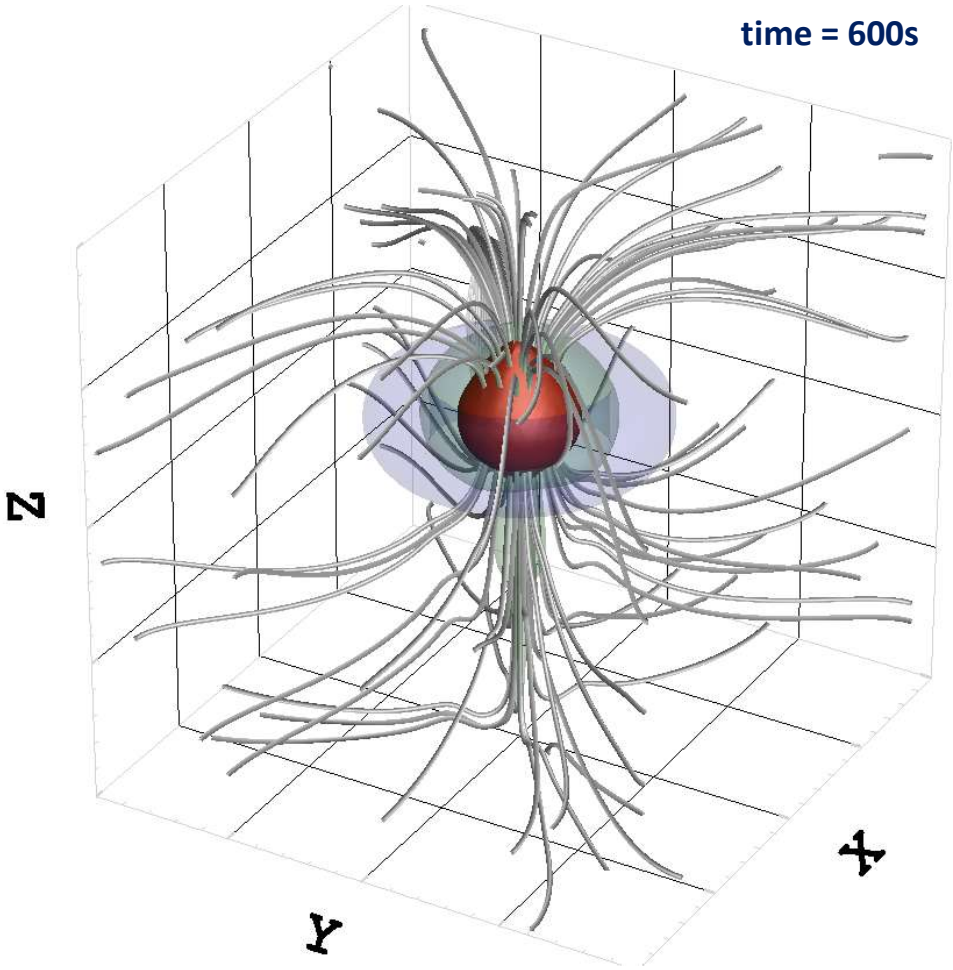

Ahmad (AIAA-2018-3498)

Mesoscale Modeling (Wake Turbulence)

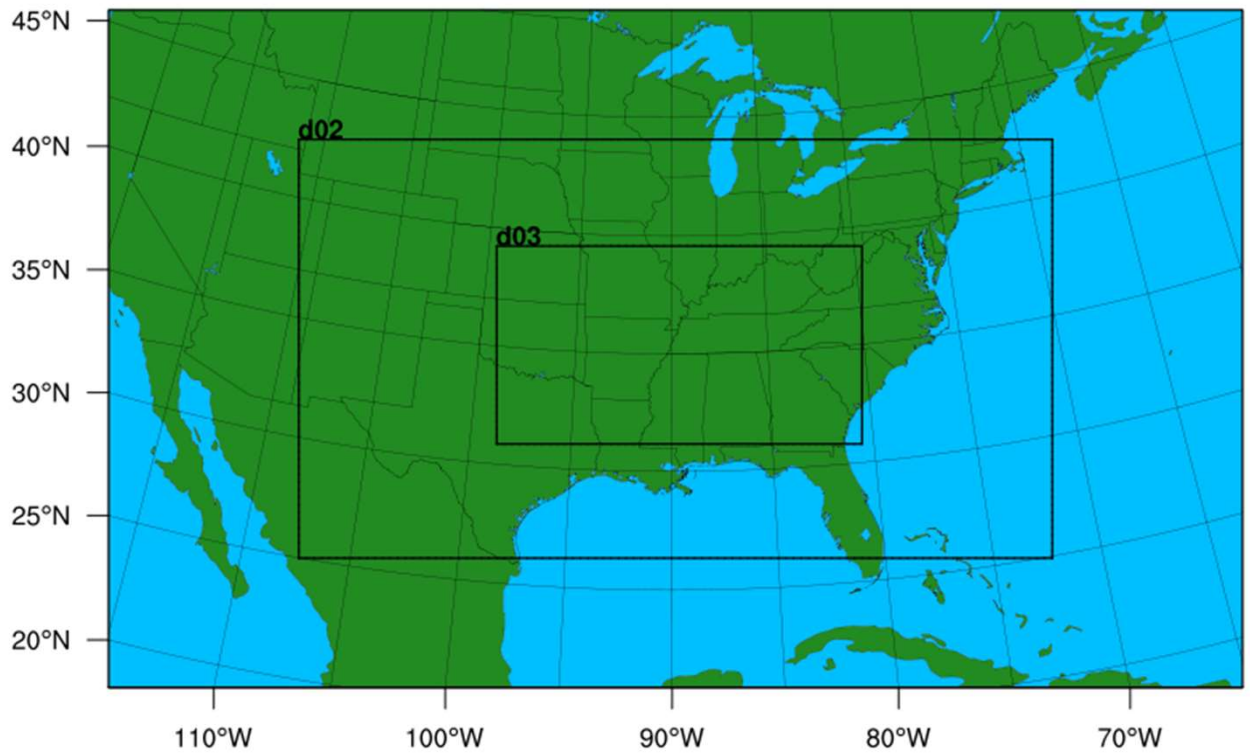

domain	latmin	latmax	lonmin	lonmax	Δx
d01	18.08°N	49.14°N	124.06°W	55.93°W	36km
d02	24.84°N	43.86°N	111.54°W	68.45°W	12km
d03	30.66°N	39.29°N	99.74°W	79.97°W	4km

Ahmad and Proctor (AIAA 2012-0429)

Mesoscale Modeling (Wake Turbulence)

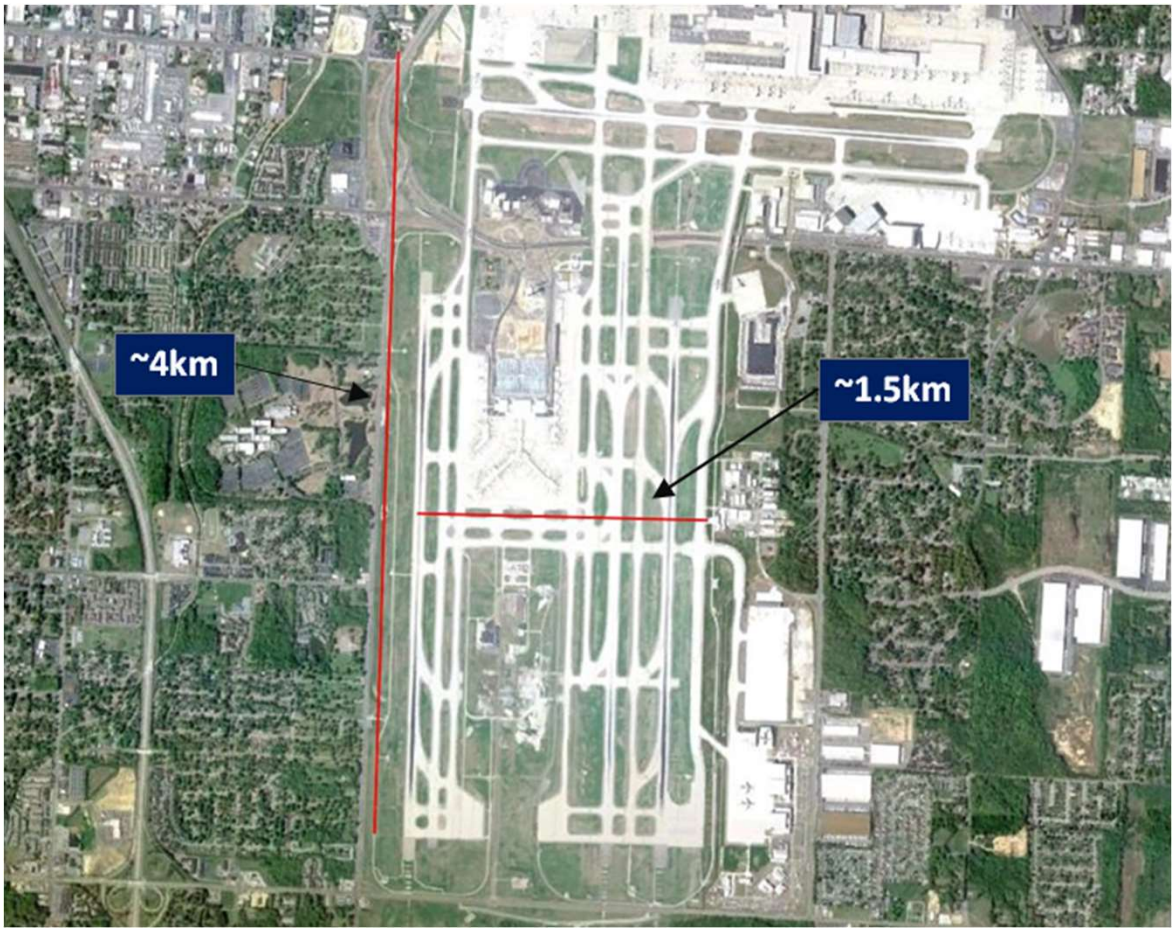

Image generated using Google Earth

Memphis International Airport

Uniform resolution (Δz = 40m) below 800m

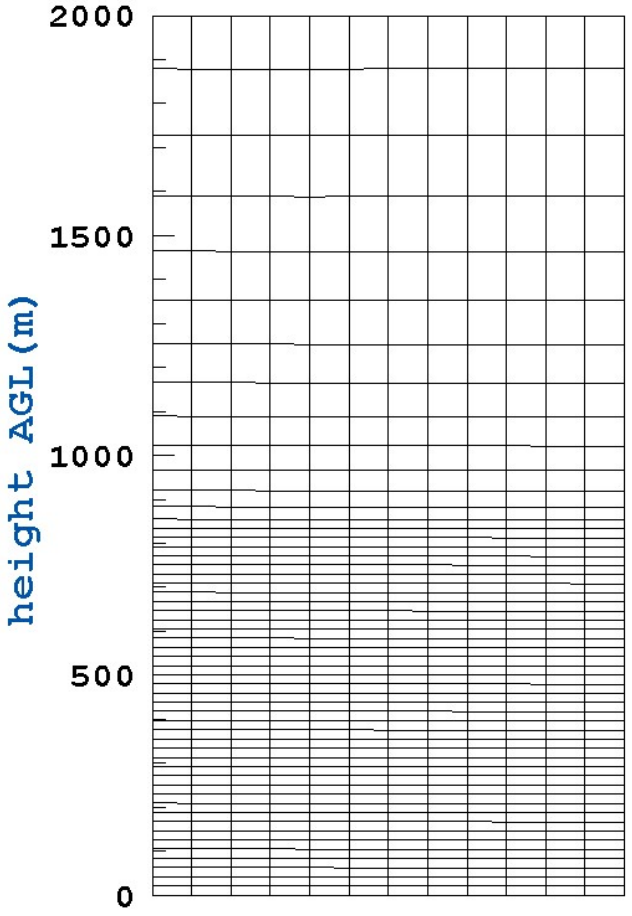

WRF Vertical Mesh

Ahmad and Proctor (AIAA 2012-0429)

Mesoscale Modeling (Wake Turbulence)

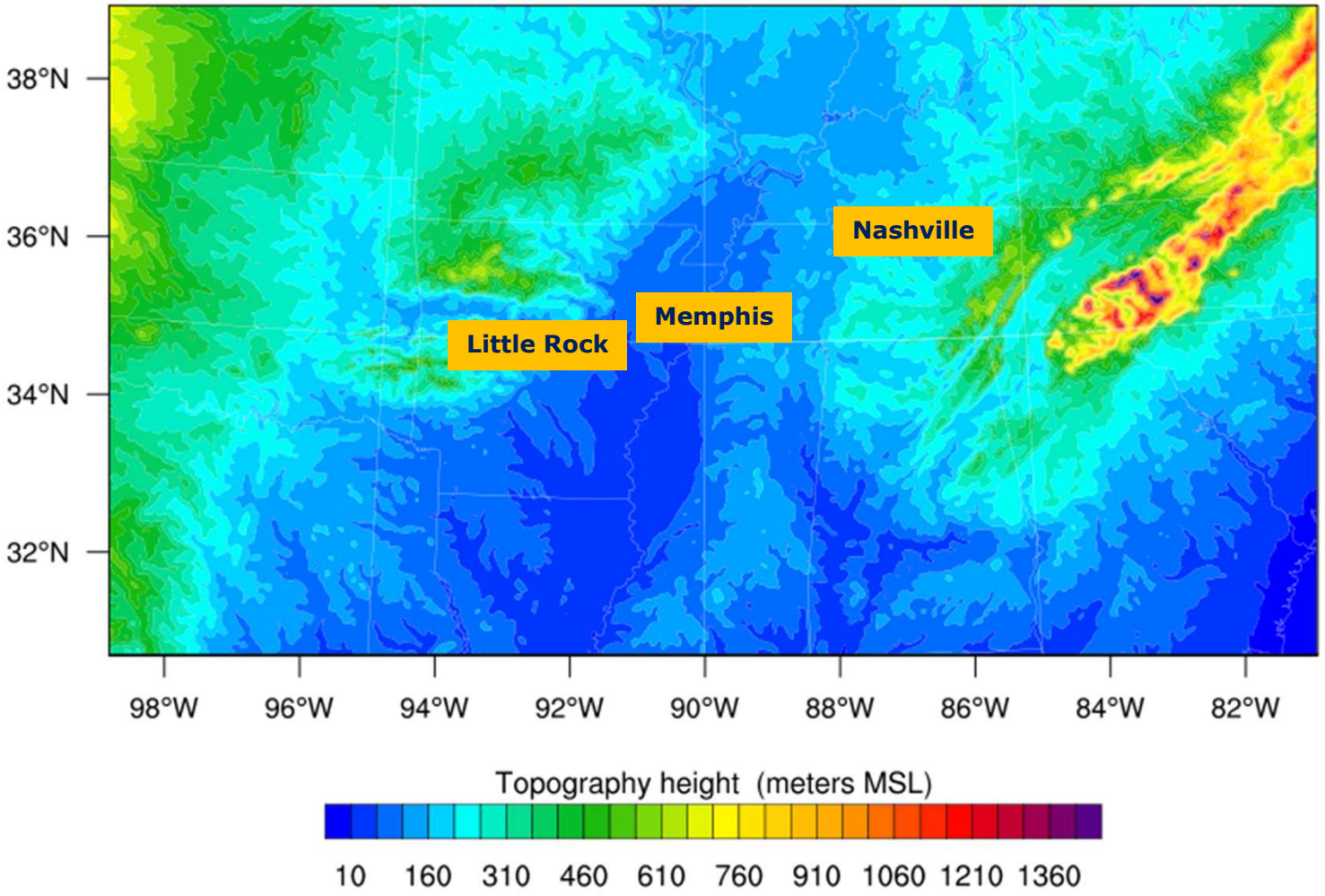

WRF innermost 4km resolution nest

Ahmad and Proctor (AIAA 2012-0429)

Mesoscale Modeling (Wake Turbulence)

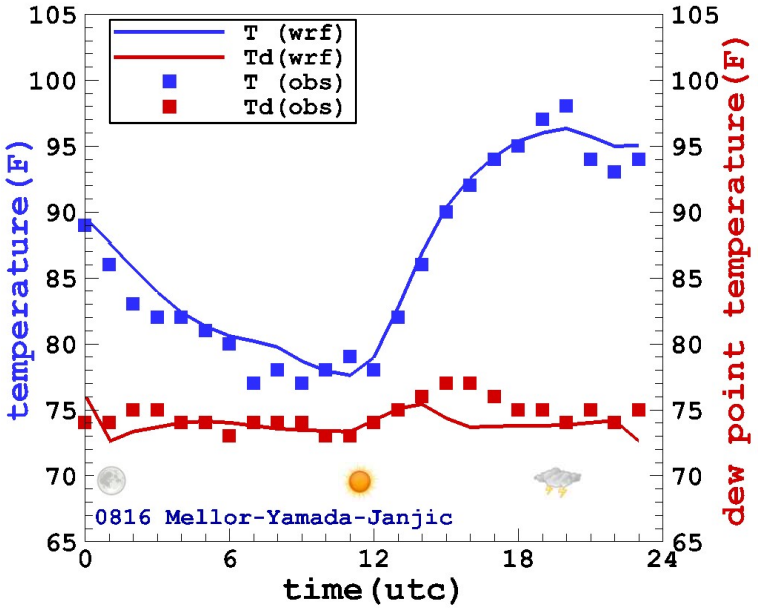

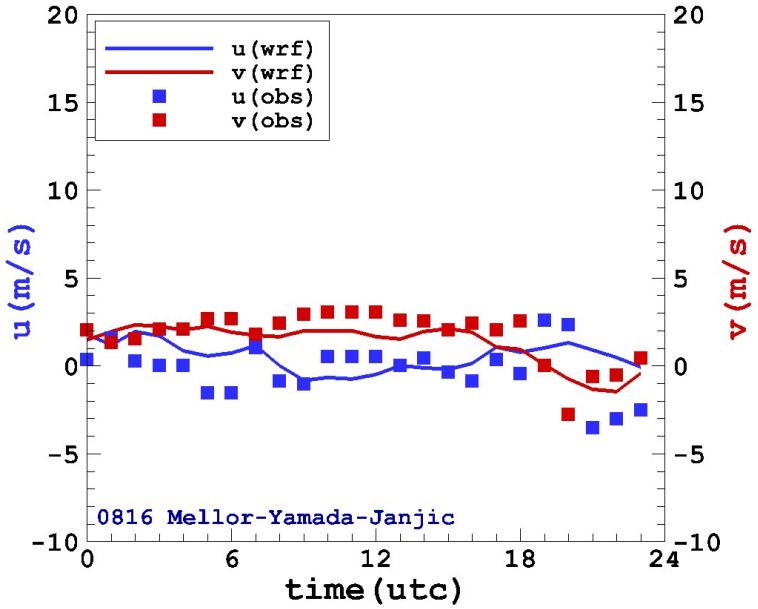

Turbulence Scheme	T(°F)			T_d(°F)			u(m/s)			v(m/s)		
	rmse	mae	bias	rmse	mae	bias	rmse	mae	bias	rmse	mae	bias
MYJ	1.53	1.25	0.96	1.28	0.99	-0.58	1.52	1.19	0.52	0.92	0.71	-0.31
BL	1.40	1.15	0.81	1.37	1.02	-0.66	1.68	1.32	0.74	0.88	0.74	-0.43

Ahmad and Proctor (AIAA 2012-0429)

Mesoscale Modeling (Wake Turbulence)

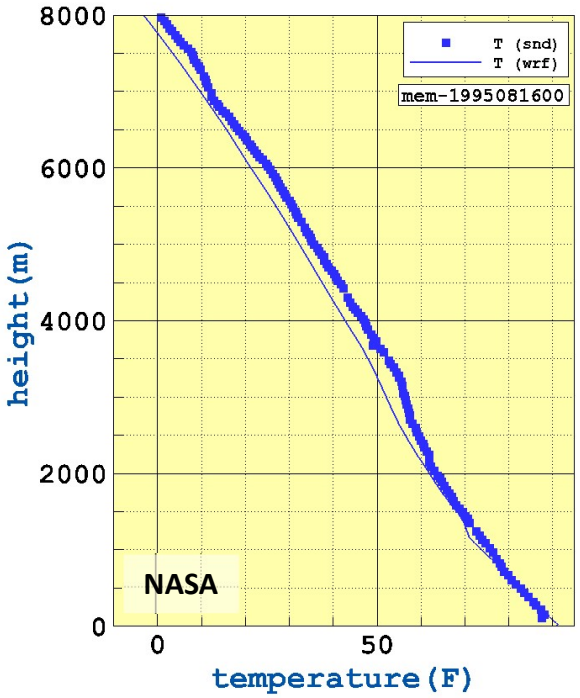

Memphis, TN

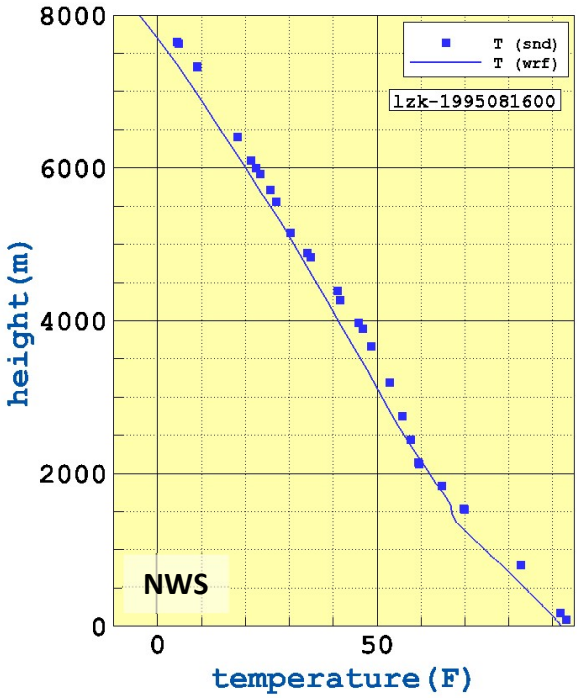

Little Rock, AR

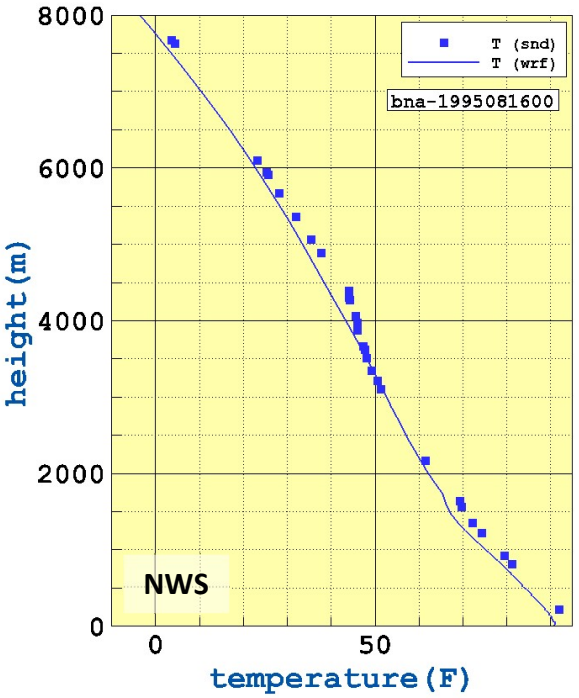

Nashville, TN

Ahmad and Proctor (AIAA 2012-0429)

Mesoscale Modeling (Wake Turbulence)

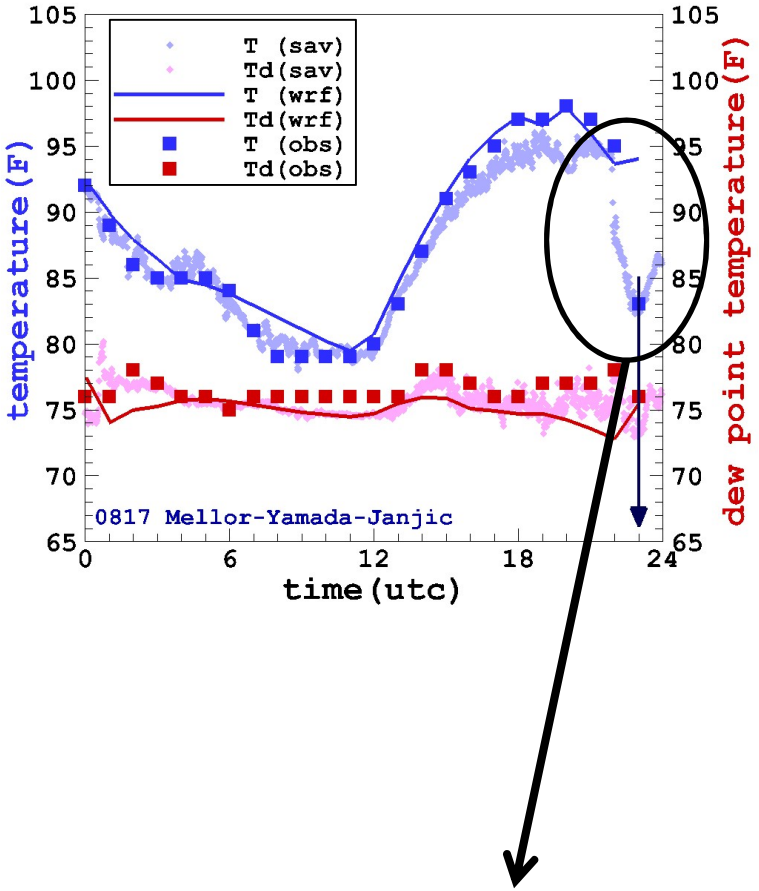

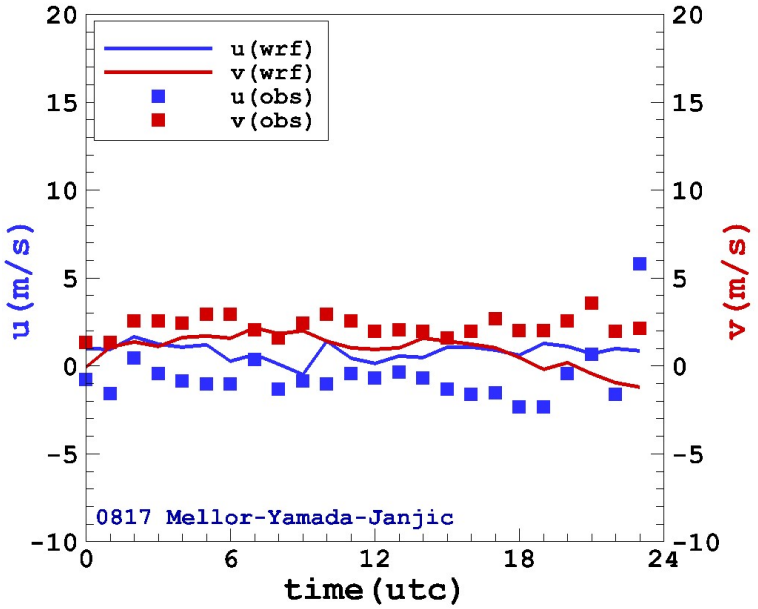

Large temperature drop in observations missed by simulation

Ahmad and Proctor (AIAA 2012-0429)

Mesoscale Modeling (Wake Turbulence)

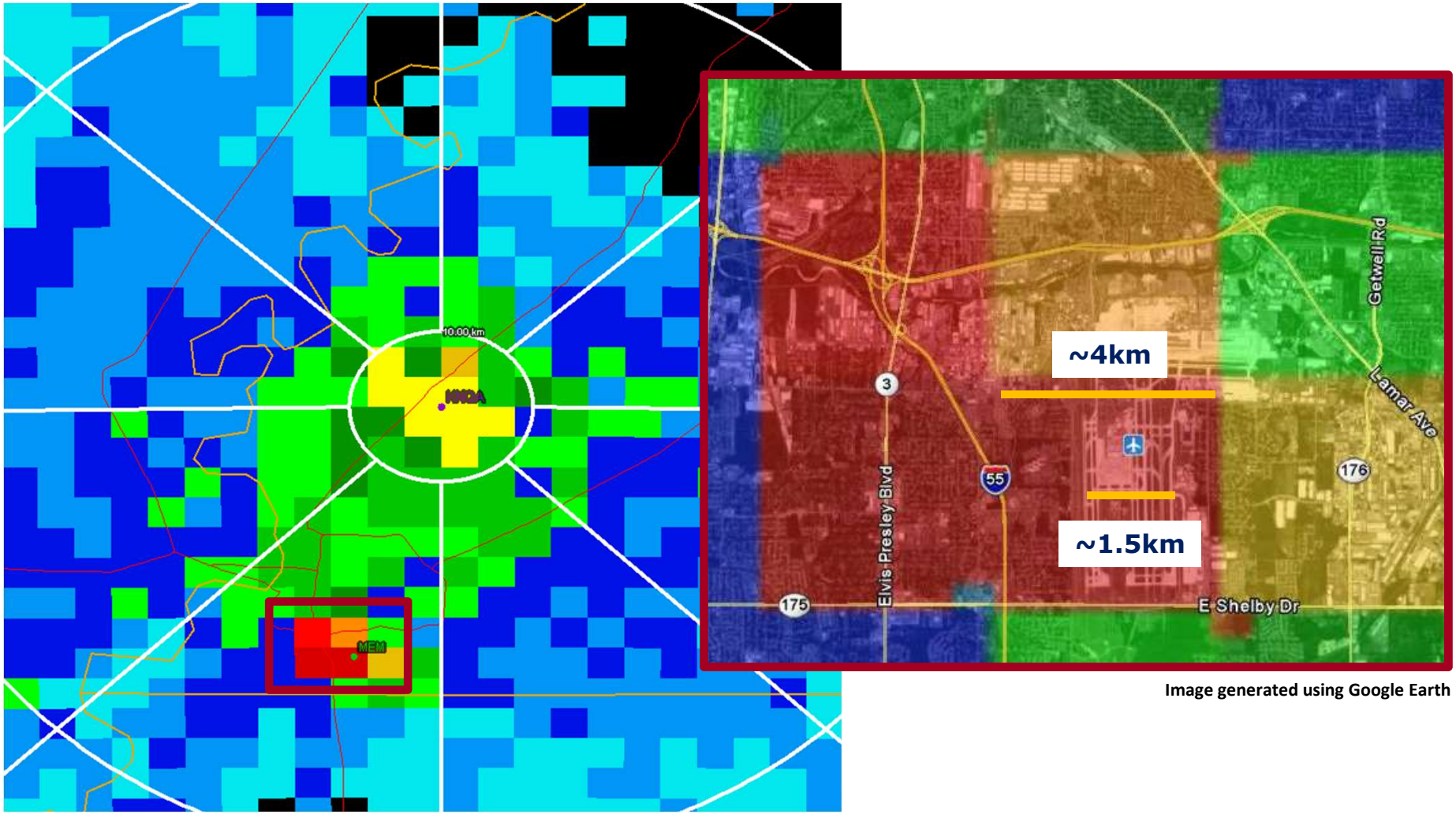

Image generated using Google Earth

Memphis NEXRAD (21:36:57UTC)

Ahmad and Proctor (AIAA 2012-0429)

Mesoscale Modeling (Wake Turbulence)

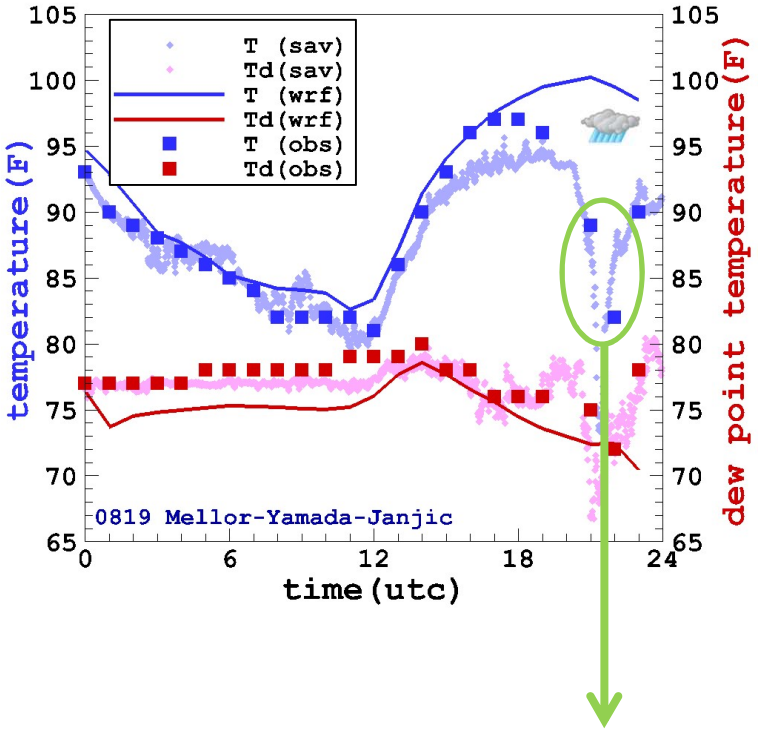

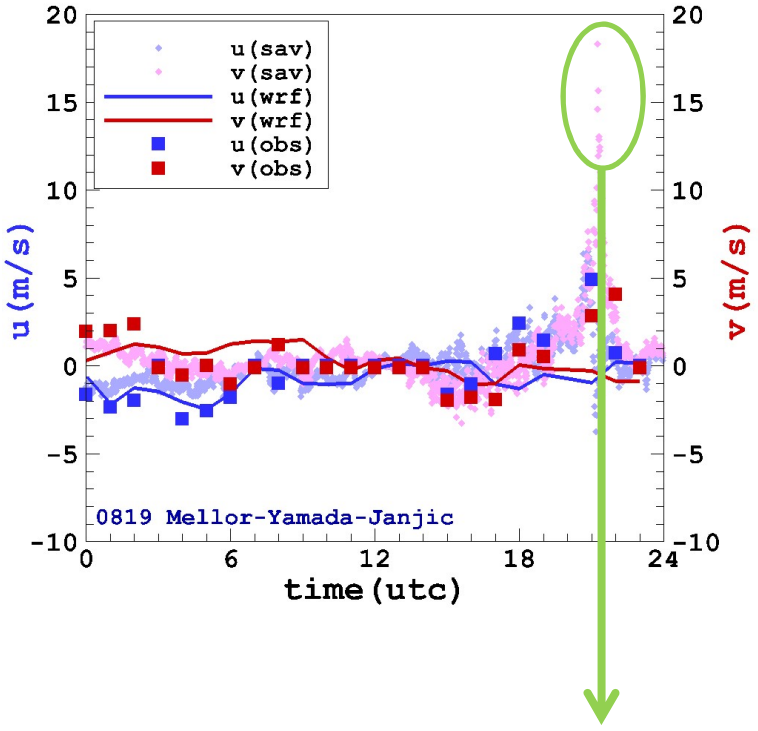

Localized subgrid scale convection

Passage of gust front

The discrepancies on this date were also due to a subgrid scale convective activity and the associated gust front which were missed by the model

Ahmad and Proctor (AIAA 2012-0429)

Mesoscale Modeling (Wake Turbulence)

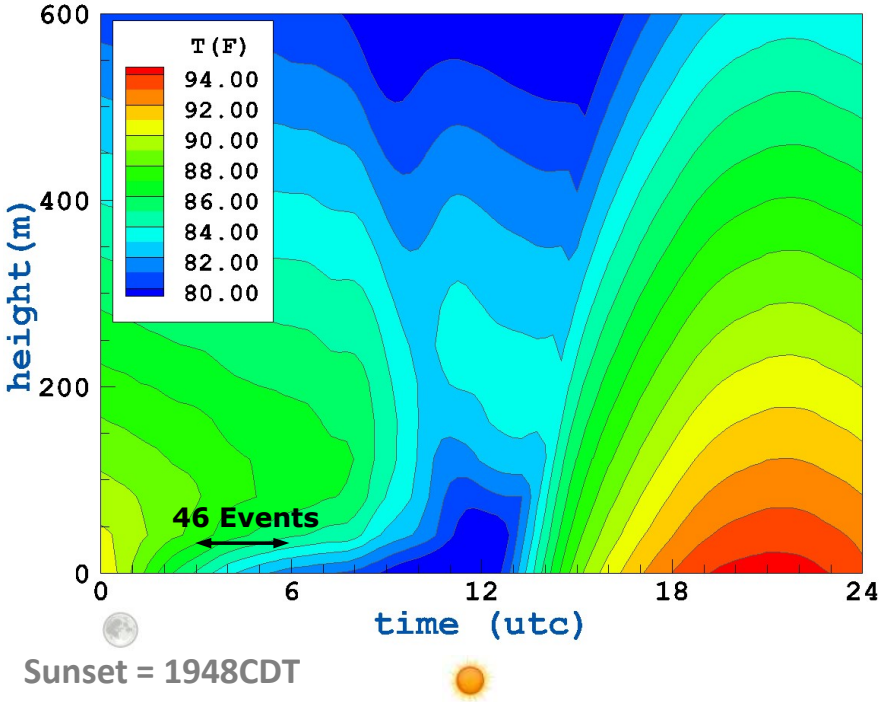

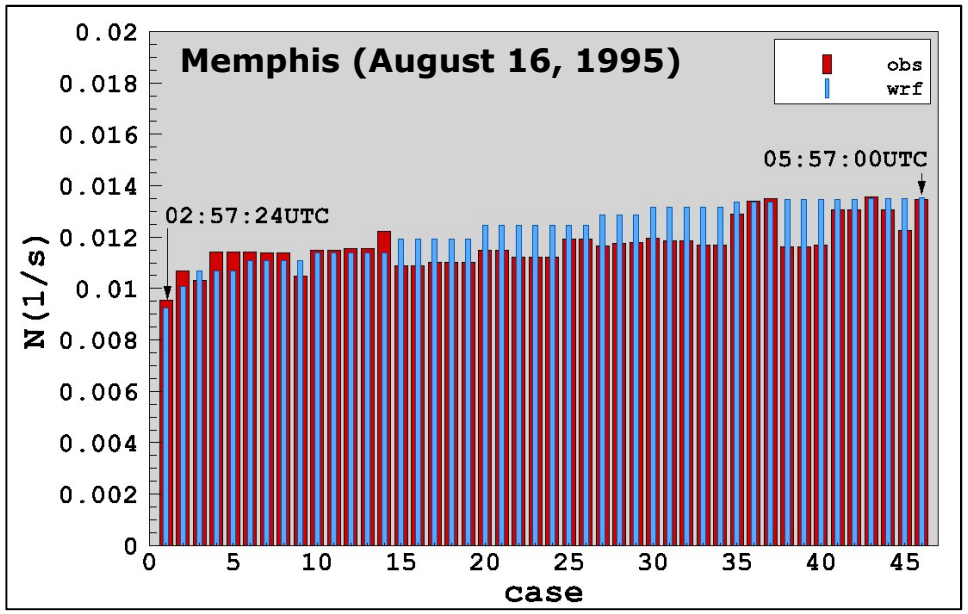

46 Events on 1995-08-16 – All in OGE
Total Events in Memphis Dataset=305

Strongest stable boundary layer for the entire data collection period

Ahmad and Proctor (AIAA 2012-0429)

Mesoscale Modeling (A380 Flight Tests)

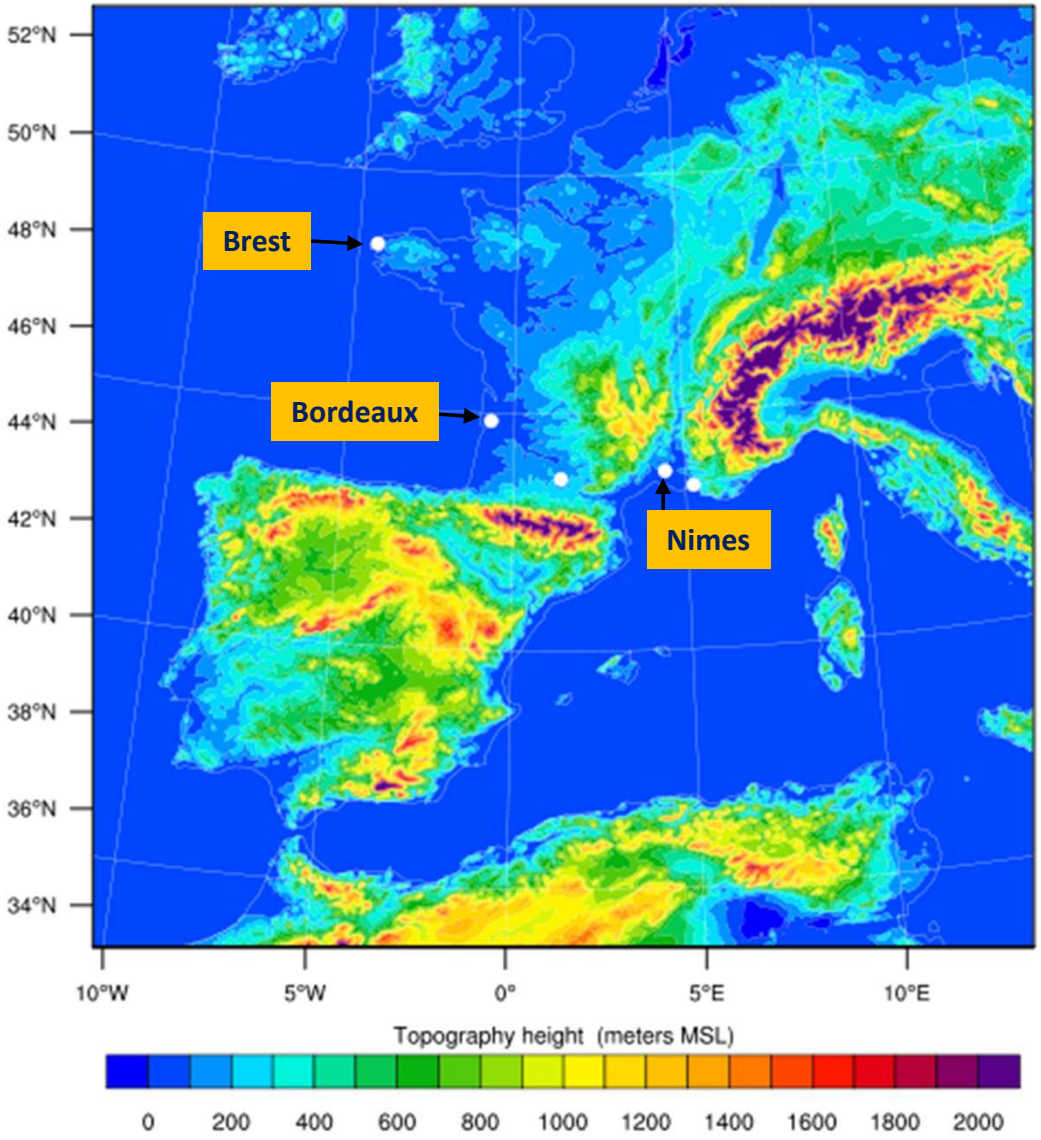

WRF Simulation Domain
4km horizontal resolution

Simulations were conducted to analyze the meteorological conditions during Airbus A380 flight tests

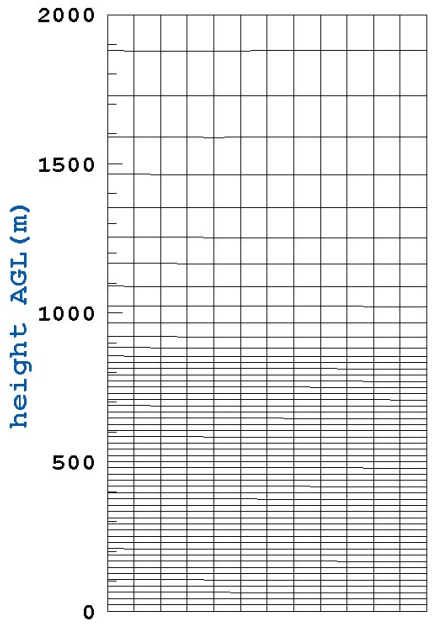

WRF Vertical Mesh
(only first 2km are shown)

Ahmad (FAA 2012)

Severe Hazard Events

- Events which are not frequent but can cause serious disruptions
  - Forest fires
  - Volcanic eruptions
  - Accidents

Release of HAZMAT (July 2007)

Train carrying toxic phosphorus compounds caught fire and derailed on July 17th, 2007 near Lviv, Ukraine. Affected area around 900 sq. km encompassing nearly 14 villages.

Eruptions of Eyjafjallajökull (2010)

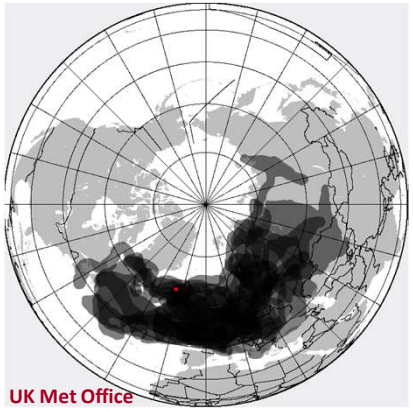

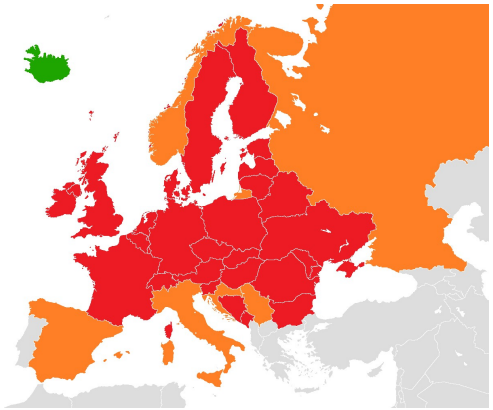

Airspace completely closed to IFR traffic (red) and partially closed To IFR traffic (orange) on April 18th, 2010
https://en.wikipedia.org/wiki/Air_travel_disruption_after_the_2010_Eyjafjallaj%C3%B6kull_eruption

California Forest Fires (October 2007)

Santa Ana Winds (Vientos de Satán)

- The hot and dry character of the Santa Ana is due to the compression of air as it descends the leeward slopes of the mountains
- Episodes of Santa Ana winds occur between September and March in response to high pressure system over the Great Basin (Nevada and parts of Utah)
- In the Northern Hemisphere, the winds flow clockwise out of a high pressure system
- The air over the dry and arid Great Basin is accelerated into the Los Angeles Basin

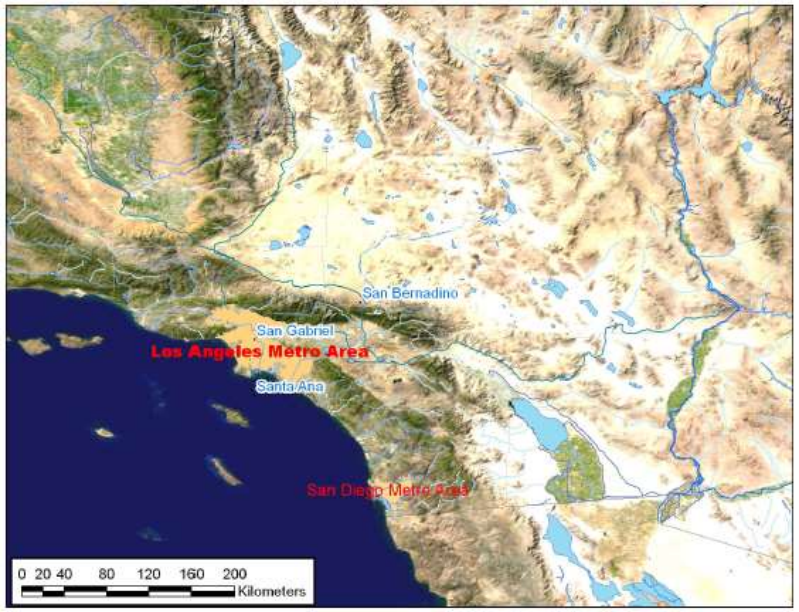

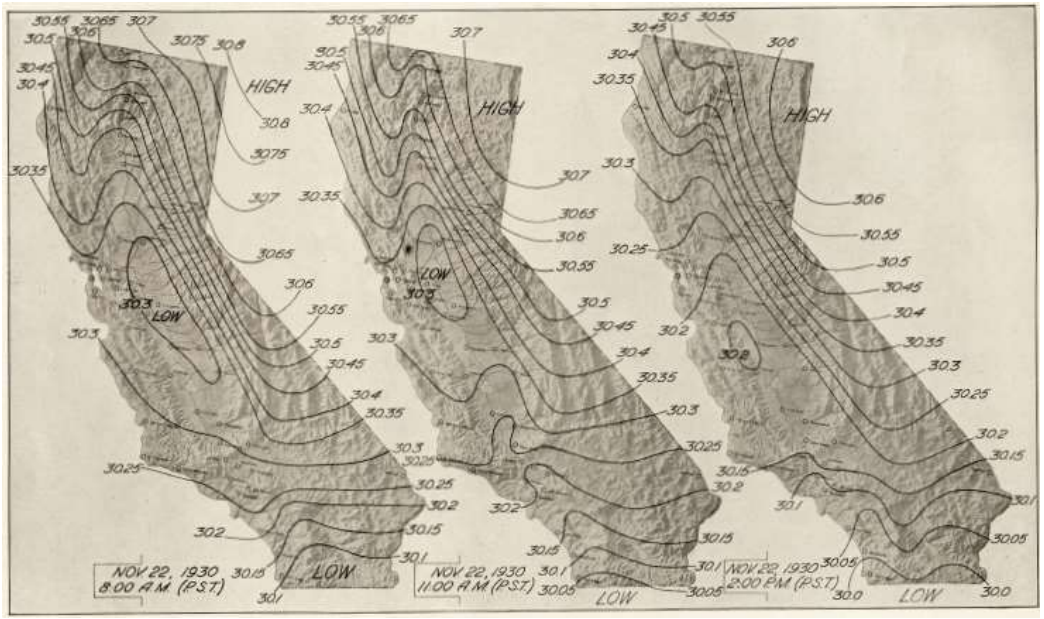

French (Monthly Weather Rev. 1931)

Santa Ana Winds (October 2007)

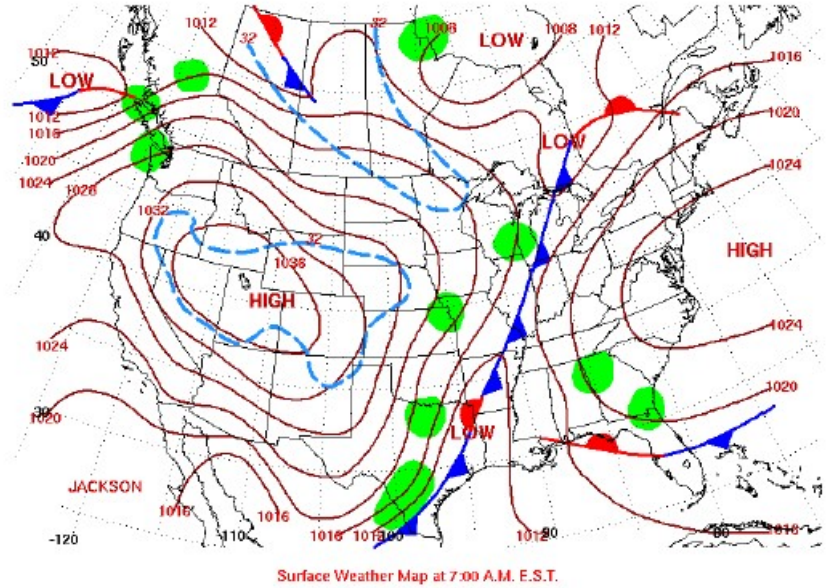

Classic conditions for the onset of a Santa Ana episode existed during the last week of October 2007.

A High Pressure System was in place over the Great Basin area resulting in a relatively large pressure gradient extending westward to Southern California

PI ≤ -4
Extreme
Drought

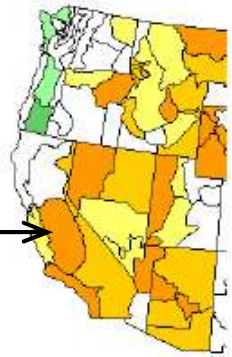

Palmer Index

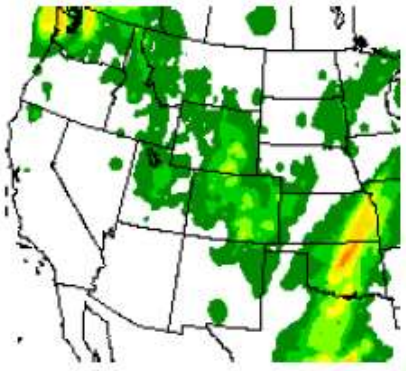

24hr Cumulative Precipitation

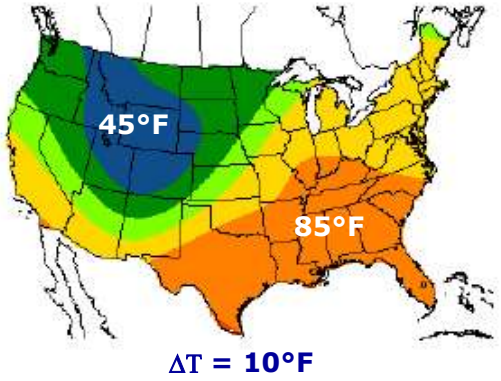

Maximum Surface Temperature

Source:
NCEP

Santa Ana Winds (October 2007)

- Loss of fourteen lives attributed to these fires
- Thousands of home destroyed
- Largest mass evacuation in state's history (650,000 by October 27th, 2007)

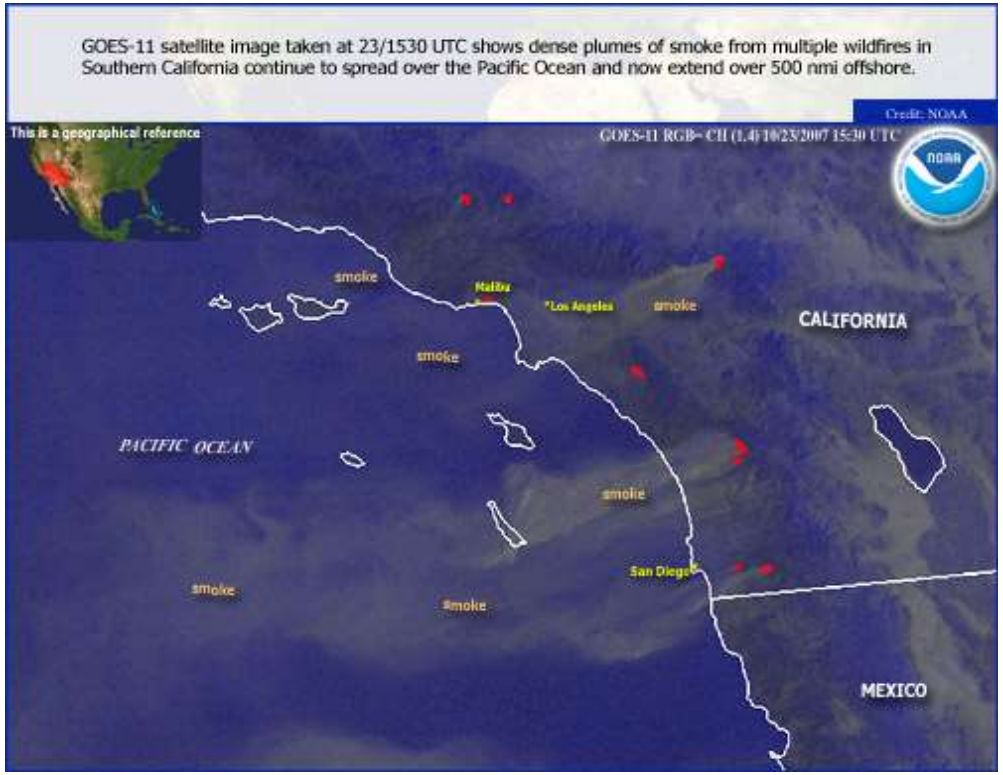

Patricia Rey (EPA) estimated that the fires dumped an equivalent of greenhouse emissions of 440,000 cars over a period of one year. Source: BBC

North East of San Diego
Damage in San Diego County estimated at $1bn

Santa Ana Winds (October 2007)

- Domain: [130°W:95°W] x [25°N:45°N]
- Mesh resolution [3km:60km]
- Initialized at 2007-10-23 (12Z) using GFS data - All available surface and upper air observations used for ICs and BCs
- A stretched grid with 35 levels was specified in the vertical. Height of level 1 was 30m AGL. A stretch ratio of 1.15 was used. Model top at approximately 21 km.
- Final simulation time = for 72hrs

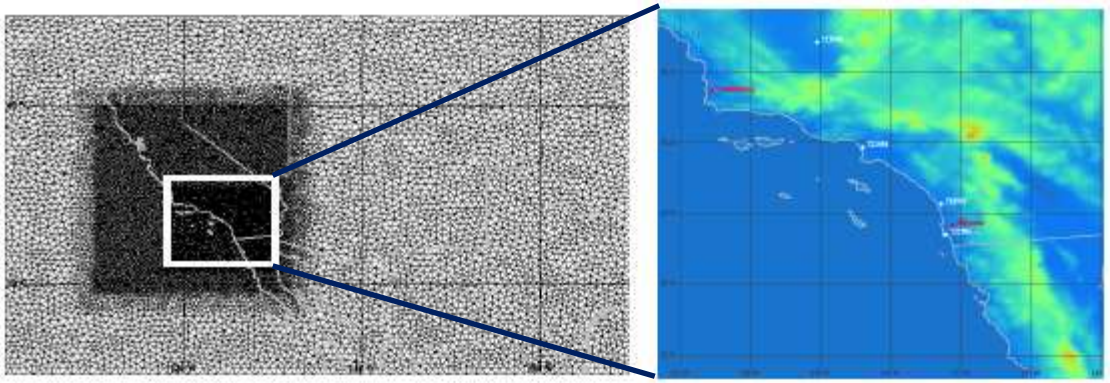

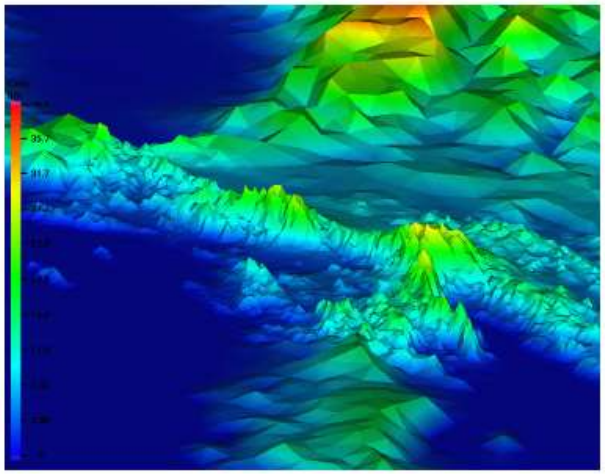

Ahmad et al. (AIAA 2009-0555)

Santa Ana Winds (October 2007)

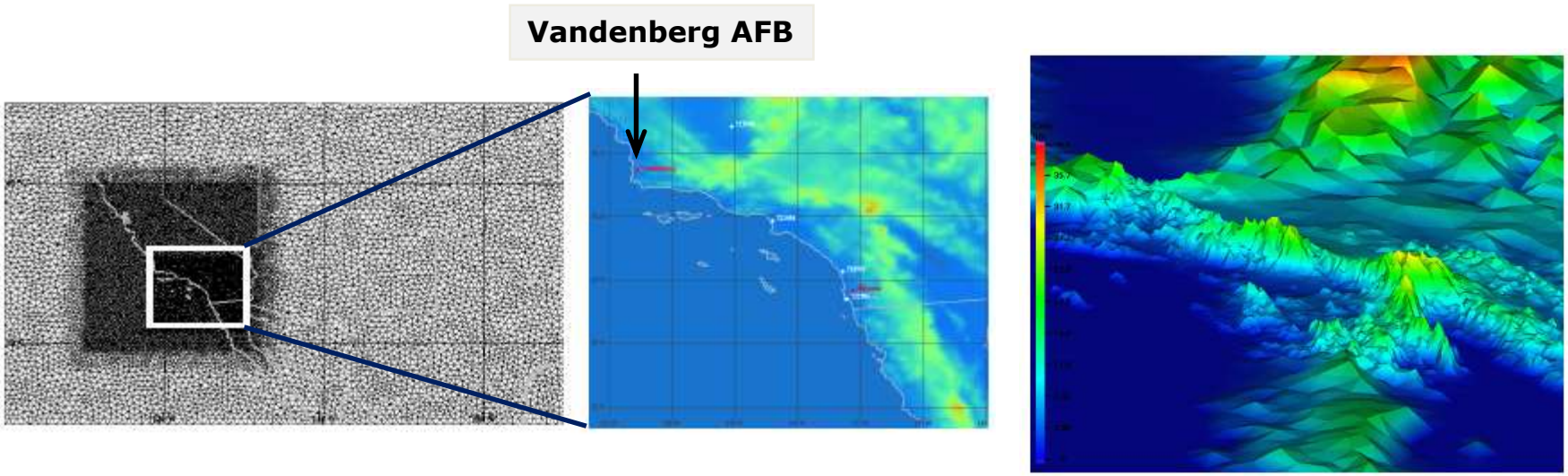

Ahmad et al. (AIAA 2009-0555)

Santa Ana Winds (October 2007)

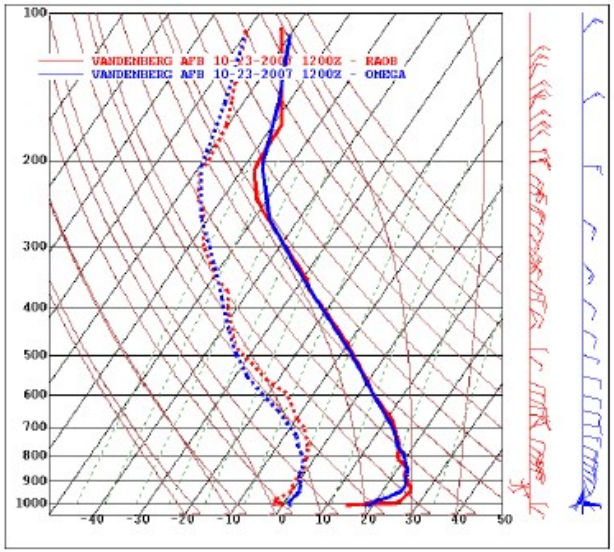

10-23-2007 12Z

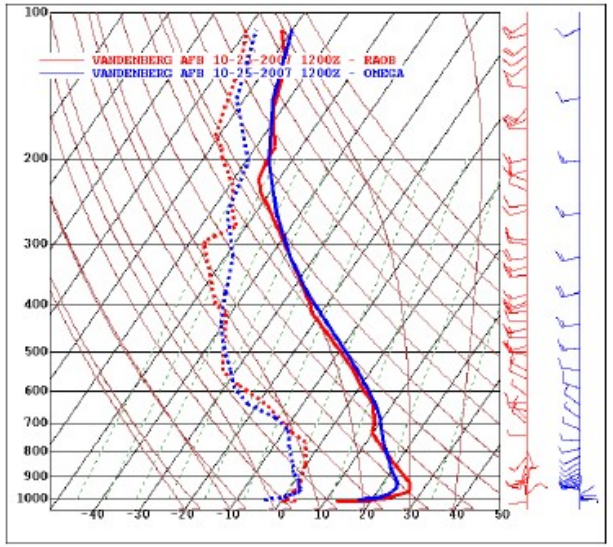

10-25-2007 12Z

Vandenberg AFB

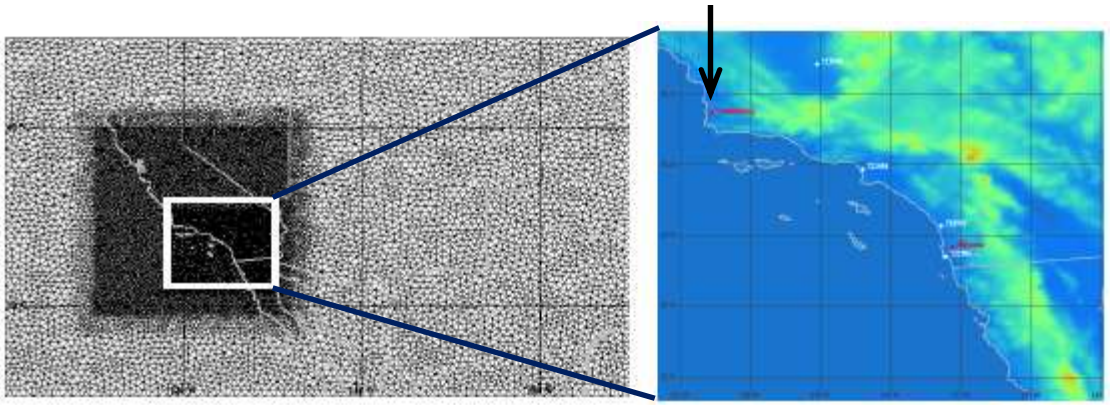

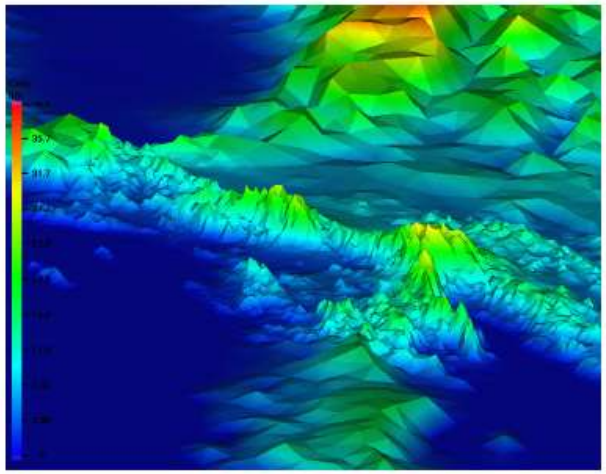

Ahmad et al. (AIAA 2009-0555)

Santa Ana Winds (October 2007)

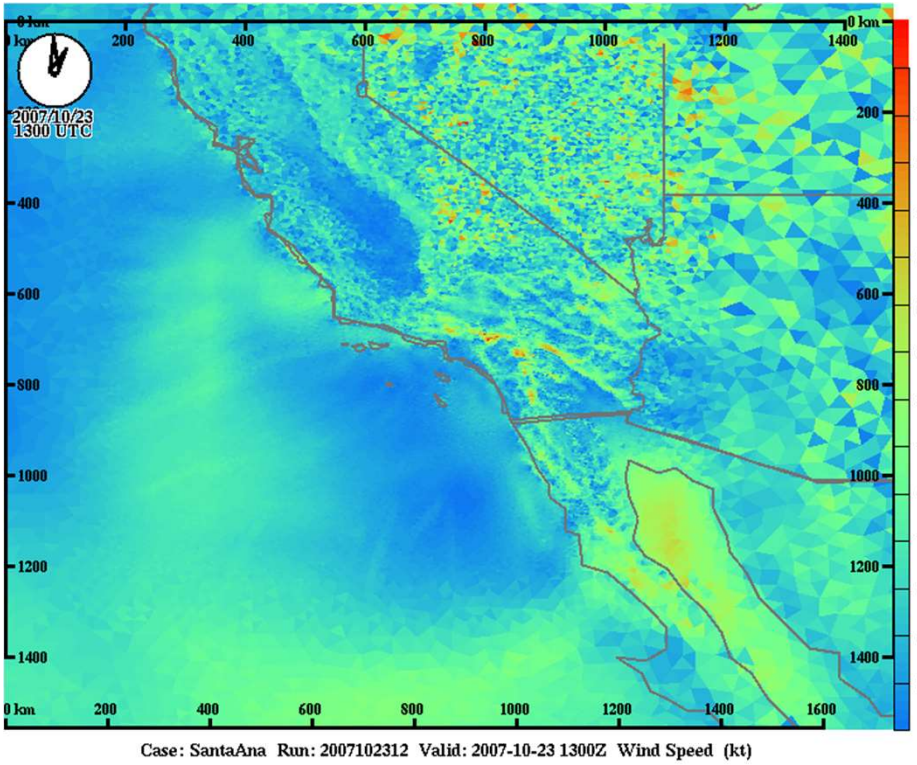

Wind speed (knots)

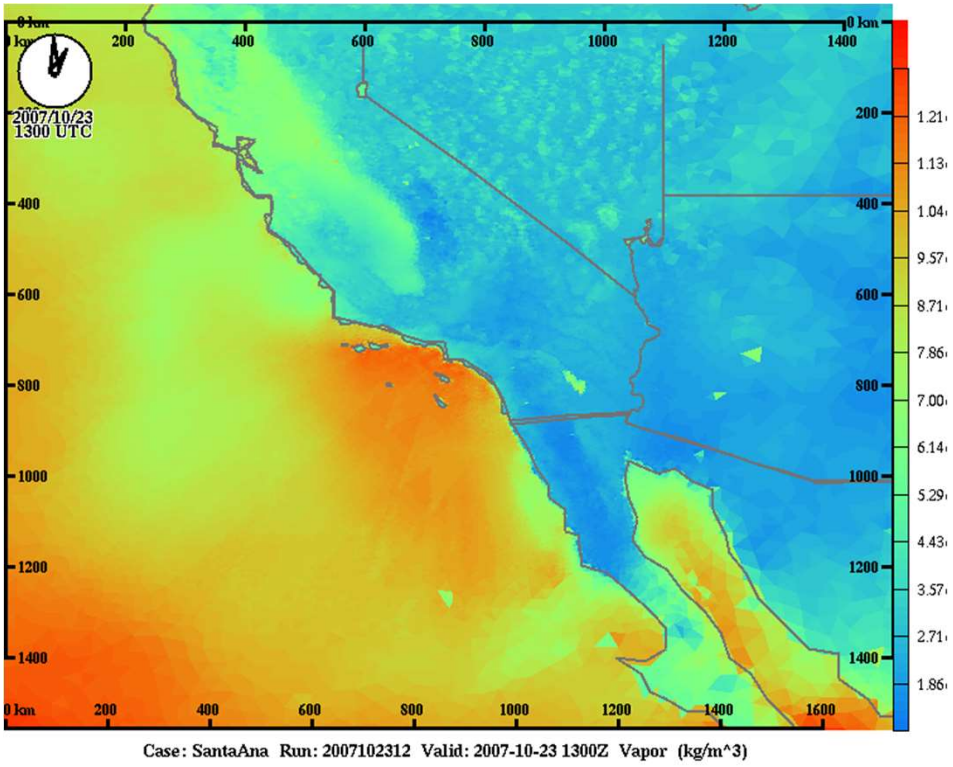

Vapor (kg/m^3)

Ahmad et al. (AIAA 2009-0555)

Hurricane Floyd (September 1999)

- Impact of Floyd
  - 57 lives lost
  - ~$3bn in damage
- 90 knots winds around 0630 UTC on 16th September
- OMEGA simulation using dynamic grid adaptation
  - Adaptation criteria set to pressure perturbation minima
- Domain: [58°W:89°W] x [13°N:40°N]
- Mesh resolution: [15km:80km]
- Initialized at 1999-09-14 (00Z) using NOGAPS data
- Final simulation time = 72 hours

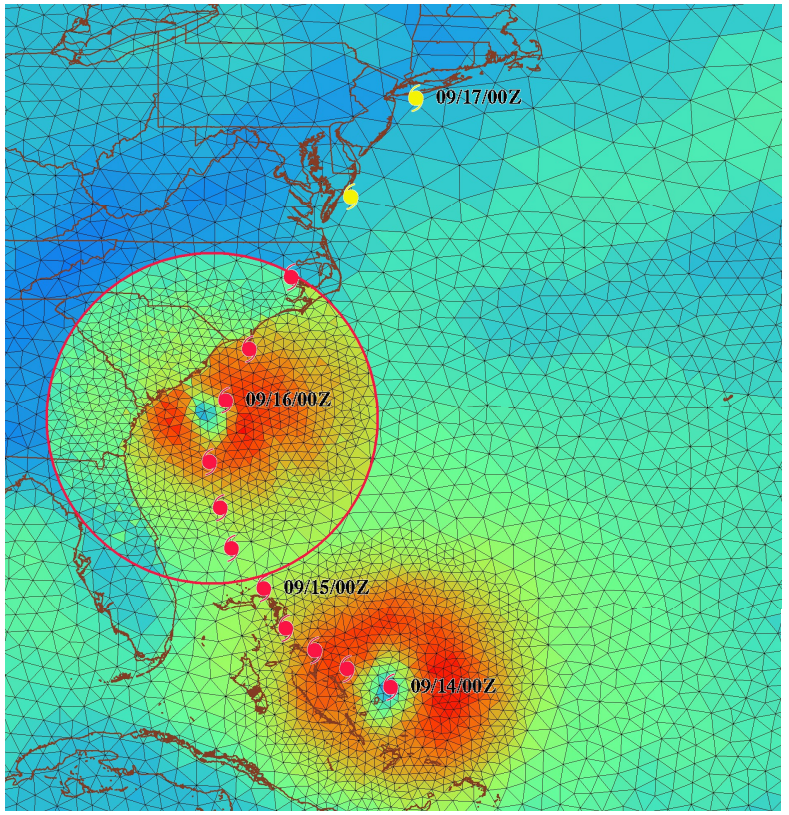

Wind speed at initialization and (inset) 48 hours into the forecast. The observed storm track is shown at six hour intervals by the symbols.

Gopalakrishnan et al. (MWR 2002)

Hurricane Floyd (September 1999)

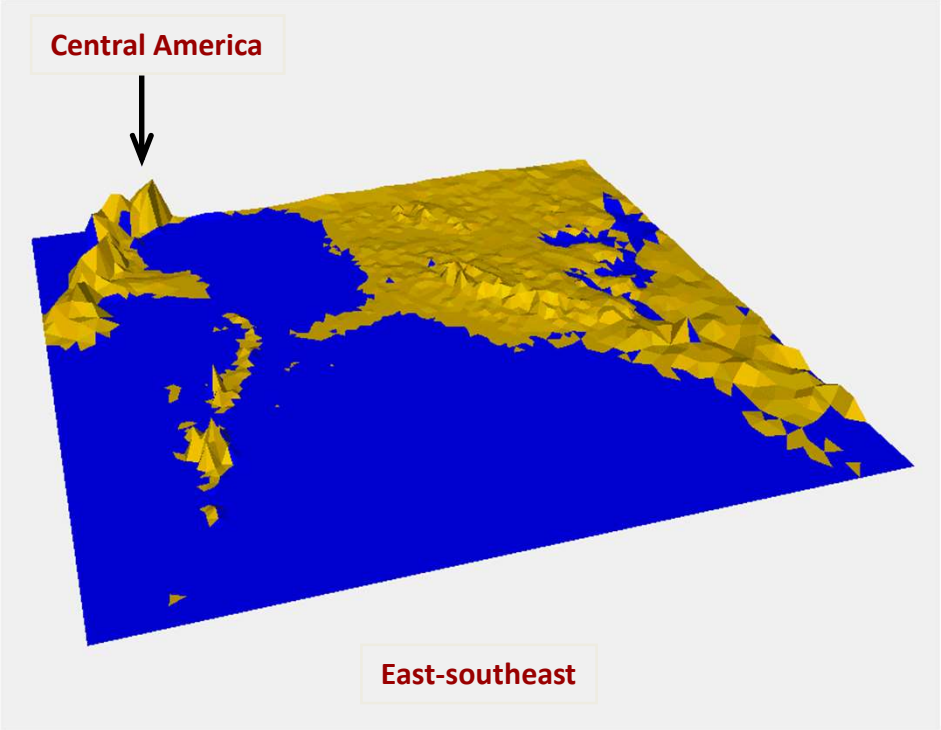

Adaptive Mesh
Adaptation criteria set to: min p’

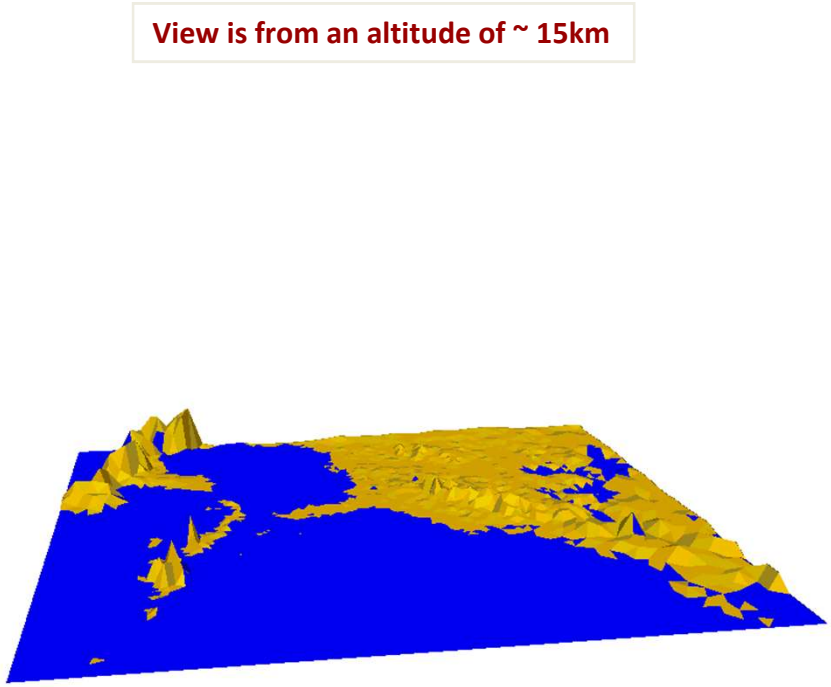

Equivalent Potential Temperature
355K Isosurface

Atmospheric Diffusion

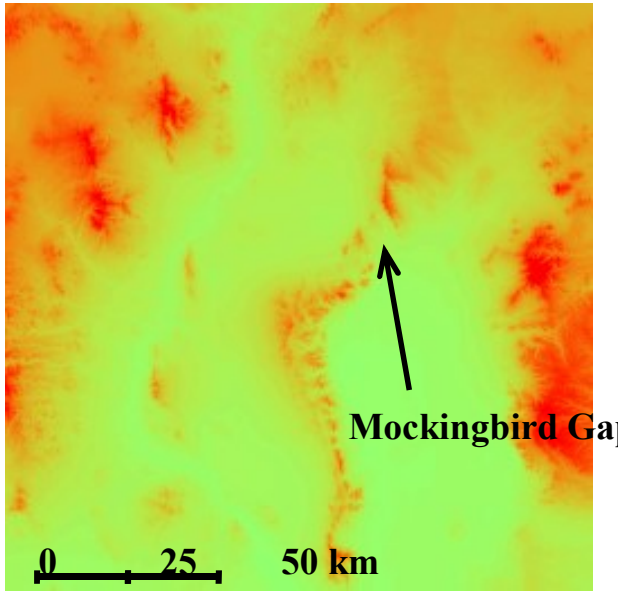

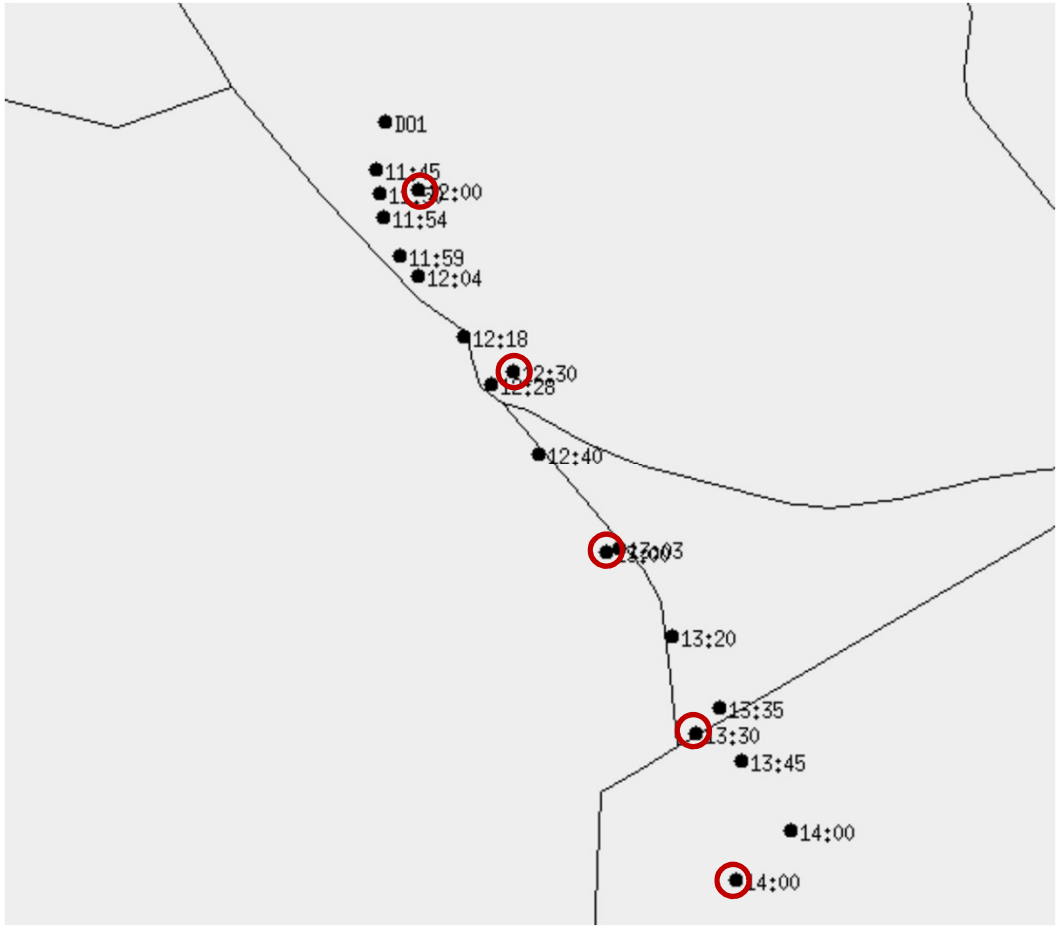

The terrain surrounding the test site at White Sands Missile Range (left) and a comparison of the OMEGA-forecasted plume centroid (circled dots) and the lidar-measured plume centroid.

Bacon et al. (AMS 1997)

Air Traffic Operations

- Spacing algorithm
  - NASA's spacing algorithm, ASTAR, enables an aircraft to precisely space behind another aircraft
- Operational goal
  - Achieve a precise spacing interval behind a target aircraft at a designated achieve-by point, which is typically the Final Approach Fix (FAF)
- An example of an Achieve-By IM operation
  - Air traffic controllers provide an IM clearance close to the aircraft's top of descent
  - The flight crew enters the information into onboard avionics
  - Pilots follow onboard speed guidance to achieve a precise spacing interval behind a lead, or target aircraft

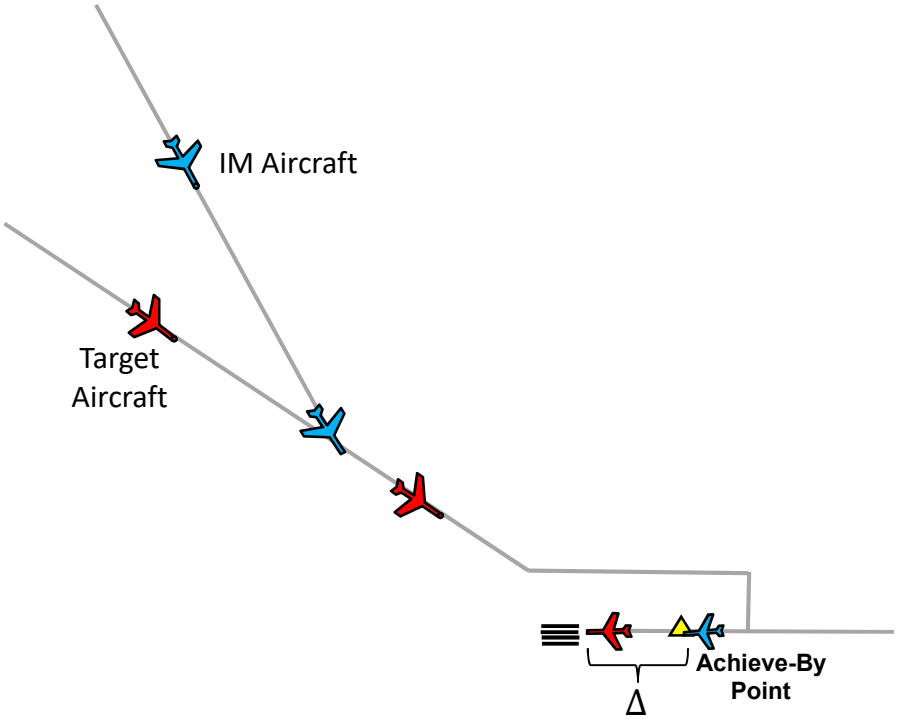

Ahmad et al. (AIAA-2015-3398)

Air Traffic Operations

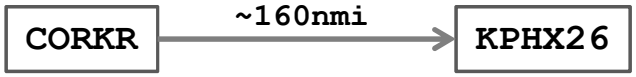

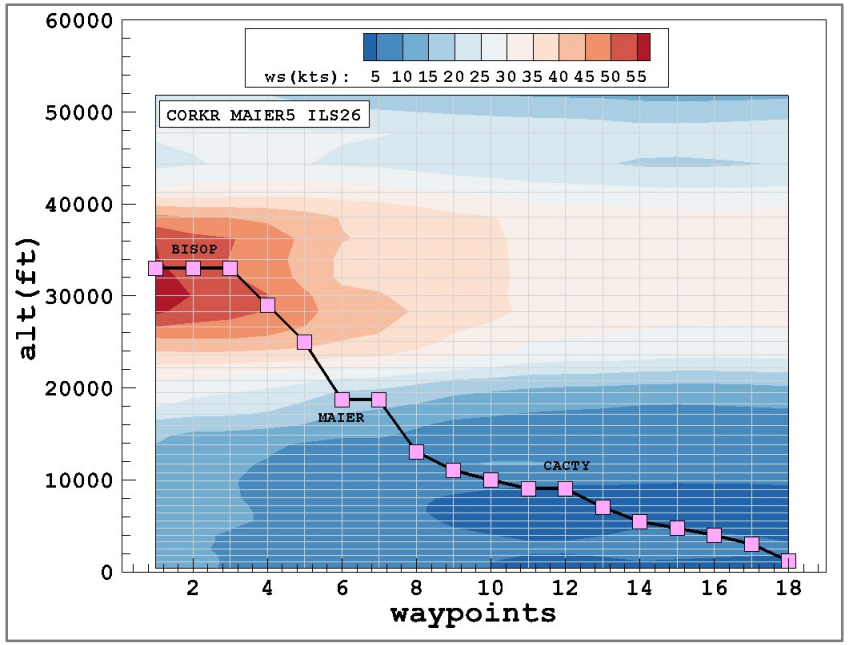

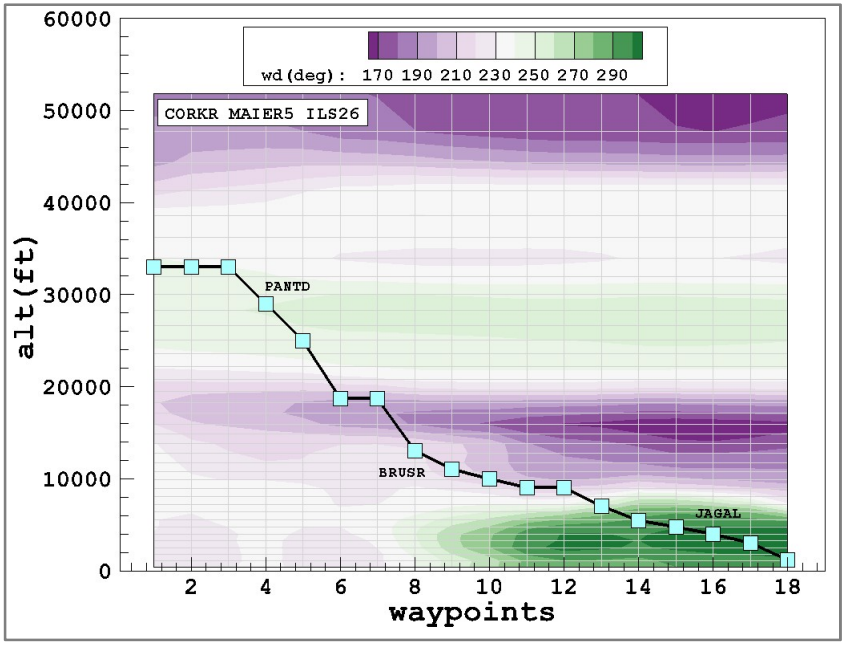

Winds along the Route

Wind Speed (left panel) and the Wind Direction (right panel)

Convection Induced Turbulence

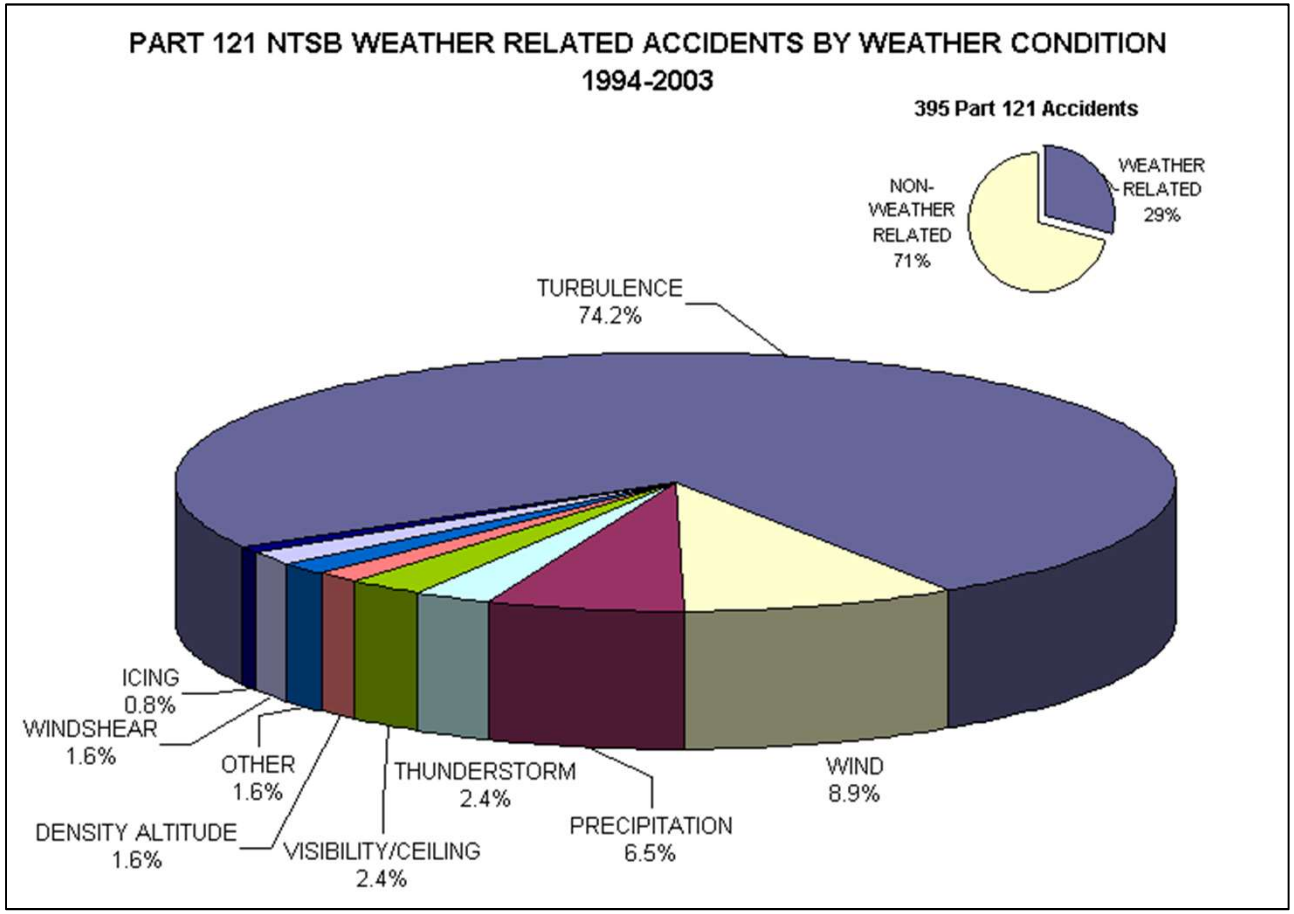

FAR Part 121 Accidents (Air Carrier Operations)

Total Accidents = 395

31% of weather related accidents occurred in the cruise phase of the flight

http://www.asias.faa.gov/aviation_studies/weather_study/studyindex.html

Convection Induced Turbulence

- Convective storms pose a serious risk to aviation operations
  - Turbulence, strong winds
  - Heavy rain, hail, icing
  - Lightning
  - Poor visibility
- Major cause of delays
  - Re-routing of flights
  - Disruption of operations at airports
- Most injuries from turbulence encounters are associated with Convection Induced Turbulence (CIT)
- Aircraft encounters with turbulence are usually unexpected and of short duration
- Encounters with CIT can occur when
  - aircraft move around high reflectivity regions to minimize deviation from the flight plan
  - convection appears invisible or harmless from aircraft's radar
  - storm tops unexpectedly rise into the aircraft's flight path
  - aircraft are inadvertently vectored into convection by ATC
- NASA's Turbulence Prediction And Warning System (TPAWS) Flight Experiments showed that the intensity of turbulence was not correlated with the level of radar reflectivity

Convection Induced Turbulence

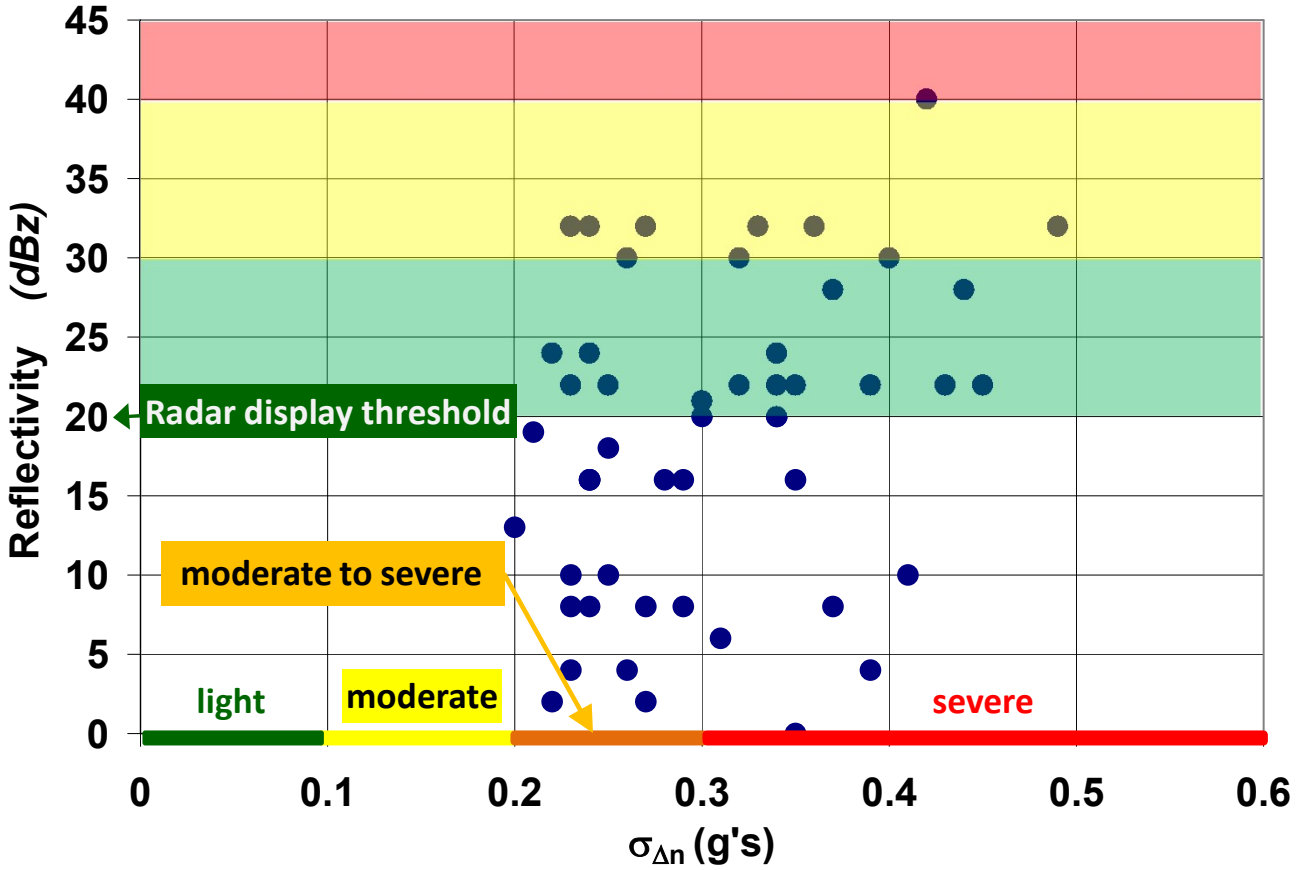

Peak RRF vs. Measured Hazard along Flight Path for Selected Events during NASA's TPAWS Experiment

Ahmad and Proctor (AIAA 2011-3201)

Convection Induced Turbulence

NTSB ID: DCA10FA076
Northwest of Guam

Vertical accelerations encountered: +1.5g and -0.3g

Encounter Duration: 5s

One flight attendant injured

NTSB conclusion: an inadvertent encounter with CAT

According to the captain, at the time of the encounter he was navigating around scattered cloud build ups

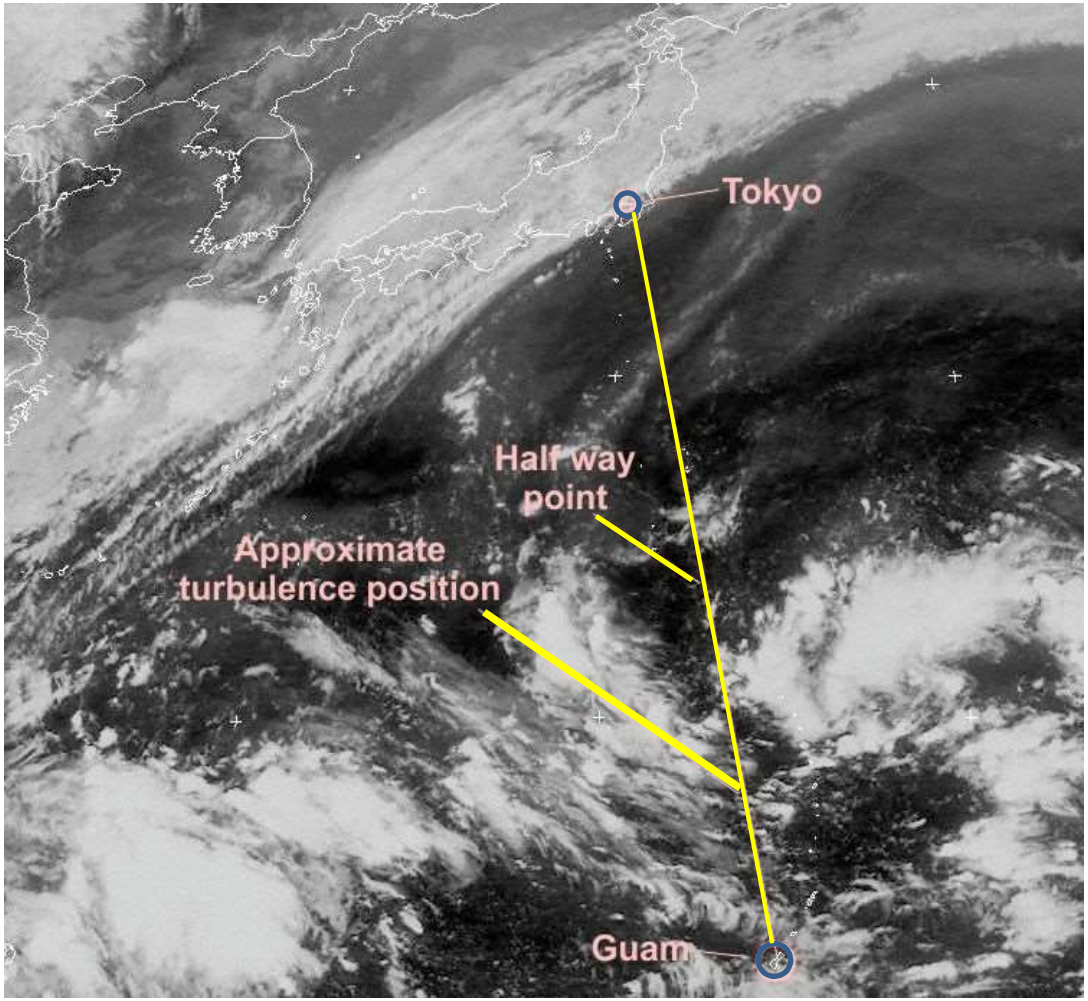

July 15, 2010 (0200 UTC) – Delta Boeing 767 – FL360

Turbulence Hazard Metric

- Root mean square of the aircraft's normal load acceleration, $\sigma_{\Delta n}$
- The metric is strongly correlated with the peak normal load on the aircraft, $|\Delta n|$
- It is airplane centric
- The metric is easy to calculate
- It statistically quantifies the sharp bumps and accelerations that passengers feel when flying in an aircraft

$\sigma_{\Delta n} \leq 0.1g$	*Light Turbulence*
$0.1g < \sigma_{\Delta n} \leq 0.2g$	*Moderate Turbulence*
$0.2g \leq \sigma_{\Delta n} < 0.3g$	*Moderate to Severe Turbulence*
$0.3g \leq \sigma_{\Delta n} < 0.6g$	*Severe Turbulence*
$0.6g \leq \sigma_{\Delta n}$	*Extreme Turbulence*

Turbulence Hazard Metric

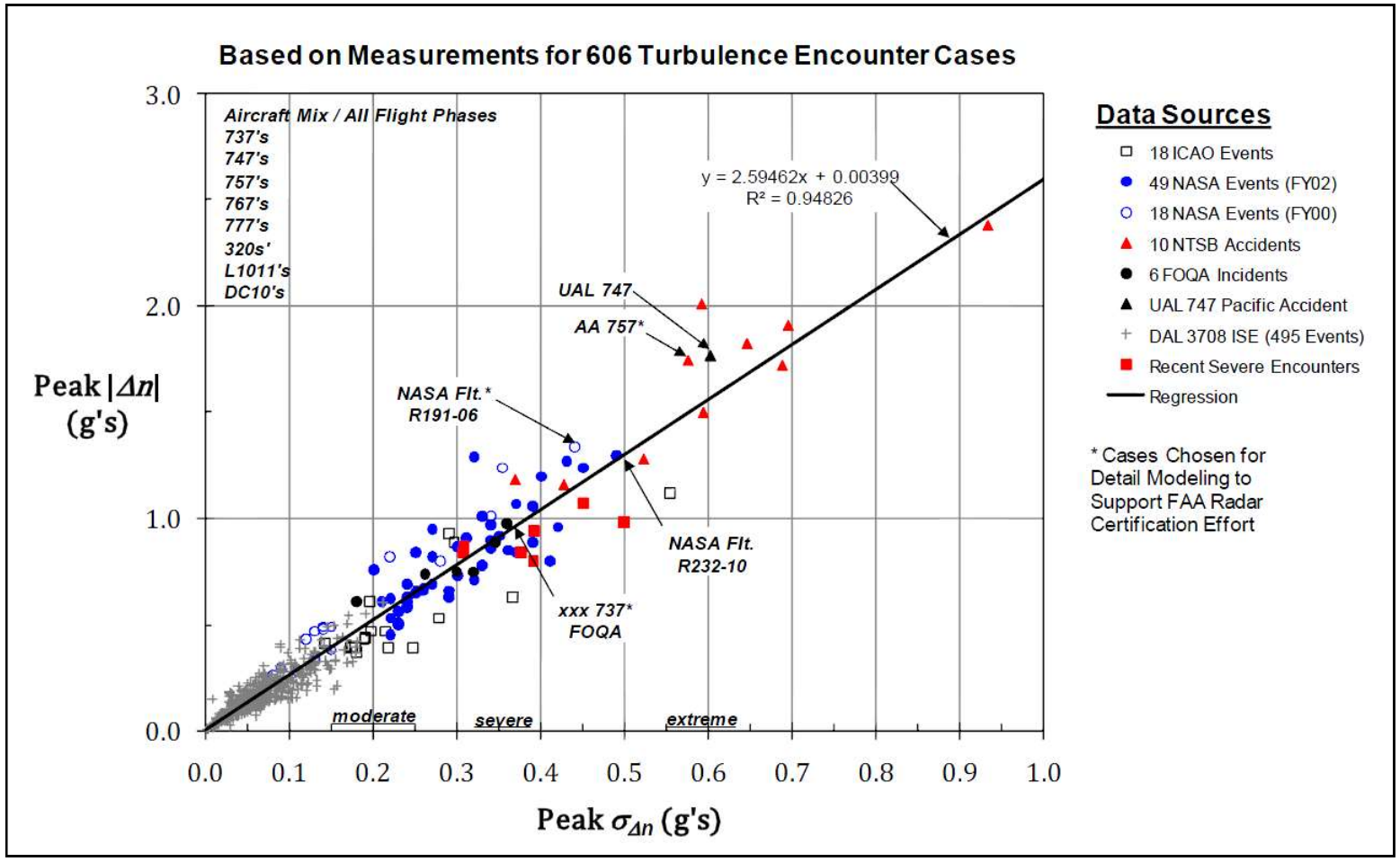

Bowles and Buck (2009)

Turbulence Hazard Metric

- Variance in the vertical velocity, σ_w is given by:

$$\sigma_w(x,y)=\left[\frac{1}{L_xL_y}\int_{x-\frac{L_x}{2}}^{x+\frac{L_x}{2}}\int_{y-\frac{L_y}{2}}^{y+\frac{L_y}{2}}\{w(x',y')-\overline{w}(x,y)\}^2\,dx'dy'\right]^{\frac{1}{2}}$$

$\overline{w}$ is the average vertical wind velocity

$L_x = L_y$ = 1km
Corresponds to 5*s* averaging period
for a typical commercial aircraft
flying at cruise speeds

- The RMS normal load acceleration, $\sigma_{\Delta n}$ is related to the variance in the vertical velocity by:

$$\sigma_{\Delta n}(x,y)=\sigma_w(x,y)\left(a(z)-b(z)\log(l)\right)\left(\frac{180}{W}\right)\left(\frac{V}{V_n(z)}\right)\times 1.09$$

  - The turbulence length scale, l is set to 500m
  - W is the weight of the aircraft, V is aircraft's true airspeed
  - Functions $V_n(z)$, $a(z)$, and $b(z)$ are aircraft dependent

Turbulence Hazard Metric

Boeing 737-300 with a weight of 100klbs

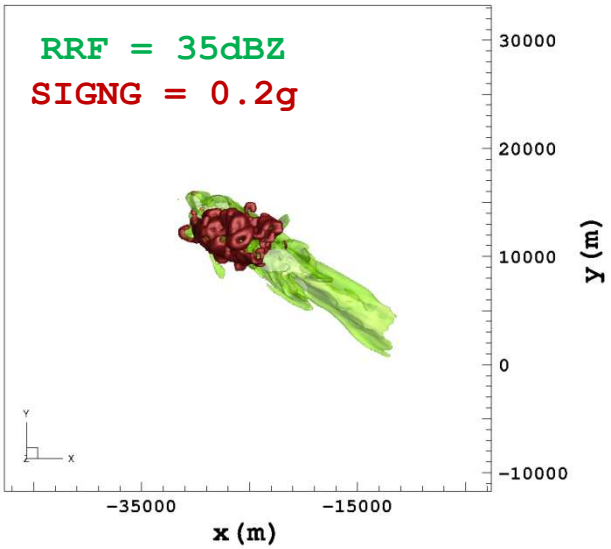

xy-plane
View is from the top

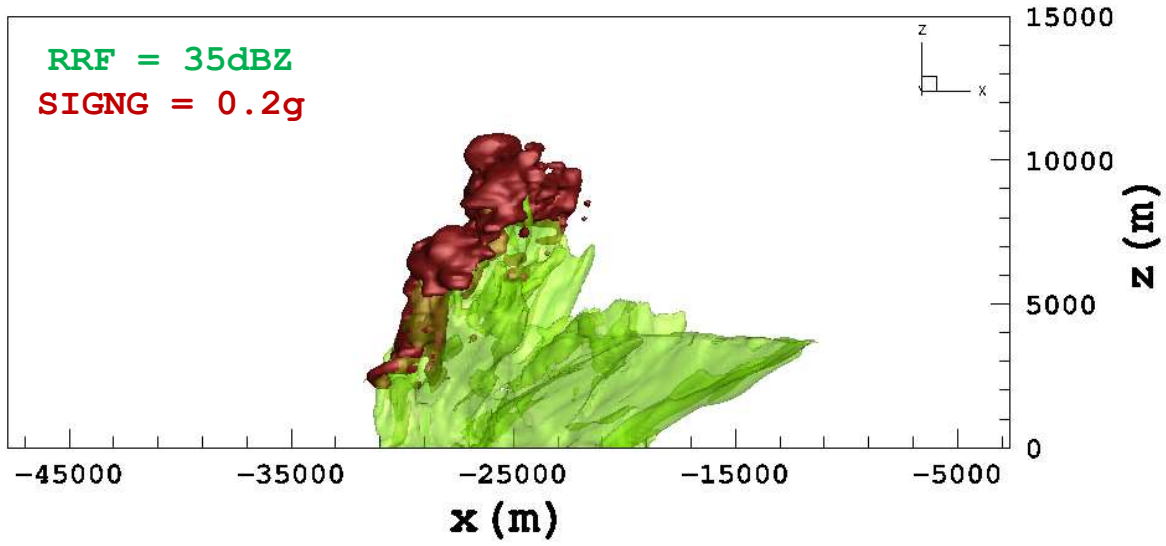

xz-plane – view is from the south

Turbulence Hazard Metric

vertical velocity (m/s) slice through the *x*-*z* plane at *y* = 12260m

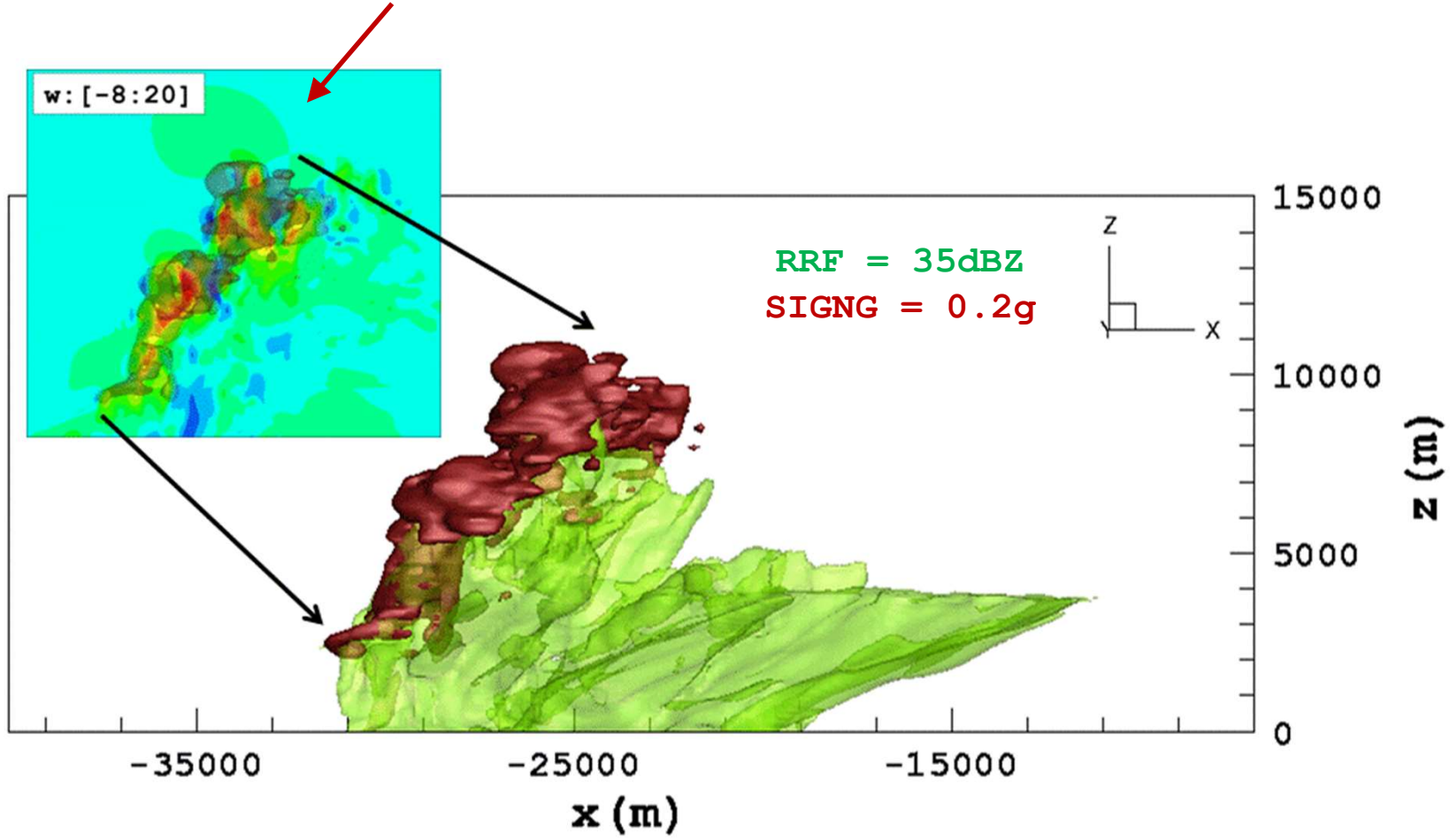

Simulation time = 43min and 15s

Turbulence Hazard Metric

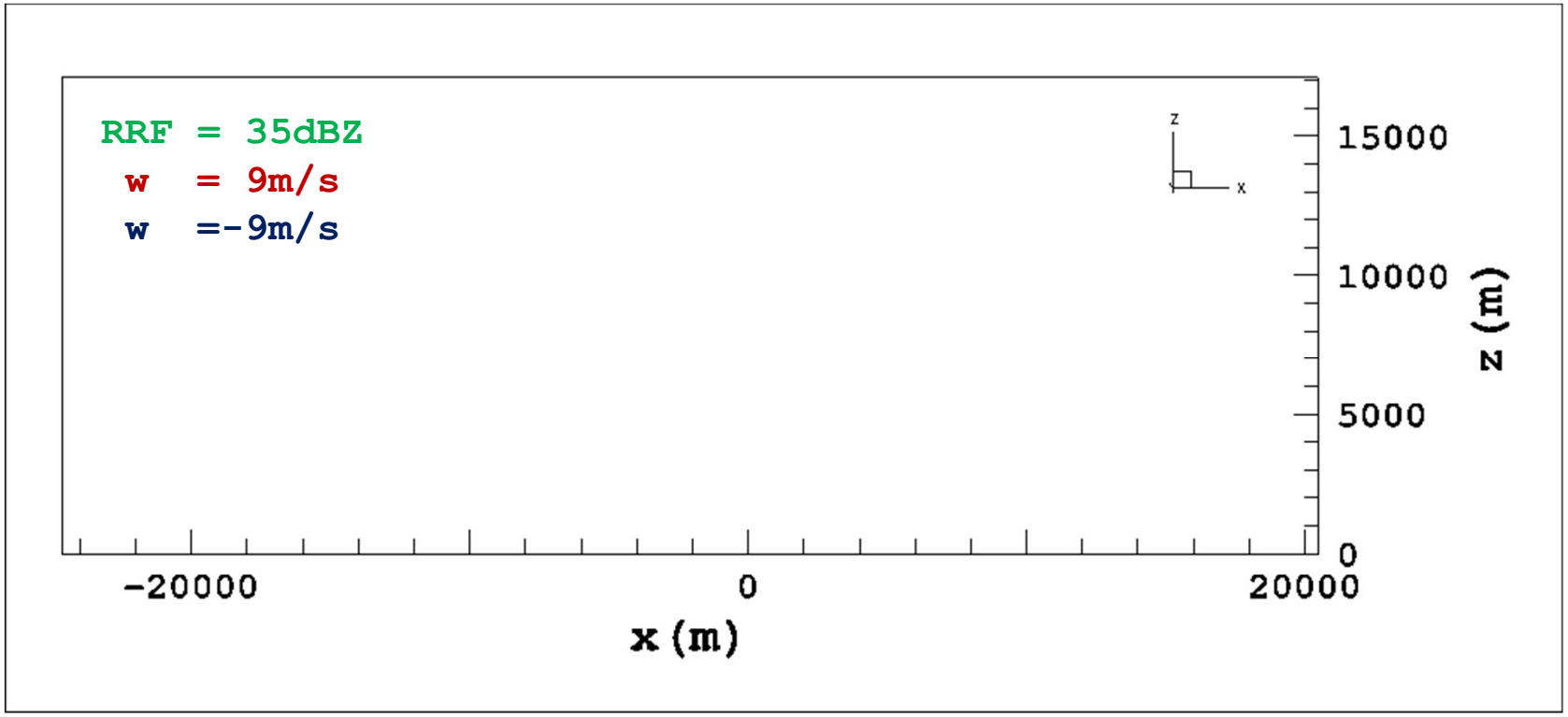

Storm evolution in time

Turbulence Hazard Metric

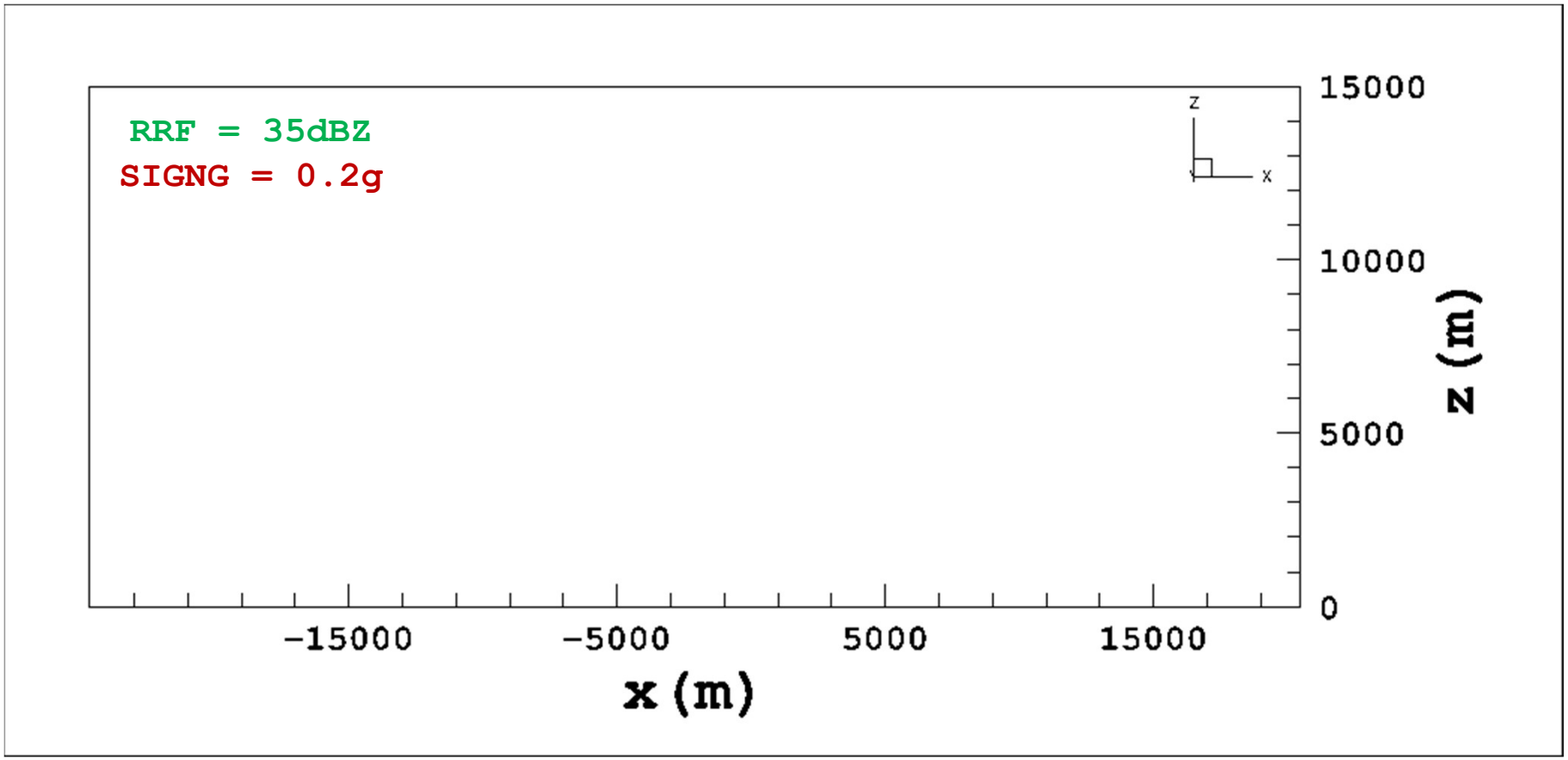

Storm evolution in time

Aircraft Wake Turbulence

- Vortices are generated by an aircraft as a direct consequence of the lift
  - First described by Fredrick W. Lanchester in his work *Aerodynamics* (1907)
- Wake spacing standards have been designed to ensure air traffic safety

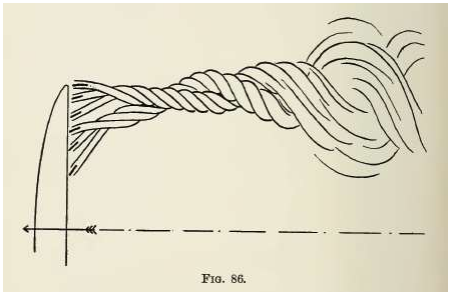

***Aerodynamics* (1907) p. 178**

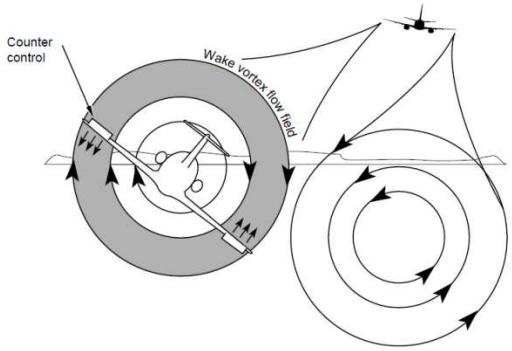

Induced roll experienced by the following aircraft (FAA AC 90-23G)

Animation generated using Google Earth

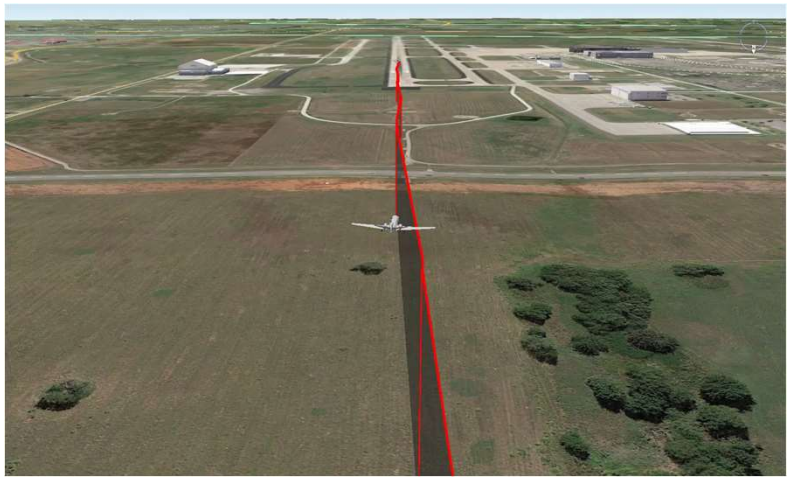

- Current wake spacing standards are a major constraint to enhancing the capacity of the National Airspace System (NAS)

Aircraft Wake Turbulence

Field Experiments
Wake & Met Data Collection



Wake Vortex Decay
Parametric Studies

Fast-Time Wake Vortex Models

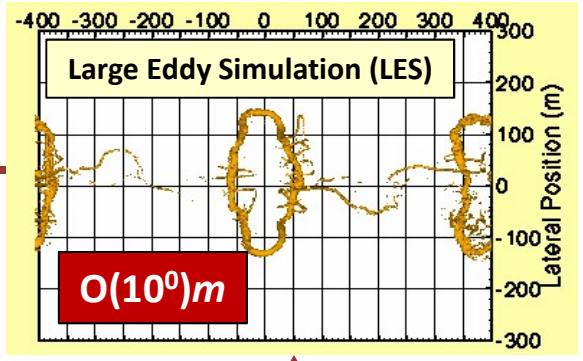

Initial Conditions for LES

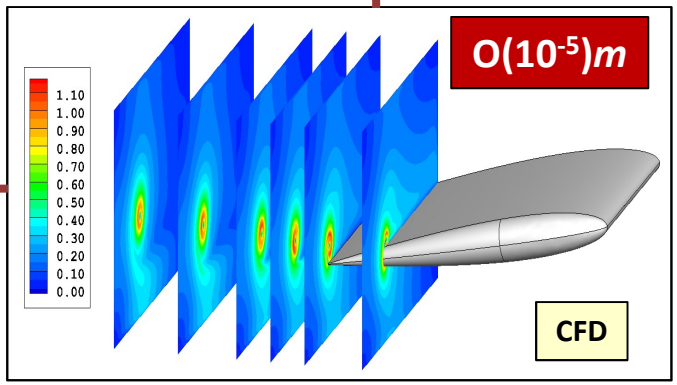

Initial Conditions for
Fast-Time Wake Models

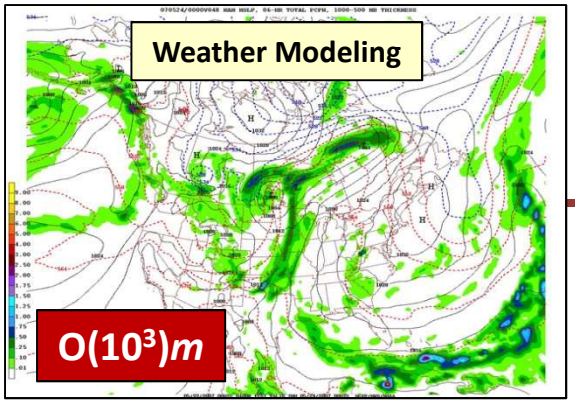

Aircraft Wake Turbulence

Field Experiments
Wake & Met Data Collection



Wake Vortex Decay
Parametric Studies

Fast-Time Wake Vortex Models

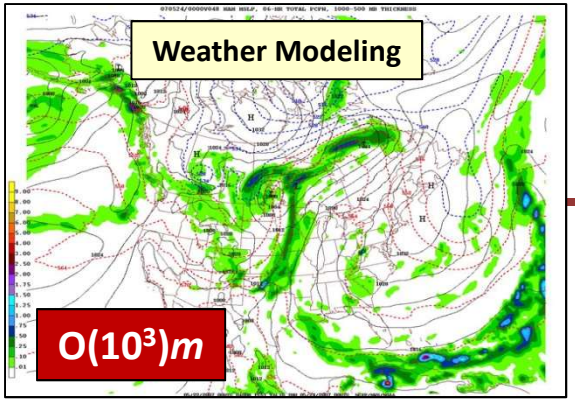

Initial Conditions for
Fast-Time Wake Models

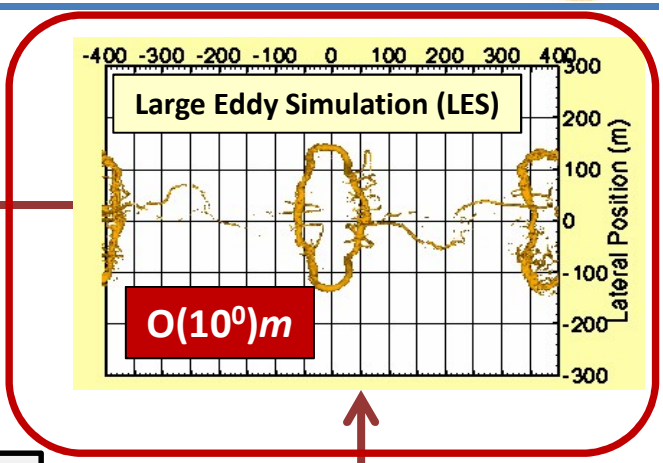

Initial Conditions for LES

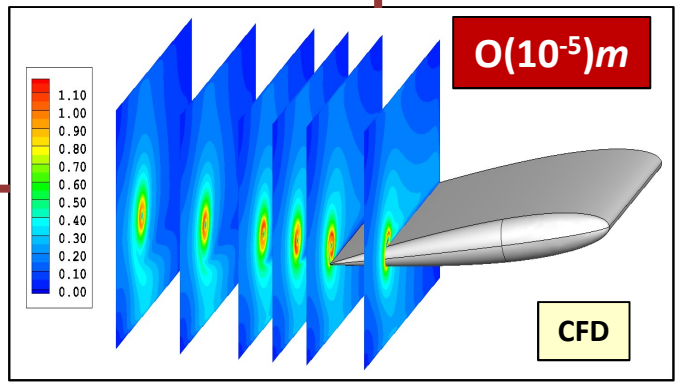

Aircraft Wake Turbulence (B767)

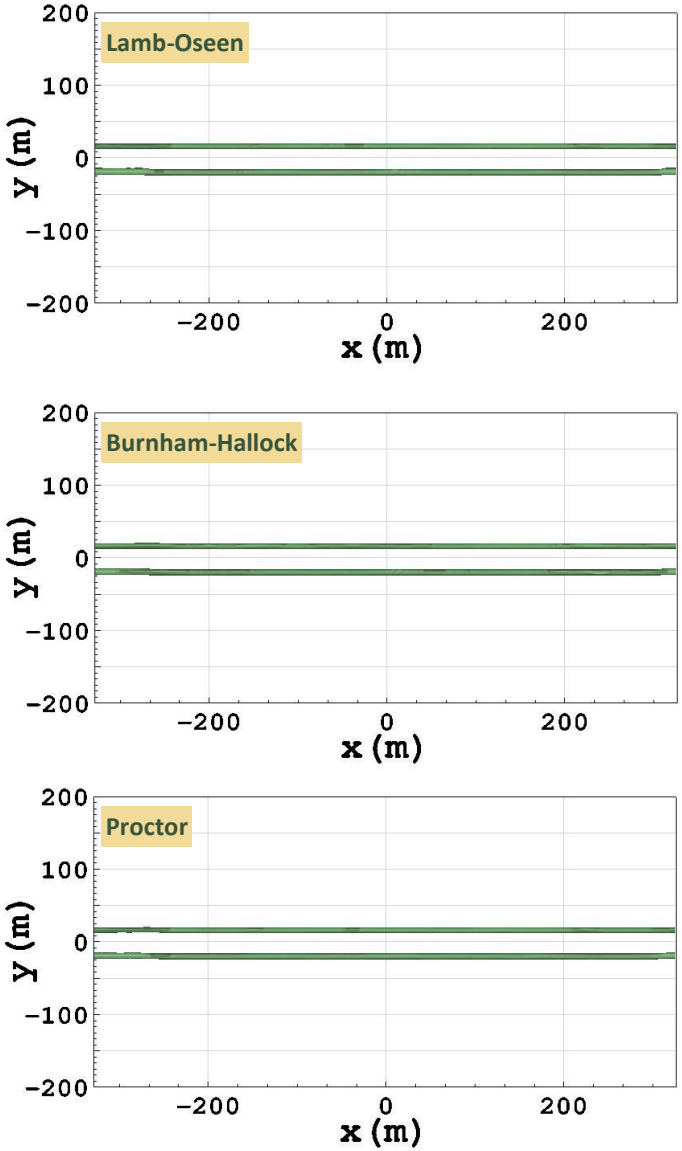

TASS Simulations

$N^* = 0$; $\varepsilon^* = 0.07$

$\Delta x = 2m$; $\Delta y = \Delta z = 1.5m$

$r_c = 3m$; $b_0 = 36m$

$\Gamma_0 = 360 m^2/s$

Ahmad et al. (AIAA 2014-0927)

Aircraft Wake Turbulence (B767)

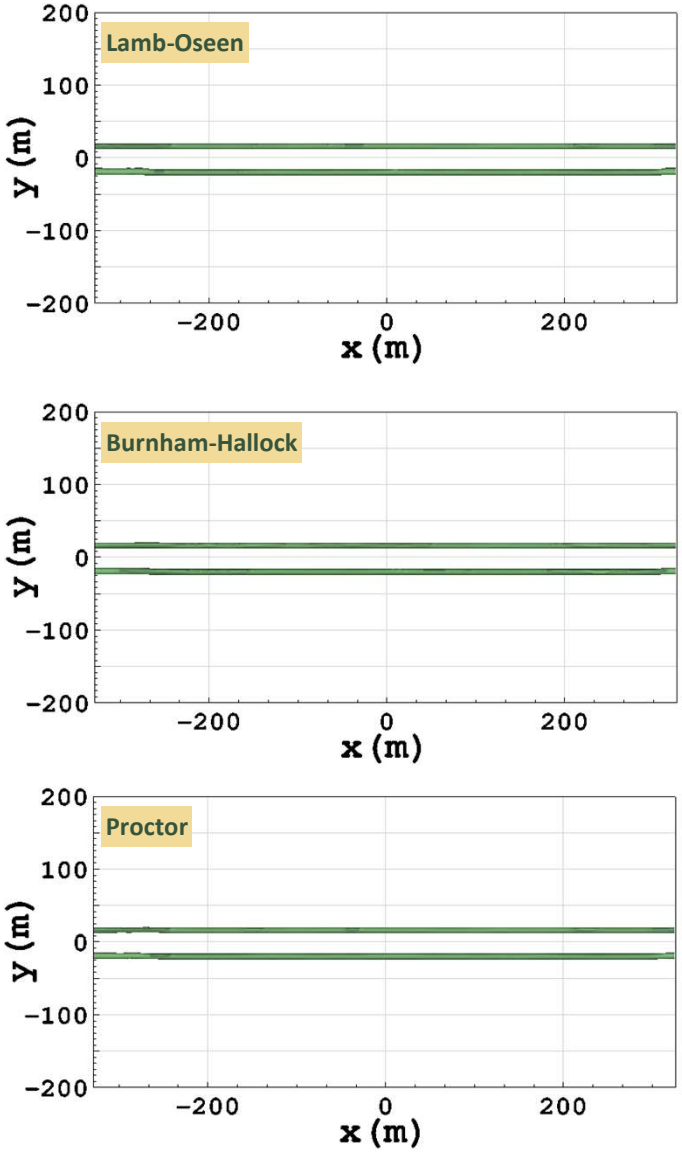

TASS Simulations

$N^* = 0$; $\varepsilon^* = 0.07$

$\Delta x = 2m$; $\Delta y = \Delta z = 1.5m$

$r_c = 3m$; $b_0 = 36m$

$\Gamma_0 = 360 m^2/s$

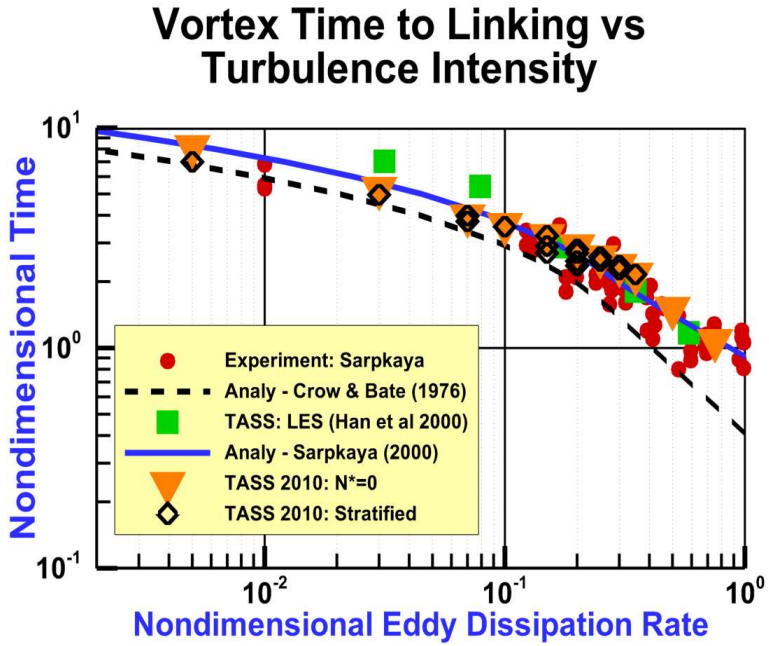

Ahmad et al. (AIAA 2014-0927)

Wake Vortex Encounter Incident

Source: O'Callaghan (NTSB Final Report – CEN13TA113)

(1) N753CC very likely encountered the right wake vortex of the Airbus, and

(2) This encounter very likely generated strong rolling moments to the left that can account for the 60° roll to the left recorded by the EGPWS on N753CC.

Meteorological and A/C Data from NTSB Report

Crosswinds, potential temperature, EDR

A/C Trajectories, Wingspans, etc.

Fast-Time Model used in Monte-Carlo: APA3.4

Wake Vortex Encounter Incident

Animation generated using Google Earth

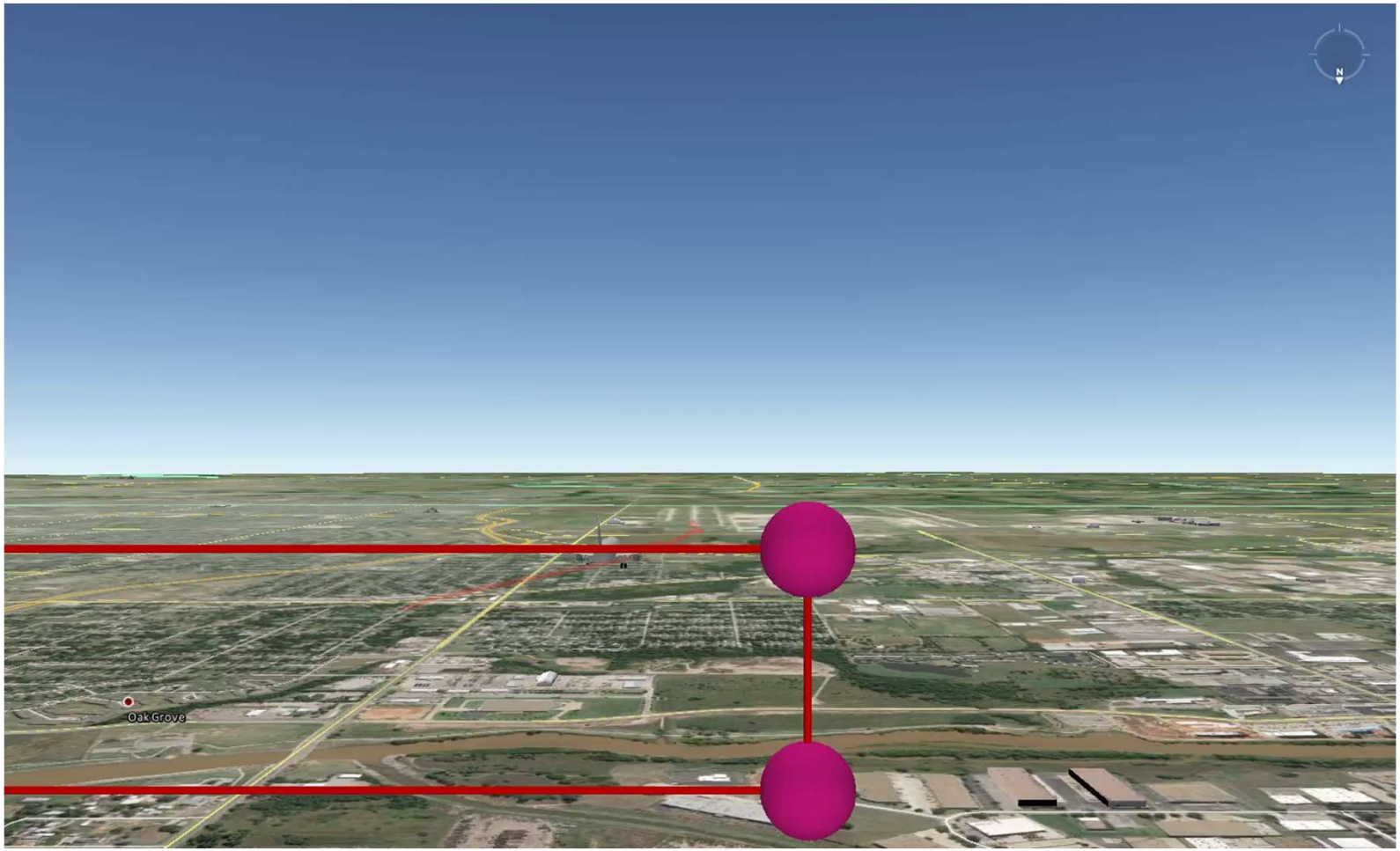

Wake Vortex Encounter Incident

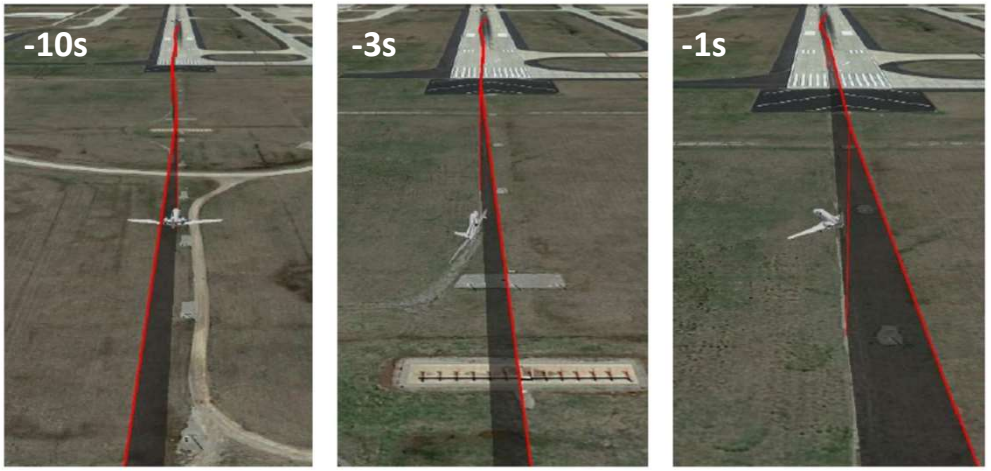

Images generated using Google Earth

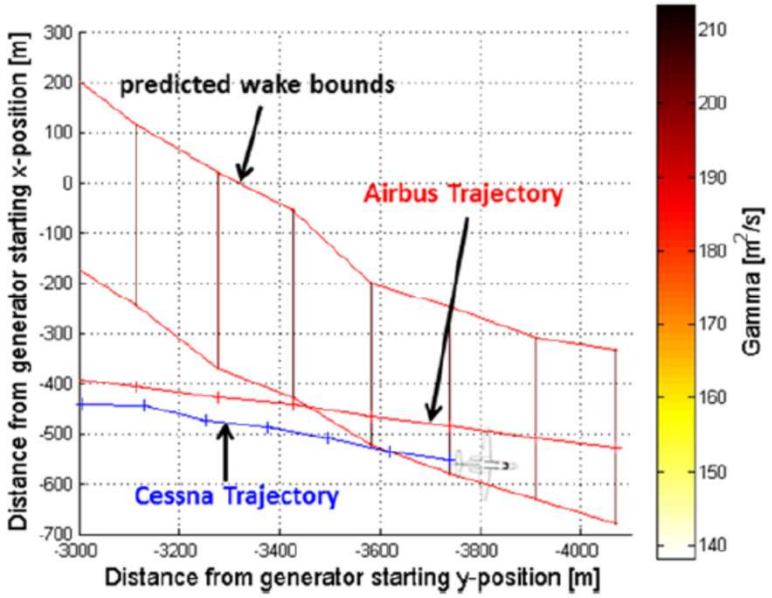

Method	C_V	
	Burnam-Hallock	Rankine
Bowles-Tatnall	0.1617	0.1841
Modified Bowles-Tatnall	0.1306	0.152
O'Callaghan (2013)	NA	0.15

Gloudemans et al. (NASA/TM-2016-219193)

Acoustic Wave Propagation

- Sound speed is a function of temperature. A 1°C change of temperature results in sound speed variation by 0.6 m/s – Atmospheric refraction
- Winds cause shifts in the wave propagation front
- Turbulence in the surface layer can result in dispersion of waves
- Atmospheric absorption on the molecular level causes dissipation of sound waves

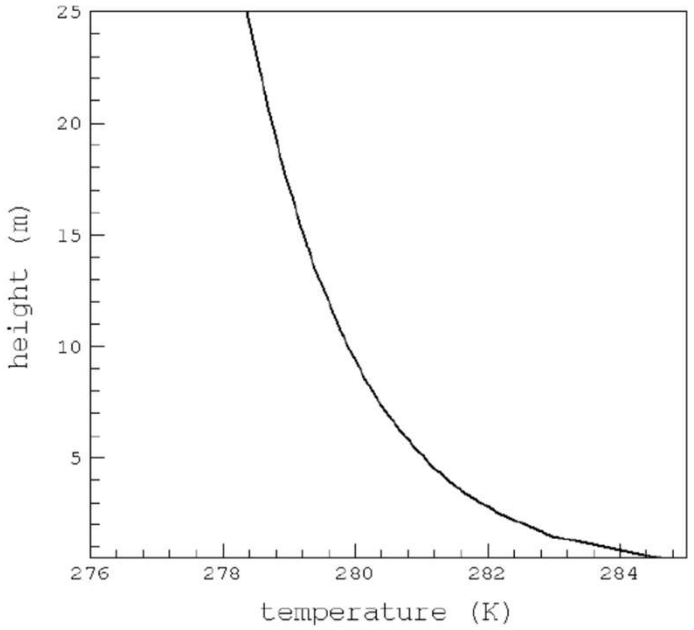

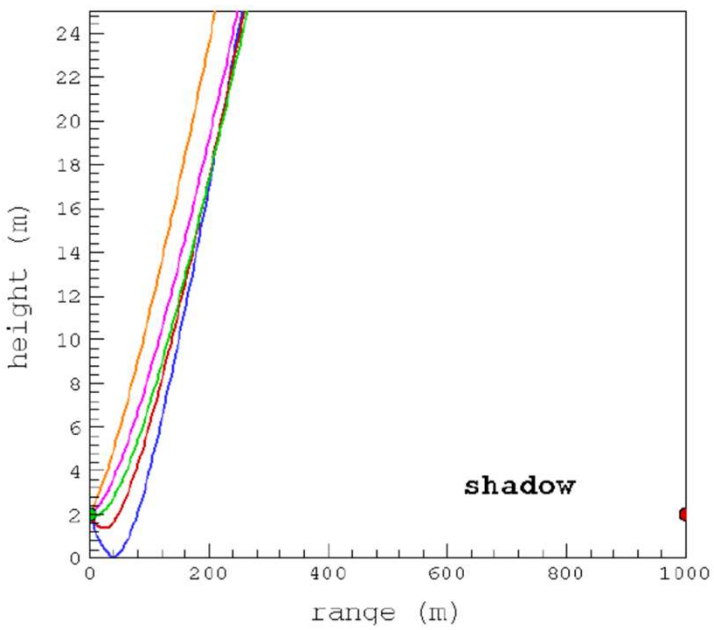

Ahmad et al. (AIAA-2008-0062)

Gettysburg – July 2nd, 1863

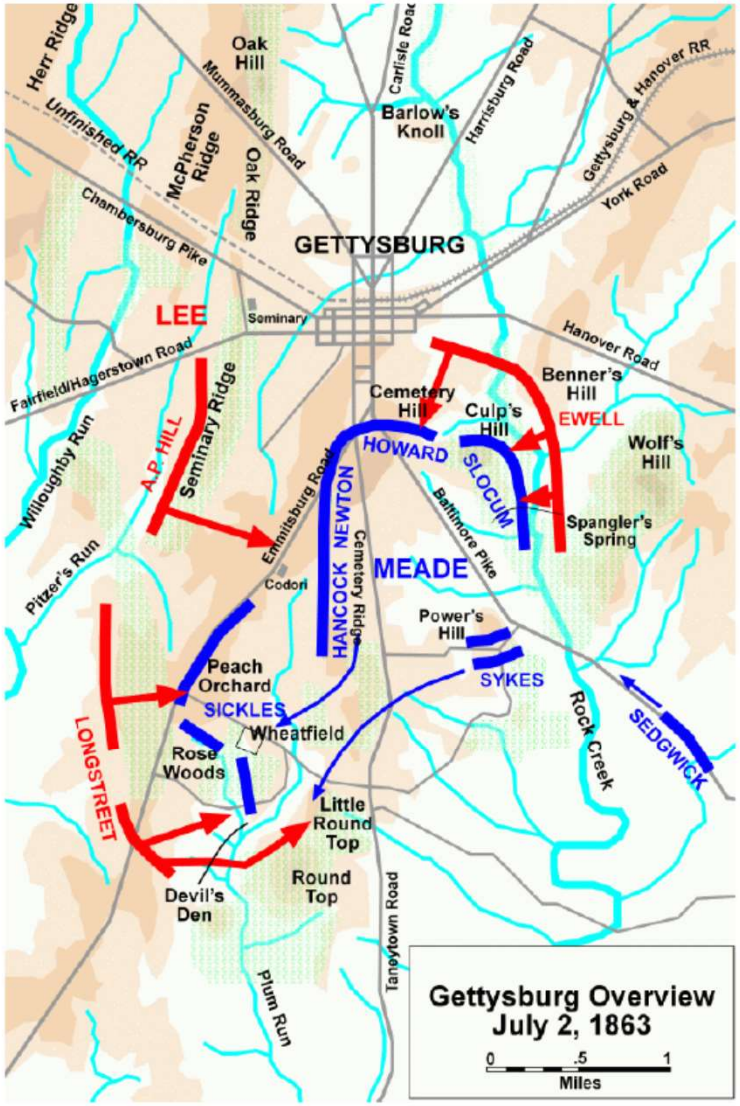

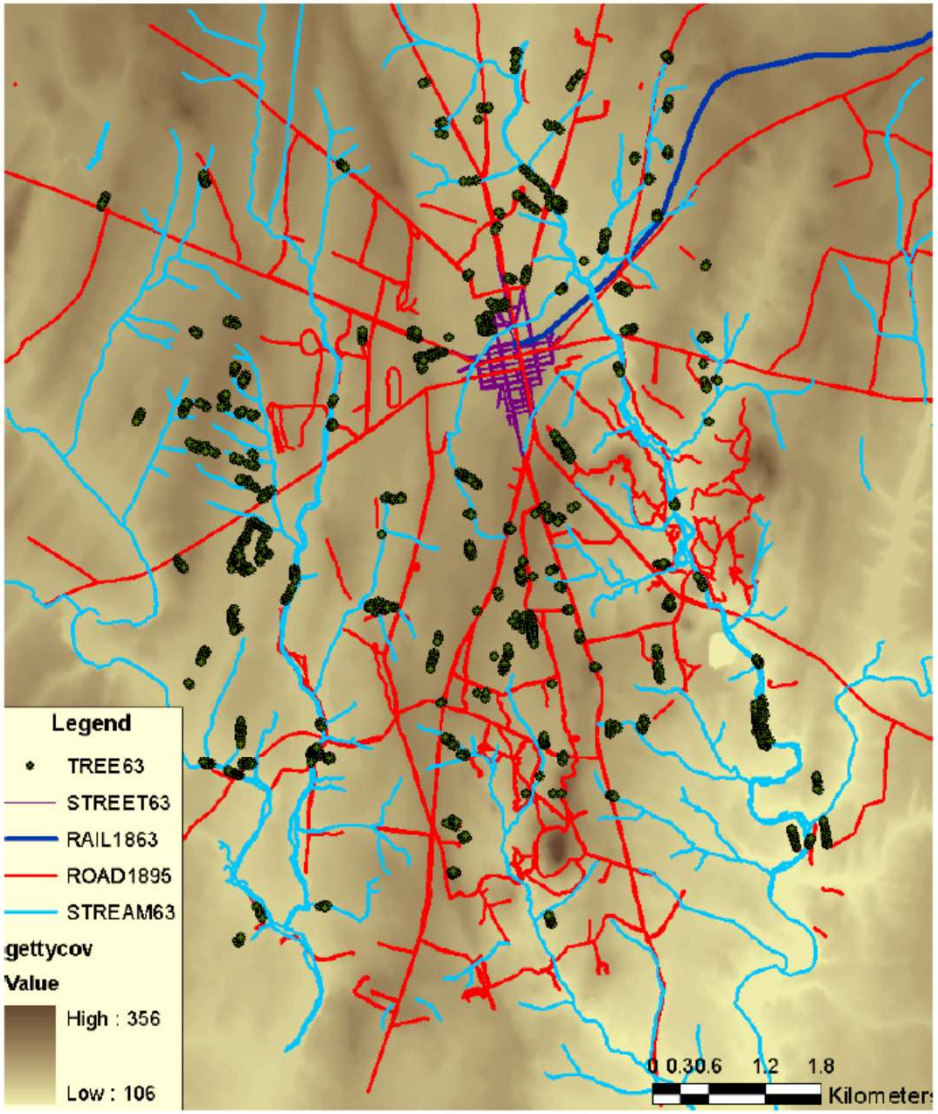

Ahmad et al. (AIAA-2008-0062)

Gettysburg – July 2nd, 1863

Table 1: Longstreet's Cannons

Army of Northern Virginia

Longstreet's Corps

Corps Artillery Reserves | **McLaws' Division** | **Hood's Division**

Alexander's Battalion | **Cabell's Battalion** | **Henry's Battalion**

Alexander's Battalion

Name	Latitude	Longitude	Altitude (ft)	Took Position
Woolfolk's Battery	39° 47′ 58″	−77° 15′ 22″	603	1630
Jordan's Battery	39° 48′ 01″	−77° 15′ 22″	588	1630
Parker's Battery	39° 48′ 02″	−77° 15′ 22″	591	1600
Taylor's Battery	39° 48′ 04″	−77° 15′ 22″	591	1600
Moody's Battery	39° 48′ 06″	−77° 15′ 22″	593	1600
Rhett's Battery	39° 48′ 08″	−77° 15′ 22″	585	1600

Gettysburg – July 2nd, 1863

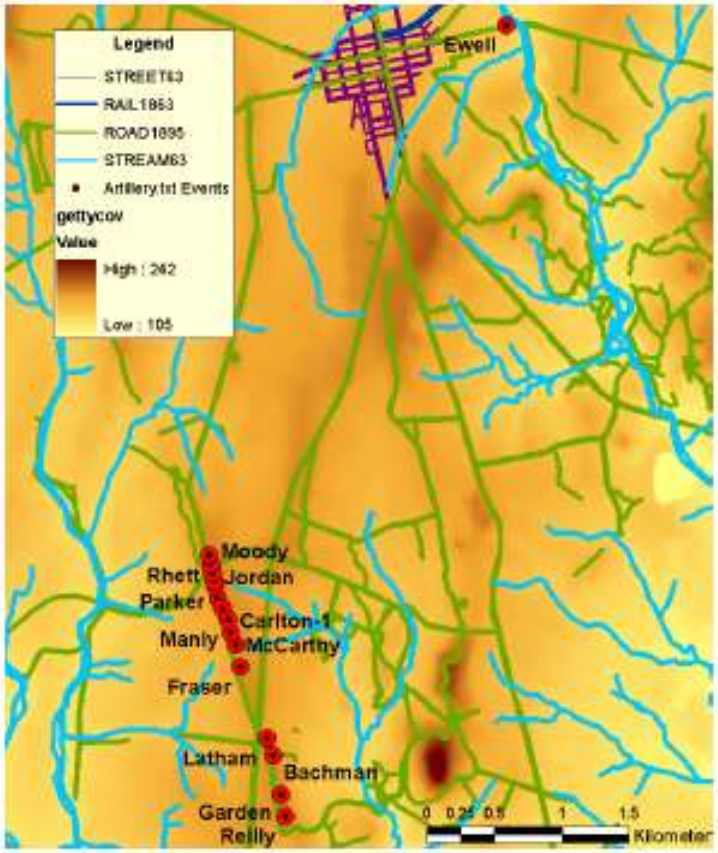

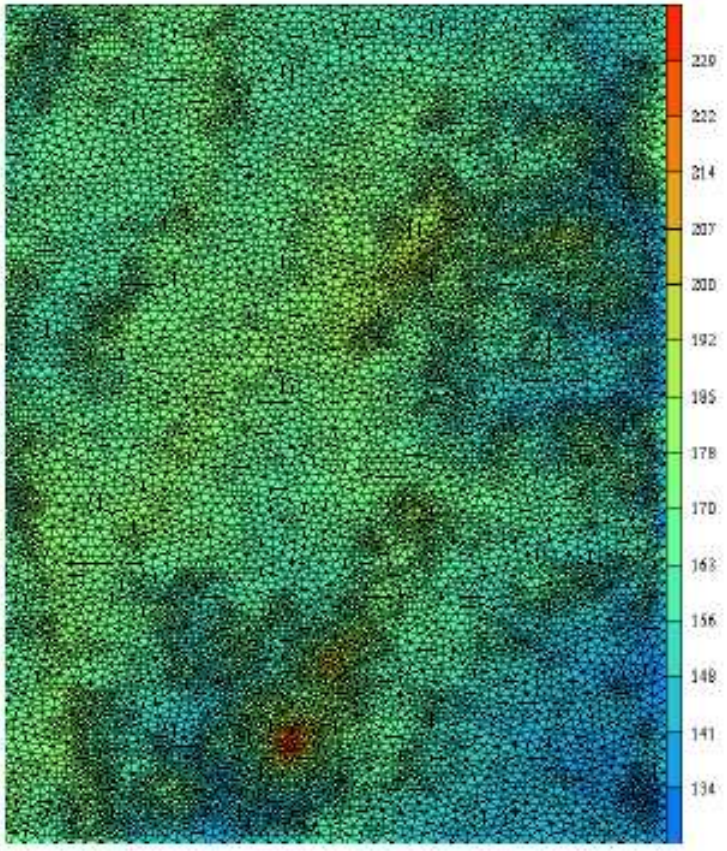

Ahmad et al. (AIAA-2008-0062)

Gettysburg – July 2nd, 1863

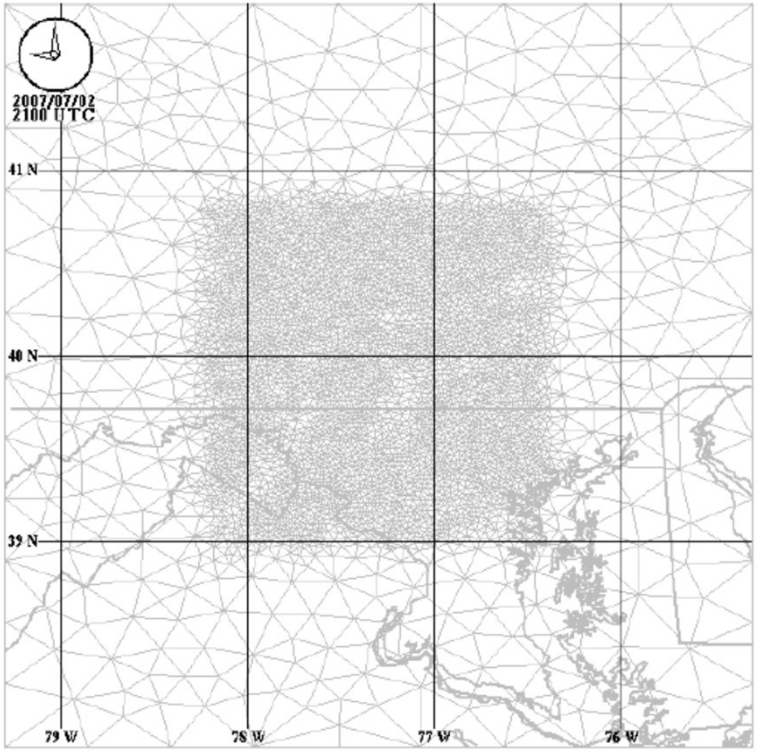

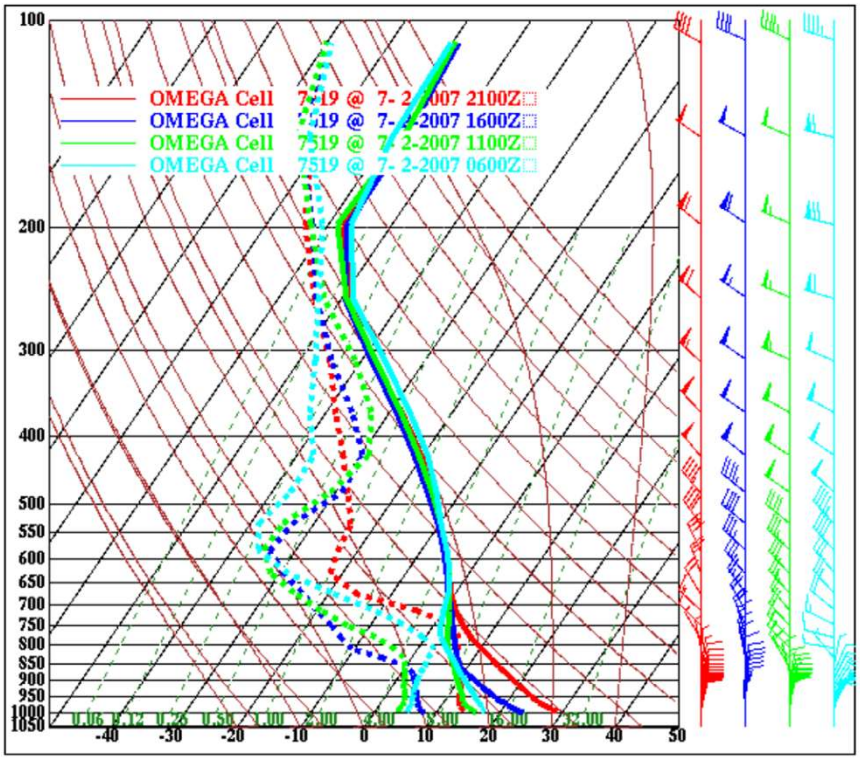

Ahmad et al. (AIAA-2008-0062)

Gettysburg – July 2nd, 1863

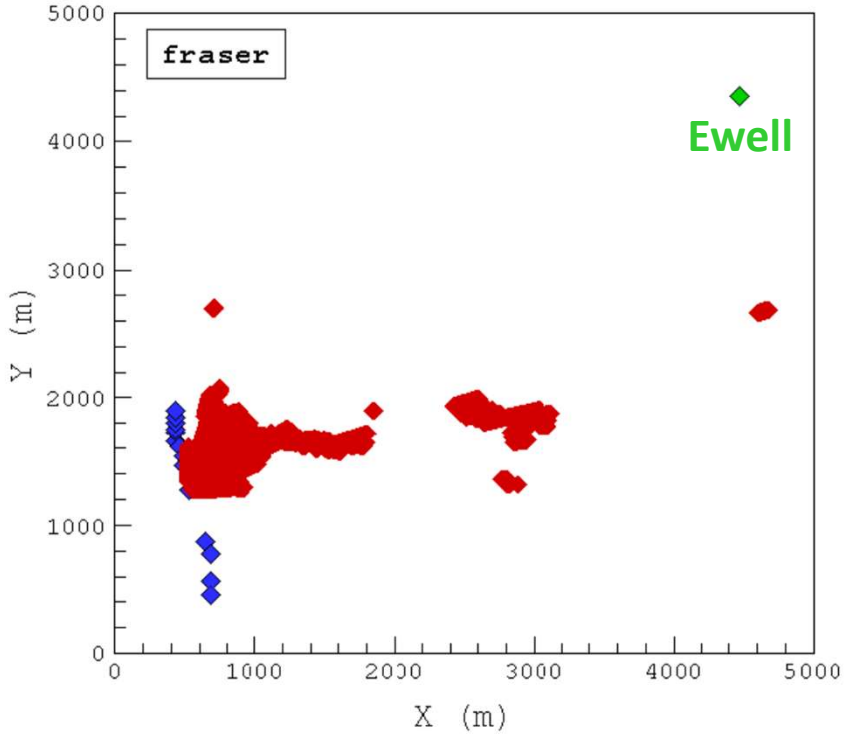

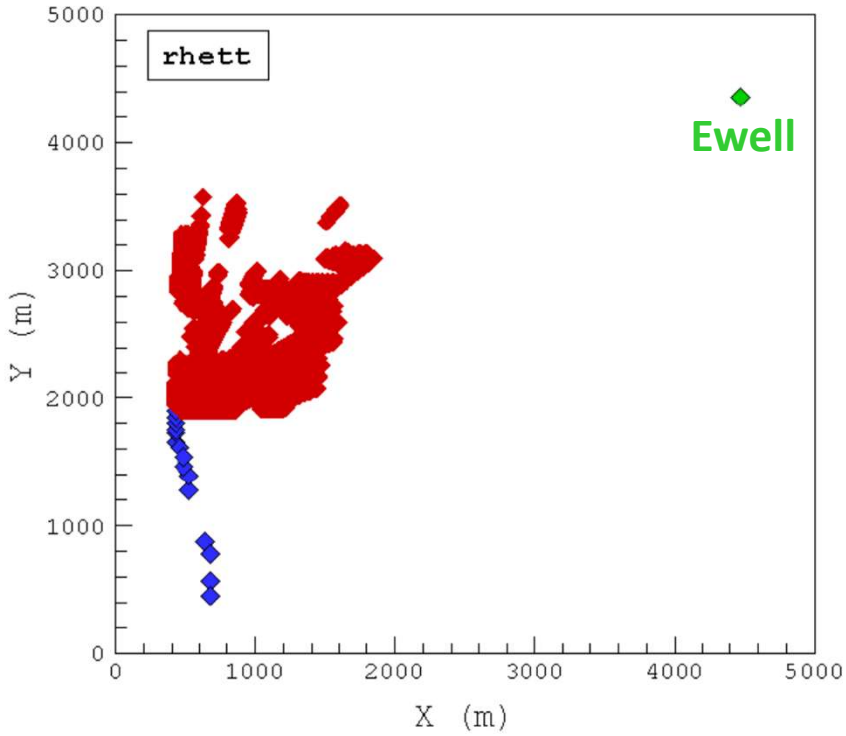

Ahmad et al. (AIAA-2008-0062)

Questions?